IMPACT OF TRUCK SUSPENSION AND ROAD ROUGHNESS ON LOADS EXERTED TO PAVEMENTS

Conducted for:

Engineering & Software Consultants, Inc.
14123 Robert Paris Ct.
Chantilly, VA 20151

Research Report FHWA-RD-07-1008-02

November 2010

Center for Transportation Infrastructure Systems
The University of Texas at El Paso
El Paso, TX 79968
(915)747-6925
http://ctis.utep.edu

TECHNICAL REPORT STANDARD TITLE PAGE

1. Report No.
FHWA-RD-07-1008-02

2. Government Accession No.

3. Recipient's Catalog No.

4. Title and Subtitle
Impact of Truck Suspension and Road Roughness on Loads Exerted to Pavements

5. Report Date
November 2010

6. Performing Organization Code

7. Authors
S. Misaghi, S. Nazarian and C.J. Carrasco

8. Performing Organization Report No.
Research Report FHWA-RD-07-1008-02

9. Performing Organization Name and Address
Center for Transportation Infrastructure Systems
The University of Texas at El Paso
El Paso, Texas 79968-0516

10. Work Unit No.

11. Contract or Grant No.
DTFH61-05-D0-00017

12. Sponsoring Agency Name and Address
Engineering & Software Consultants, Inc.
14123 Robert Paris Ct.
Chantilly, VA 20151

13. Type of Report and Period Covered
Final Report July 2008-November 2010

14. Sponsoring Agency Code

15. Supplementary Notes
Research Performed in Cooperation with FHWA.
Contacting Agency: Engineering and Software Consultants, Inc. (FHWA)

16. Abstract

A software package, called IntPave, an Integrated Pavement Damage Analyzer, was developed at the Center of Transportation Infrastructure Systems at The University of Texas at El Paso with the capacity to calculate the pavement distress for flexible pavements under any type of traffic load, and to make a comparison of the level of distress caused by a standard and a non-standard, assuming statically exerted loading. However, what has been lacking is a tool to measure the dynamic impact on the pavement due to vehicle-road interaction. In this report, the interaction of truck suspension systems with the roughness of the road surface was analyzed to calculate the additional forces to the pavement. The aim of this research was to quantify the impact of truck suspension system and road surface condition on the damage exerted to the road. Based on the suspension system and the road roughness based on the International Roughness Index (IRI), the truck-pavement interaction was modeled to estimate the dynamic load applied to the pavement. These analyses were incorporated in a new module of IntPave to modify the static load amplitudes to dynamic ones.

17. Key Words
Pavement Response, Suspension, Model Response, IRI, ISO Road Profile, Displacement PSD, DLC, Dynamic Impact

18. Distribution Statement
No restrictions. This document is available to the public through the National Technical Information Service, 5285 Port Royal Road, Springfield, Virginia 22161, www.ntis.gov

19. Security Classified (of this report)
Unclassified

20. Security Classified (of this page)
Unclassified

21. No. of Pages
104

22. Price

Form DOT F 1700.7 (8-69)

IMPACT OF TRUCK SUSPENSION AND ROAD ROUGHNESS ON LOADS EXERTED TO PAVEMENTS

by

Shahram Misaghi, MSCE
Soheil Nazarian, Ph.D., P.E.
and
Cesar Carrasco, Ph.D.

Research Report FHWA-RD-07-1008-02

Conducted for
Federal Highway Administration

November 2010

The Center for Transportation Infrastructure Systems
The University of Texas at El Paso
El Paso, TX 79968-0516

NOT INTENDED FOR CONSTRUCTION, BIDDING, OR PERMIT PURPOSES

ACKNOWLEDGEMENT

The successful progress of this project could not have happened without the help and input of many New York State DOT, FHWA, Texas DOT, and Ohio DOT personnel. The authors acknowledge Dr. Julian Bendaña of NYSDOT for his guidance and valuable input. The interaction with Ms. Katherine Petros, Mr. Eric Weaver both from FHWA has been very beneficial to us. We also acknowledge very valuable input by Dr. Magdy Michael of TxDOT and Mr. Roger Green of ODOT.

EXECUTIVE SUMMARY

The implementation of North American Free Trade Agreement (NAFTA) opened the borders to international traffic coming from both Canada and Mexico. As a consequence, highway networks will be subjected to trucks with new axle configurations and heavier axle loads, causing concern on the impact of super-heavy vehicles on highway's infrastructure. This pooled fund study is aimed at providing tools to address these issues.

A software package, called IntPave, an Integrated Pavement Damage Analyzer, has been developed at the Center of Transportation Infrastructure Systems at The University of Texas at El Paso to estimate the pavement distress for flexible pavements under any type of traffic load, and to make a comparison of the level of distress caused by a standard and a non-standard, assuming statically exerted loading. However, what has been lacking is a tool to include the additional dynamic loads on the pavement due to vehicle-road interaction. In this report, the interaction of truck suspension systems with the roughness of the road surface was analyzed to calculate the dynamic load amplification of forces exerted on the pavement. Based on the suspension system and the road roughness, the truck-pavement interaction was modeled to estimate the dynamic load applied to the pavement. These analyses were incorporated in a new module of IntPave to modify the static load amplitudes to dynamic ones. The dynamic Load Coefficient (DLC) is used to modify the traditional static load from the displacement power spectral density and frequency response function of a suspension system. The displacement power spectral density is correlated to the International Roughness Index (IRI).

In this report the process of incorporating the vehicle-pavement interaction is discussed followed by parametric studies of four suspension systems. The suspension systems studied were quarter car, single tandem, single tridem and walking beam. The impact of the stiffness, damping and mass of the suspension system on DLC were evaluated. It was found that as stiffness increases the DLC increases, whereas the latter decreases as damping coefficient or mass increases. The impact of the vehicular speed on DLC was also studied. As vehicular speed increase the DLC increases. Based on the correlation between vehicle speed and road roughness a DLC model prediction has been developed.

TABLE OF CONTENTS

LIST OF TABLES

LIST OF FIGURES

CHAPTER 1: INTRODUCION

Trucking accounts for about 80% of freight transportation in the United States. The impact of heavier axle loads and new axle configurations on the US highway networks is not well understood. Highways designed to carry vehicle loads of 80 kips (36,000 kg) could be trafficked with gross vehicle loads of over 120 kips (51,000 kg) by trucks with different tire and axle configurations. The use of heavy loads and new vehicle configurations has a major impact on the structural and functional performance of the highway network. New analytical tools are needed to predict the additional damage and to quantify the economic impact of allowing such trucks to use the highway system. A software package called Integrated Pavement Damage Analyzer (IntPave) has been under development at The University of Texas at El Paso (UTEP) for this purpose.

IntPave structural model is a finite element program that calculates pavement responses and estimates the progression of distresses to predict performance and damage to pavements. The finite element program makes use of an optimized mesh that becomes more refined in the proximity of load application points, namely the tire contact areas thus needing fewer elements resulting in a faster computational time. The meshing both in 2D and 3D is carried out automatically without the input from the user. Any user who is familiar with the major layered elastic pavement design algorithms can utilize this code without the knowledge of the finite element method.

The fact that the highway system accommodates a vast variety of vehicles serving a multiplicity of uses has led to the incorporation of a permit fee model in IntPave that seeks to compare the damage that various groups of trucks impose to the pavement with the costs to maintain it. Under this approach, each user pays the highway costs that it creates.

OBJECTIVES

IntPave currently conducts the damage analysis and permit fee allocation assuming the axle loads are exerted statically. The interaction of truck suspension system with the roughness of the road surface may exert additional forces to the pavement. The aim of this research is to quantify the impact of truck suspension system and road surface condition on the damage exerted to the road. Different common suspension systems are modeled. The International Roughness Index (IRI) was used to simulate the road roughness. Based on these two parameters, the truck-pavement interaction was modeled to estimate the dynamic load applied to the pavement. These analyses were incorporated in a new module of IntPave to modify the static load amplitudes to dynamic ones.

SCOPE OF WORK

The aim of this research is to relate the truck suspension system and the road roughness to the additional load that may be exerted to the pavement. To that end, a model that estimates the dynamic impact of the load for a given suspension and road roughness has to be developed. The dynamic impact explains how much the dynamic load can be greater than the static load.

IntPave is a software package which was developed to calculate fatigue and rutting damage of pavement under static loads. As a result of this study, a new module that calculates the potential dynamic loads has been added to IntPave. The flow chart of the module is shown in Figure 1.1. A frequency-domain solution has been implemented because the time-domain solutions are time consuming. The road roughness is quantified based on the International Roughness Index (IRI). To implement this concept in the frequency domain solution, the IRI has been related to a series of power spectral density of the road displacement. Every suspension system in frequency domain has a corresponding frequency response function (FRF). These FRF's have been formulated for a number of common suspension systems. Knowing the power spectral density of the road roughness and the frequency response function of the suspension, a dynamic load coefficient (DLC) is calculated. The DLC along with the static load can be used to calculate to the modified static load. The modified loads are then used instead of the traditional static loads to calculate the damage and costs.

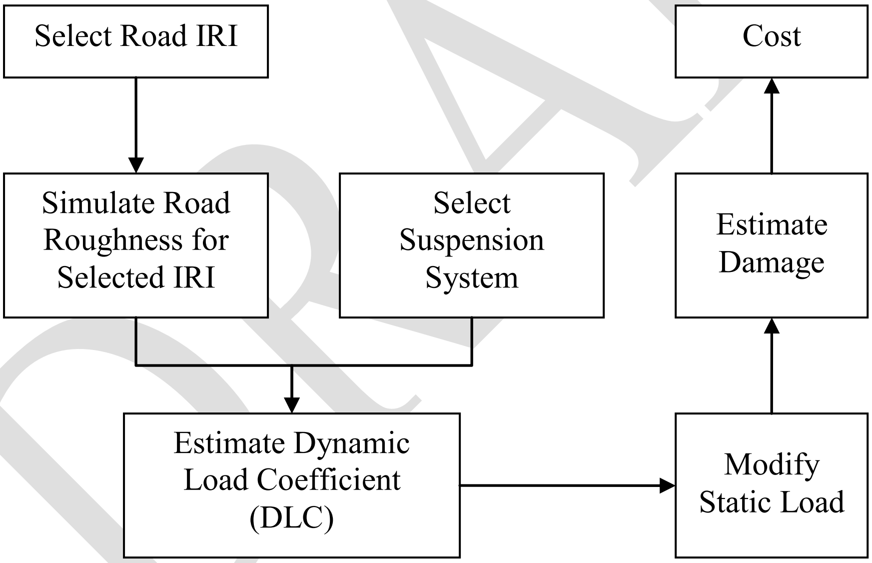

Figure 1.1 – Flowchart of Incorporating Road Roughness in Calculation of Loads

ORGANIZATION

Chapter 2 of this report contains an overview of common suspension systems, and a brief review of the literature on the subject. A brief description of road roughness simulation using the International Organization for Standardization (ISO) method is included in Chapter 3, along with the pertinent formulation of the relationship between IRI and initial spectral density. Chapter 4 discusses the methodology developed to estimate dynamic load coefficient. A series of parametric studies are presented in Chapter 5 to show how the dynamic load coefficient varies with different suspension parameters and pavement conditions. Finally, Chapter 6 includes the summary of the work accomplished and the status of the project.

CHAPTER 2: BACKGROUND

This chapter introduces several suspension systems commonly used in heavy vehicles and some essential terminologies associated with them. A historical background on this topic is also provided.

SUSPENSION SYSTEMS

Three types of suspensions are popular in the US and throughout the world. Based on a survey of manufactures, Morris (1987) estimated the popularity of different truck suspension systems used in different vehicles. As reflected in Table 2.1, the most common suspension types are the Walking Beam, Air Spring and Leaf Spring. These suspension types are described briefly in the next section.

Table 2.1 – Percentage Usages of Different Suspension Systems (from Morris, 1987)

Suspension	Percent Usage	
	Tractors	Trailers
Walking-Beam	15-25	<2
Air Spring	15-20	10-15
Leaf spring	55-77	>80
Other	2-4	Nil

LEAF SPRING SUSPENSION

Leaf spring suspensions are usually used in tandem, tridem or more than three axles. As shown in Figure 2.1, several strips (leaves) of steel with rectangular cross sections are formed into semi-elliptical arcs and tied together. The axle is secured to the center of the arc, while the two ends are connected to the vehicle frame. The stacked strips act as a spring to carry the payload of the truck elastically. These springs also absorb the energy by dry ('Coulomb') friction among leaves and contact points. Leaves are assembled from shorter to longer from bottom to top. Parabolic leaf spring is the newest design that uses fewer leaves. In this design, the thickness of the leaves changes from the center to the end following a parabolic curve. If the friction between the springs decreases, the efficiency of the system may increase. Spacers are added to minimize the contact at other points. Benefits of this type of design are reducing weight and better flexibility. Traditionally, the behavior of leaf springs is modeled using simple beam theory.

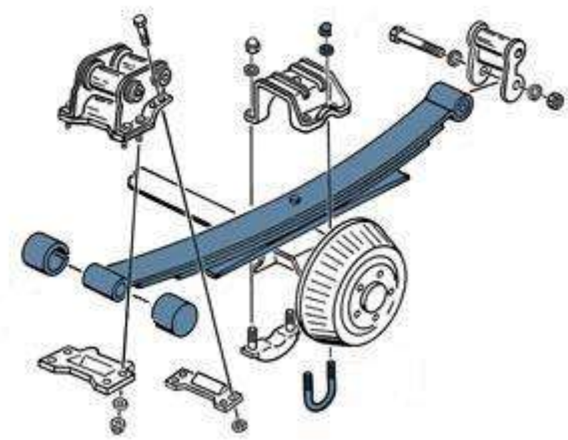

Figure 2.1 – Typical Leaf Spring Suspension System used in Tandem and Tridem Axles

A variation to the leaf spring suspensions is the single point spring as shown in Figure 2.2. In this type of suspension, axles are attached to the two ends of the leaf spring, and the center of these leaves is linked to the chassis. Single point springs are similar to the walking beam suspension to be discussed later.

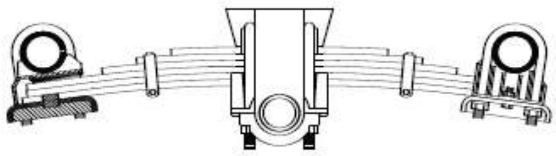

Figure 2.2 - Single point spring

AIR SUSPENSION SYSTEM

In air suspension systems, pressurized air in airbags, instead of leaves, work as spring and several shock absorbers provides the system damping. Trapped air in sealed rubber membranes provides nonlinear spring stiffness in the system. Hydraulic absorbers provide energy dissipation. Air suspension systems have several advantages. Automatic control devices can be added to these systems to optimize the use of variable wheel deflection. They can also provide a steady vehicle height. Riding comfortably is another of their advantages. In spite of these advantages, they have some limitation such as the load carrying capacity.

Figure 2.3 - Air suspension system

WALKING BEAM

This type of truck and tractor rear suspension consists of two centrally pivoted beams, one at each side. These beams are connected to each other via a shaft passing through the center of the beams. The walking beam suspension system consists of two set of leaf springs rigidly supported by beams that transmit the load to a beam centrally pivoted. The rigid beam links the two axles. A large beam connects the two axles. Upper and lower shock insulators are attached to the beam at each side of the walking beam, and a large cap clamps the insulators to the axles. No shock absorbers are used in this system.

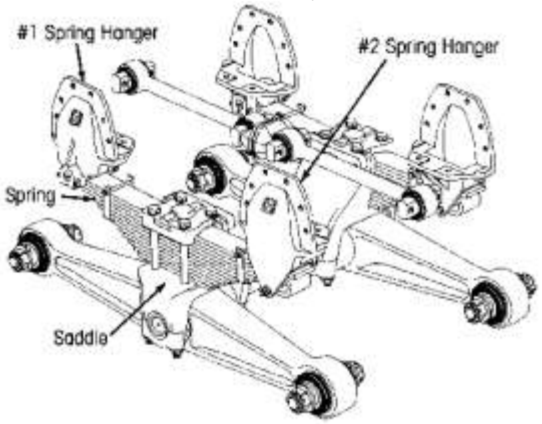

Figure 2.4 - Sample of Walking Beam

HYDRAULIC SHOCK ABSORBER

This suspension works like air suspension system but it utilizes hydraulic fluid rather than air to absorb the energy. Energy dissipation is provided by trapped oil inside a metallic chamber. Hydraulic shock absorbers are commonly used in commercial vehicles. The nonlinear force generated by this kind of suspension system depends on characteristics of imposed motion such as frequency and amplitude. Studies focused in this type of suspension systems are limited to passenger cars. Segal and Lang (1981) developed a model based on internal pressure/flow process. That complex model requires 82 parameters. Karadayi (1989) published a nonlinear damper model based on an experimental study of two passenger car shock absorbers. The results from that model agreed with the experimental results at 0.2 Hz, but there were no experimental results for higher frequencies to further verify the model. Wallaschek (1990) showed that the behavior of such absorber cannot be predicted with small number of parameters.

Figure 2.5 – Hydraulic Shock Absorber

DYNAMIC LOAD COEFFICIENT (DLC)

The dynamic forces due to the road roughness and the speed of the truck may exert additional loads under each wheel. These additional loads are normally centered around the traditional static loads. A typical dynamic axle load probability density distribution, as shown in Figure 2.6, represents the likelihood that the wheel load would have a particular magnitude in as it moves along a pavement section. The distribution has a mean value, ($\bar{F}$), which usually is assumed to be equal to the static load, and a standard deviation, σ. The Dynamic Load Coefficient (DLC) is defined as a dimensionless variable obtained by dividing the standard deviation by the mean static load (Gillespie, 1993). In an equation form, this relationship is shown as

$$DLC = \frac{\sigma}{\bar{F}} \tag{2.1}$$

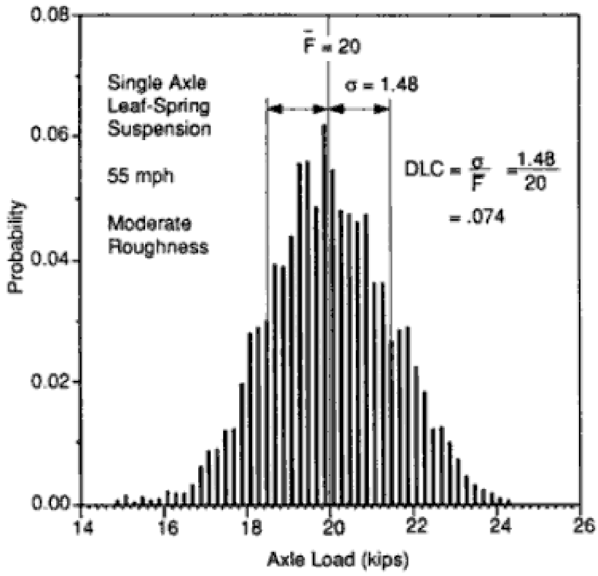

Figure 2.6 - Probability of Distribution of Dynamic Load under Wheel

Tire force time-history can be used to determine the statistical distribution parameters. If N measurements of tire forces are available, the standard deviation is derived by Equation 2.2:

$$\sigma^2 = \frac{1}{N}\sum_{k=1}^{N} f_k^2 \tag{2.2}$$

where f_k is the k-th force measurement. The DLC concept allows the probabilistic magnitude of the dynamic axle load at a certain vehicle speed and road roughness to be determined. Theoretically, a truck passing over a smooth pavement should have a DLC close to zero. The maximum experimentally observed DLC is in the range of 0.3 to 0.35.

LOAD SHARING COEFFICIENT

The distribution of loads between the axles is not usually the same. Sometimes the load carried by each axle is important. The load sharing coefficient (LSC) is a measure of how well a suspension group distributes the total axle group load between the axles (Potter et al., 1996). The LSC can be found from:

$$LSC = \frac{F_{mean}(i)}{F_{stat}} \quad \textbf{(2.3)}$$

where

F_{stat} = nominal static tire force $F_{\text{group(total)}}/n$
$F_{\text{group(total)}}$ = total axle group force
$F_{\text{mean}}(i)$ = mean force on tire i
n = number of tires in the group

INTERNATIONAL ROUGHNESS INDEX

Traditionally, the serviceability of a pavement is determined by its smoothness. The serviceability concept was first described by Carey and Irick (1960) at the AASHO road test. The serviceability index, ranging between 0 and 5 (impassible to excellent), was measured by a panel of raters driving a car over a pavement. The World Bank developed the International Roughness Index (IRI) as a quantitative expression of the smoothness of a pavement (Sayers et al. 1986). The IRI is defined as the average rectified slope (ARS) which is a ratio of accumulated suspension motion to the distance traveled. A mathematical model of a quarter car one-wheel vehicle passing a measured profile at 50 mph (80 km/m) is used for this purpose. The unit of IRI is either in./mile or m/km, where IRI of 1 m/km is excellent. ASTM E 1926 explains the calculation of the IRI. The raw data, which is in the form of a longitudinal road profile measurement, along with a mathematical process provide an estimate of the highway IRI.

LITERATURE REVIEW

Magnusson et al. (1984) published a review of the dynamic axle loads applied to pavements. They indicated that the minimum dynamic loads were achieved by using soft suspension springs and tires. They recognized that an optimal level of viscous damping usually exists, depending on the condition and Coulomb friction. Aurell (1991) carried out an experimental and theoretical parametric study which confirmed Magnusson et al.'s results. Heath (1987) showed that lower stiffnesses of suspension system and tire are desirable, but he mentioned very low tire stiffness sometimes imposes low frequency forces that may exaggerate the sprung mass motion.

Sweatman (1987) studied the influences of the vehicle speed and roughness on DLC with different suspension systems. His study showed that the DLC is linearly related to the speed.

Cebon (1985) experimentally measured the dynamic loads under rigid 3- and 4-axle trucks. Sprung mass, unsprung mass and dynamic tire forces were measured during his tests. The results explained several essential features of heavy vehicle vibration behaviors. Cebon also attempted to validate the 2- and 3-dimensional numerical models developed for the simulation of those vehicles. The agreement between the behaviors of the models and measurements was acceptable. He indicated a two- dimensional model provided reasonably realistic dynamic tire forces as long as the following two conditions are met:

1. The vehicle speed should be high enough to prevent the excitation of the sprung mass.

2. The unsprung mass vibration mode should have similar damping and frequency in bounce and roll, or the unsprung mass mode should not contribute significantly to the dynamic tire forces.

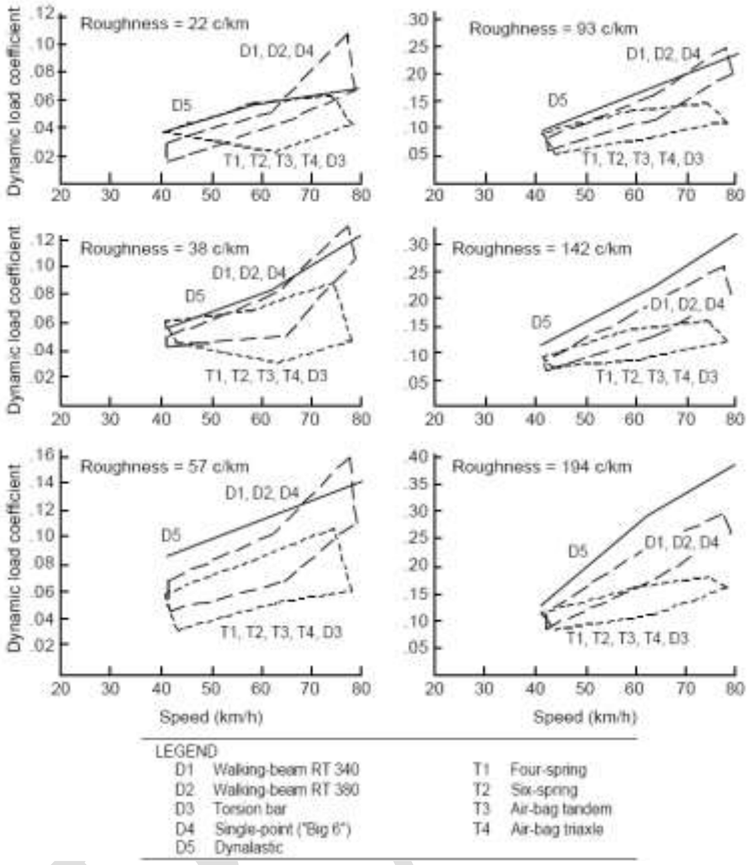

Figure 2.7 - Effects of Speed and Roughness on Dynamic Load Coefficient Generated by Various Suspensions (after Sweatman, 1987)

Cebon (1999) drew the following guidelines for obtaining accurate results from numerical simulations:

1. Road surface roughness must be known accurately enough, because it is one of the most important factors that cause the variations between the model and measurements.
2. The model must meet the nonlinear characterization of the suspension system.
3. The payload distribution is significant and should be considered.
4. Wheel spacing should agree with the actual vehicles.
5. Truck frame flexibility should be ignored.
6. Behavior of tire is considered linear and any nonlinearity of tire should be neglected.
7. At normal highway speeds, the influence of road roughness short waves can be ignored.

Cebon and Winkler (1990) tried to show the senility of the force with respect to speed. A 38-meter test track was equipped with 96 capacitive weigh-in-motion (WIM) strips. Seven different articulated heavy vehicles were used to perform 612 tests for a range of speeds between 8 km/h and 85 km/h.

Gillespie, et al. (1992) studied the effects of heavy trucks on pavement performance. They confirmed that in addition to the number of axles and axle configuration, the suspension system impacts the damage to a pavement. They analyzed the truck road interaction mechanism to correlate the truck characteristics with the fatigue and rutting of the pavement.

O'Connell et al. (1993) performed numerous parametric studies of the vehicle and pavement variables. The following three conclusions were derived from that study:

1. Damage factor of dynamic tire force could be up 25% depending on the vehicle and pavement conditions.
2. Air suspensions have the least damping and walking beam causes the most damage to the pavement.
3. Tandem axles increase slightly the dynamic loads and theoretical cracking damage, but decrease dramatically the rutting damage.

Potter et al. (1994) studied a road in the UK which was subjected to 1500 heavy vehicles. The dynamic tire forces were measured by 144 strip sensors. The recorded data were studied to find the relative pavement damaging capacity of the different types of vehicles, and the degree of spatial repeatability of wheels passing over a highway section. About half of the vehicle tested showed a spatially repeatable pattern. In that study, the vehicles with air suspensions exhibited lower dynamic load coefficients relative to those with steel suspensions.

Cole and Cebon (1996) reported how the load contact area might affect the generation of dynamic tire forces. They compared the characteristics of a wide single tire and a dual-tire configuration. On roads with thinner asphalt layers, they observed that the wide single tires caused up to seven times more fatigue cracking damage than the dual tires carrying the same loads. For the thicker pavements, the wide single tires caused 1.5 to 2 times more permanent deformation damage than dual tires. For rigid pavements, the wide single tires caused a relatively small increase in the fatigue damage. By optimizing the suspension system, the wide single tires generated less dynamic loads and less road damage. The reduction of the road damage was about 12% for the optimal suspension design. They indicated that if the dual tires were changed to a single wide tire, a suspension system with 25% less damping was needed to cause less damage.

de Pont (1996) used accelerometers to study the impacts of the dynamic axle loads on the pavement response. Both air and steel suspension systems were tested for vehicles with weights ranging from 2000 to 6000 kg. The air suspension system generated dynamic forces under the wheel that were less than the steel suspension system. The ratio of the forces generated by the air suspension system relative to the steel suspension system was about 0.5.

Magdy and Michael (1997) developed a finite element model to show the variability of the dynamic loads for different vehicle speed, vehicle type, suspension type, level of roughness and pavement stiffness. This study indicated that the dynamic load variation from a walking beam suspension was more than an air suspension or leaf spring system. The DLC of the walking beam suspension was approximately twice the others. They also indicated that the rutting of a pavement is very sensitive to the vehicle speed. For example, a vehicle moving at 20 km/h might cause ten times more permanent deformation than one moving at 130 km/h.

DIVINE (1998) indicated that the pavement under a steel suspension might wear at least 15% faster than under air suspension, and the magnitude of the load under an air suspension system was about half of the steel one. It defined a road-friendly suspension system as one with low spring stiffness and a certain level of viscous damping. Those properties, which are usually found on well-designed air suspension systems, cannot be probably found on a steel suspension system.

Several researchers such as Whittemore et al. (1970) and Ervin et al. (1983) in USA; Leonard et al. (1974), Addis et al. (1986), Mitchell (1989), Gyenes and Simmons (1989) and Cole (1992), Cebon et al. (1994) in UK; Sweatman (1980) in Australia; Woodrooffe et al. (1986) in Canada; Gorge (1984) and Hahn (1987) in West Germany reported about this field of study. The conclusions of those studies can be summarized in the following manner:

1. All results indicate that dynamic load increases with speed.
2. Decreasing the suspension stiffness reduces the tire dynamic load (Sweatman, 1980)
3. Walking beam suspensions as a centrally-pivoted tandem suspension system always generate more dynamic load because lightly damped pitching modes at around 8-10 Hz.
4. Walking beam suspension systems can be improved by suitable use of hydraulic dampers (Hahn, 1987)
5. Four-spring tandem axles generate smaller dynamic load than walking beam suspensions.
6. The axle spacing for an air tandem suspension does not significantly affect the dynamic loads, whereas the DLC of a four-spring suspension varies significantly with the axle spacing (Woodrooffe et al., 1986).

OECD (1998) allowed air-sprung heavy vehicles to carry more load. Australian road authorities found the dynamic loads in that type of air suspension is not uniformly distributed, resulting in more severe road damage (Potter, 1996). For a uniformly distributed load, the load sharing coefficient (LSC), defined as the load on the heaviest axle divided by the average axle load should be close to one. Sweatman (1983) reported the LSC's of steel suspensions in the range of 0.79 and 0.96. Davis (2009) reported the LSC's of air suspension systems of about 0.90 to 0.93.

Sun (2001) initiated a numerical simulation of the IRI by using the power spectral density (PSD) using Newmark sequential integration. Statistical analysis of this simulation showed a linear relation between IRI and the standard deviation of relative sprung mass vertical velocity. That study showed that if the PSD of roughness is defined by a polynomial function, the IRI can be calculated simply by means of the square root of the sum of the weighted regression coefficients of PSD roughness.

CHAPTER 3: ROAD ROUGHNESS PROFILE

As indicated above, two parameters contribute to the additional dynamic loads due to vehicle-road interaction, the type of suspension and the road roughness profile. Different types of suspensions were described in Chapter 2. Ideally, the road roughness profile is available for a given pavement by using a number of available tools. However, the raw roughness profile may not be available for all projects. In this chapter the process of estimating the road roughness profile either from the IRI or from a subjective description of the road roughness is presented. The steps required to carry out this task include the following:

1. Simulating a road roughness profile based on road condition, and
2. Estimating the IRI of the simulated road profile as per ASTM 1926

These steps are described below.

SIMULATING ROAD ROUGHNESS PROFILE

ASTM E 1926 categorizes the road roughness into five classes from Very Good condition with IRI of less than 2, to Very Poor with IRI in excess of 8 for paved road. The goal of this project is to utilize this subjective ranking to simulate a representative road roughness profile (elevation vs. distance) as shown in Figure 3.1. The profile exhibits from "sharp (short wavelength)" to "gradual (long wavelength)" changes in the profile. Depending on the suspension type, one or more wavelengths are of importance.

It is difficult to delineate the magnitudes of change associated with different wavelengths in Figure 3.1. To rigorously express the magnitude as a function of wavelength, the Fourier transform can be utilized. Fourier transforms describe a function as a summation of harmonic waves. Each harmonic wave is defined by a magnitude and frequency. The variation of the magnitude of the power with frequency is called the power spectral density (PSD). The power spectral density of road displacement is defined as variation of magnitude squared divided by wavenumber with frequency. In many frequency-domain analyses dealing with the spatial instead of temporal variations (such as this problem), the frequency is replaced by a parameter called the wavenumber. Wavenumber (in cycles/m) expresses rate of change with respect to distance in the same way as frequency f (in cycle/s) expresses the rate of change with respect to time. Wavenumber is simply the reciprocal of wavelength (in meter). As an example, the frequency domain representation of the road profile in Figure 3.1 is shown in Figure 3.2.

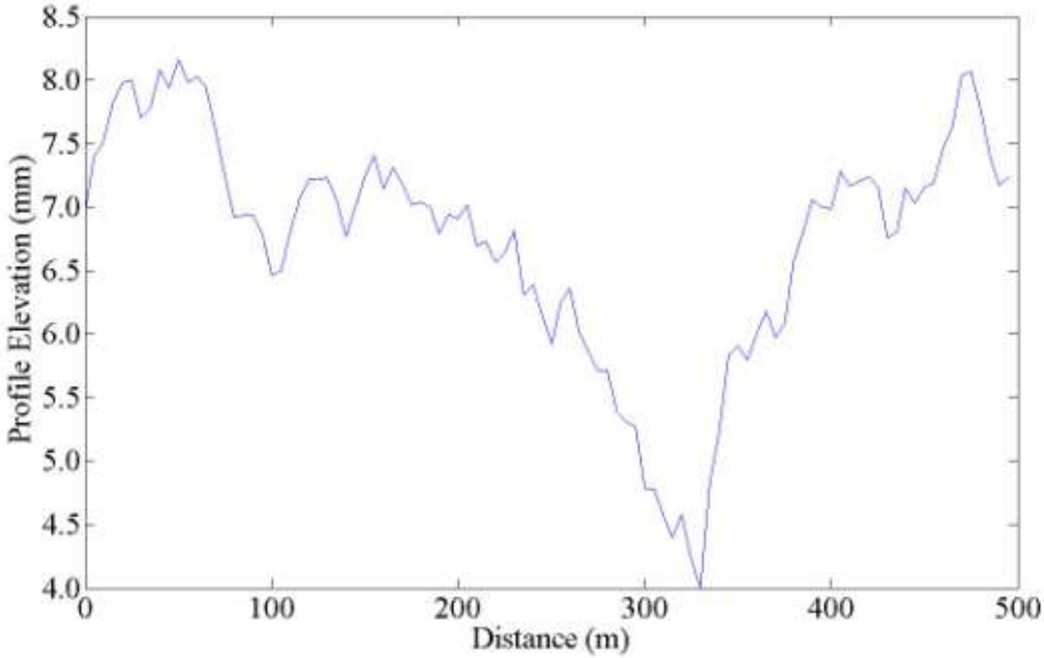

Figure 3.1 – Simulated Road Roughness Profile with Average Road Condition ($S_u(\kappa_0)$ =32x10^{-6} m³/cycle)

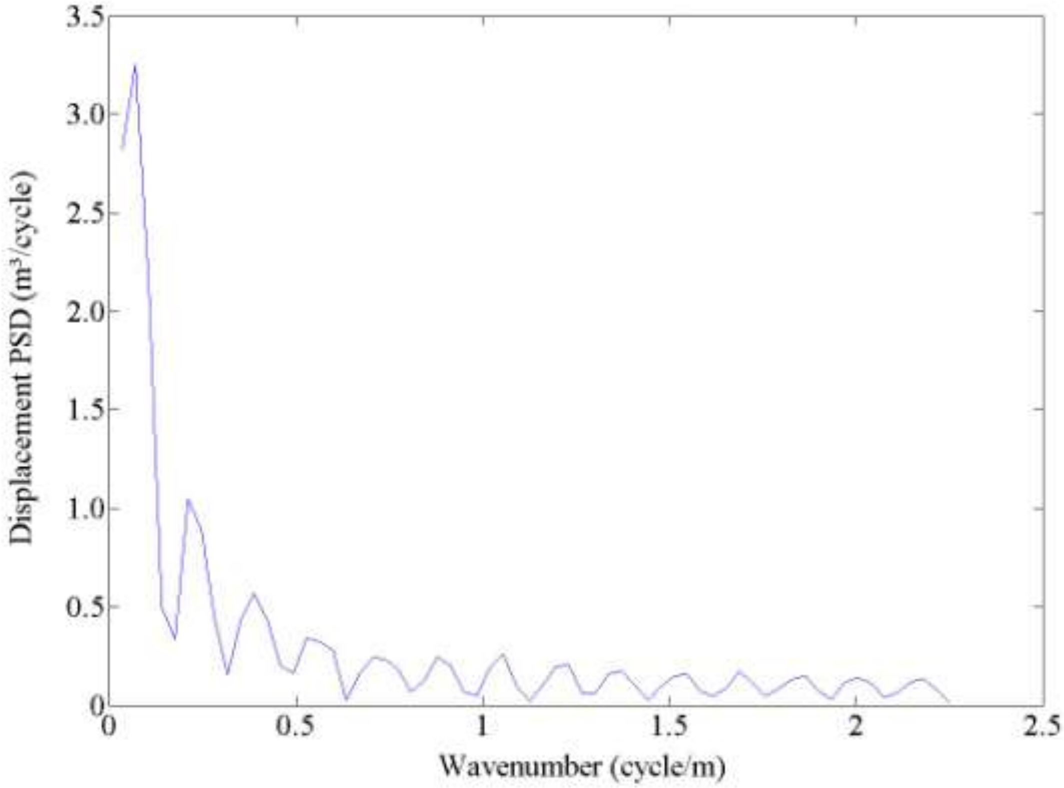

Figure 3.2 – Spectral Density of Simulated Road with Average Road Condition

Based on measurements on European roads, ISO (1995) proposed the equation 3.1 to relate the vertical profile (u) spectral density to wavenumber:

$$S_u(\kappa) = \begin{cases} S_u(\kappa_0)(\frac{\kappa}{\kappa_0})^{-n_1} & \frac{\kappa}{\kappa_0} \le 1 \\ S_u(\kappa_0)(\frac{\kappa}{\kappa_0})^{-n_2} & \frac{\kappa}{\kappa_0} > 1, \end{cases} \quad \textbf{(3.1)}$$

where

κ =wavenumber, cycle/m
κ_0 =datum wavenumber, cycle/m
$S_u(\kappa)$ =displacement spectral density, m^3/cycle
$S_u(\kappa_0)$ =spectral density at κ_0, m^3/cycle or initial spectral density.

After several iterations, Cebon (1999) recommended the following values for other parameters in Equation 3.1, n_1=3, n_2=2.25, k_0=1/(2π) cycles/m. The initial power spectral density is the power of spectral density at datum wavenumber (1/2π). The Initial power displacement spectral density $S^u(\kappa_0)$ is the parameter which generates different road conditions. Table 3.1 provides a relationship between $S_u(\kappa_0)$ and the subjective road roughness. Utilizing these values, the solution for Equation 3.1 is shown in Figure 3.3.

Table 3.1 – Relationship between Constant S_u (κ_0) and Road Roughness (from Cebon, 1999)

Road Class	$S_u(\kappa_0)/10^{-6}$ m³/cycle
Very Good	2-8
Good	8-32
Average	32-128
Poor	128-512
Very Poor	512-2048

The inverse Fourier transform (DFT) of $S_u(\kappa)$, provides a harmonic road profile (elevation vs. distance) that is associated with a given wavenumber, k. To simulate a road profile, a large number of wavenumbers should be considered and summed up as reflected in Equation 3.2:

$$Z_r = \sum_{k=0}^{N-1} \sqrt{S_k}\, e^{i(\theta_k + \frac{2\pi kr}{N})} \quad r = 0,1,2,...,N-1 \text{(from Cebon, 1999)} \quad \textbf{(3.2)}$$

where

N = Number of wavenumbers considered
S_k = $(2\pi/N\Delta)S_{11}(\gamma_k)$
$S_{11}(\gamma_k)$= target spectral density
γ_k = $(2\pi k/N\Delta)$=the wavenumber in rad/m
Δ = the distance interval between successive ordinates of the surface profile
$\{\theta_k\}$ = a set of independent random phase angles uniformly distributed between 0 and 2π.

Figure 3.4 shows a sample of road profile spectral density for an average road condition ($S_u(\kappa_0)$ = 32×10^{-6} m³/cycle). To develop this graph, k was varied between 0.02 and 5 at 0.01 increments.

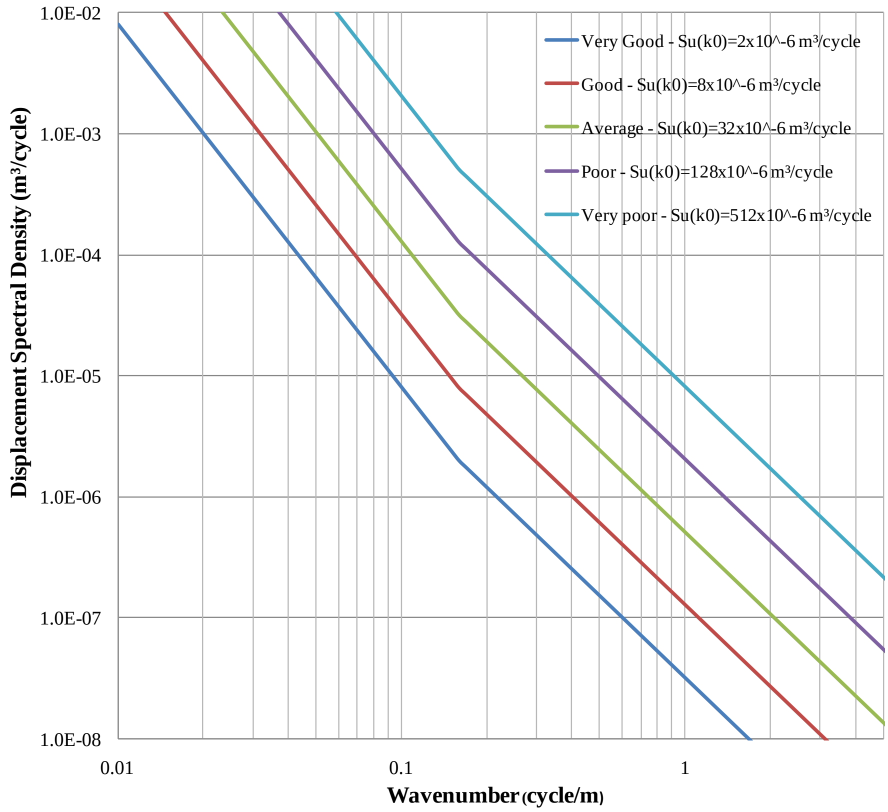

Figure 3.3 – Draft ISO Classification for Road Roughness Spectral Densities.

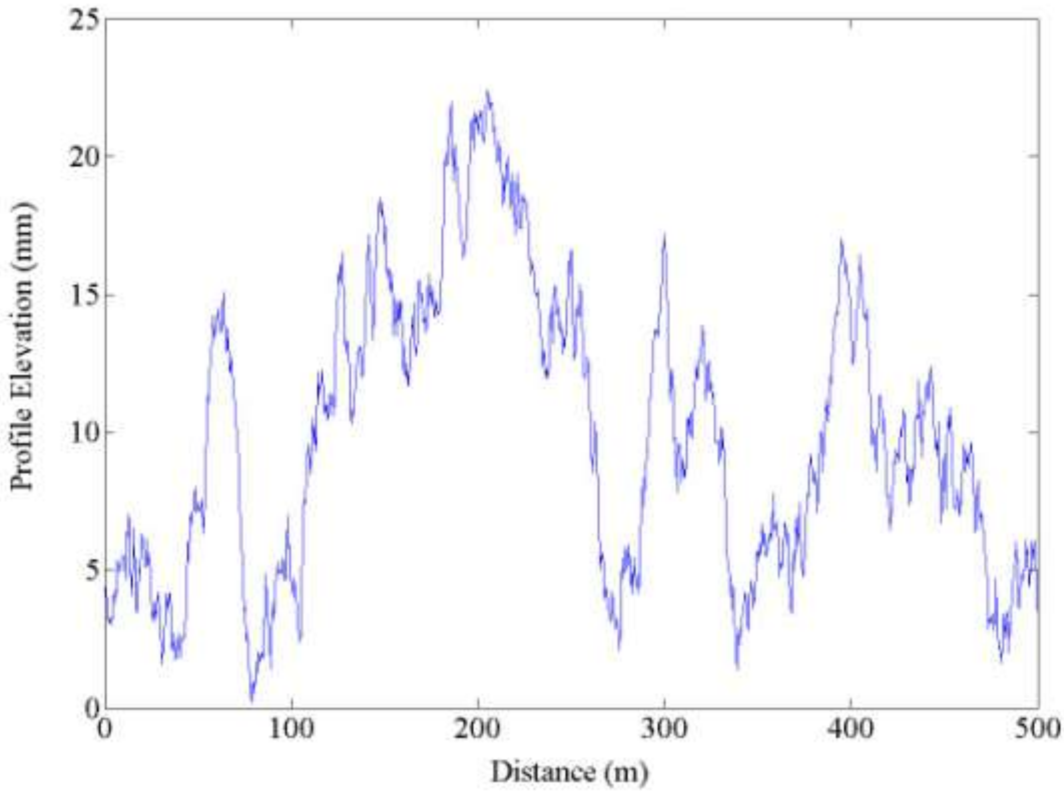

Figure 3.4 – Simulated Road with Average Road Condition ($S_u(\kappa_0) = 32\times10^{-6}$ m³/cycle)

ESTIMATING IRI OF SIMULATED ROAD PROFILE

As indicated before, the IRI is a filtered ratio of a standard vehicle's accumulated suspension motion divided by the distance traveled by the vehicle during the measurement. A specific quarter car is used in the calculation of the IRI. ASTM E-1926 contains a detailed algorithm for filtering the data to remove the road grade and the very long undulations from the measured data and transforming the data to the motion of the suspension of the quarter car. A virtual slope, which is the sum of the absolute values of the profile divided by the distant travelled is then calculated to represent the IRI.

MATLAB ROUTINE

A Matlab subroutine was developed and added to IntPave to calculate the IRI of the simulated road roughness. The flow chart of the subroutine is shown in Figure 3.5. The road roughness class from Table 3.1, the distance interval between successive ordinates of the surface profile, Δ, and the number of points to be measured, *N*, are input to the subroutine. According to ASTM E1364, the interval between measure data should be less than 0.3 m, with a preferred spacing of 0.25 m. The appropriate initial spectral density corresponding to the selected road roughness class is selected by the Matlab code. A series of random phase angles are generated by the program and inputted into Equation 3.2 to simulate the road roughness profile.

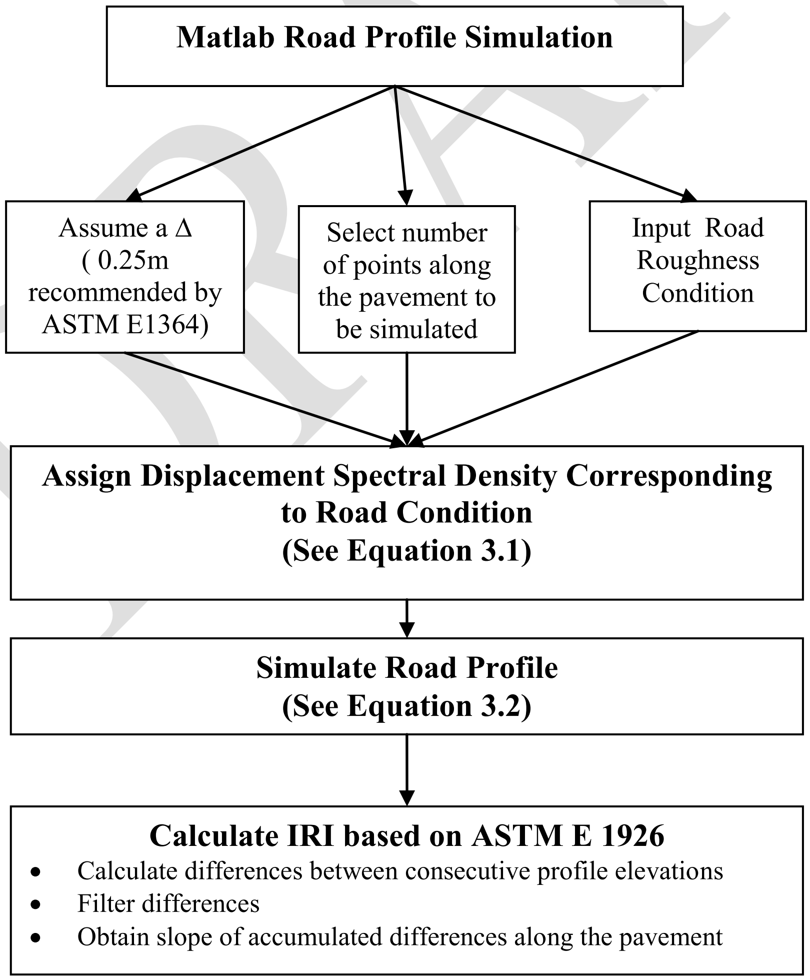

Figure 3.5 – Matlab Routine Flowchart

CORRELATING IRI TO INITIAL SPECTRAL DENSITY $S_u(\kappa_0)$

Figure 3.6 shows 100 simulations of the road roughness profiles for a road with a good road condition ($S_u(\kappa_0)$ = 8x10^{-6} m³/cycle). These profiles appear substantially different. One concern is whether the IRI calculated for all these simulated sections are similar. The statistical information about the estimated IRI is shown in Table 3.2. For the $S_u(\kappa_0)$ = 8 x10^{-6} m³/cycle, the average IRI is about 1.4 mm/m with a coefficient of variation of 6%. This indicates that the IRI's estimated for a given road roughness class is reasonably unique. Same conclusion can be drawn for different ranges of $S_u(\kappa 0)$ of 2 x 10^{-6} m³/cycle (very smooth) to 2048 x10^{-6} m³/cycle (very rough) as reflected in Table 3.2.

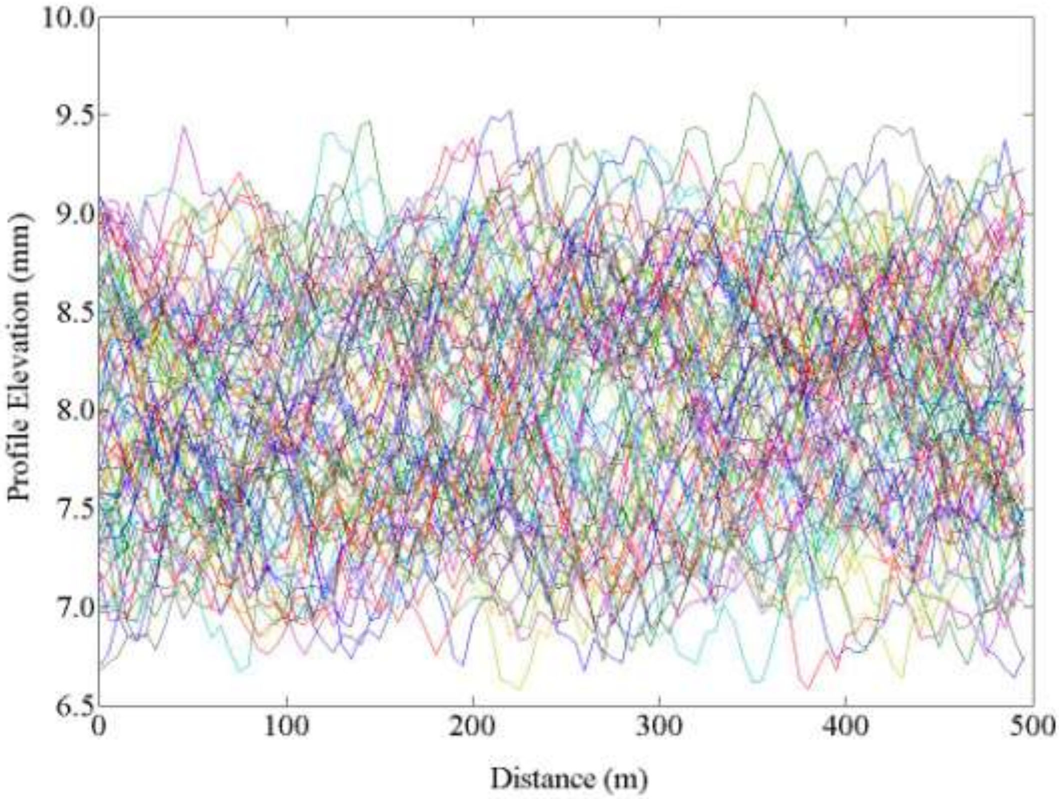

Figure 3.6 –100 Simulations of Road Roughness Profile for Good Road Condition

Table 3.2 – Statistical Information about IRI for 1000 simulations

$S_u(\kappa_0)$ (10^{-6}m³/cycle)	2	8	32	128	512	2048
Average of IRI (mm/m)	1.1	1.4	2.7	5.2	9.7	17.4
Standard Deviation	0.1	0.1	0.1	0.3	0.5	1.2
Coeff. of Variation	6%	6%	5%	5%	5%	7%

The correlation between the average IRI and $S_u(\kappa_0)$ in Table 3.2 is shown in Figure 3.7. The two parameters correlate quite well with an R^2 value of close to unity. The proposed equation for estimating $S_u(\kappa_0)$ from IRI is

$$S_u(k_0) = 2.52(IRI)^{2.37} \quad \textbf{(3.3)}$$

This equation is very convenient in terms of estimating the abstract parameter $S_u(\kappa_0)$ from the commonly known IRI. Table 3.3 provides a guideline for selecting appropriate $S_u(\kappa_0)$ for a given IRI.

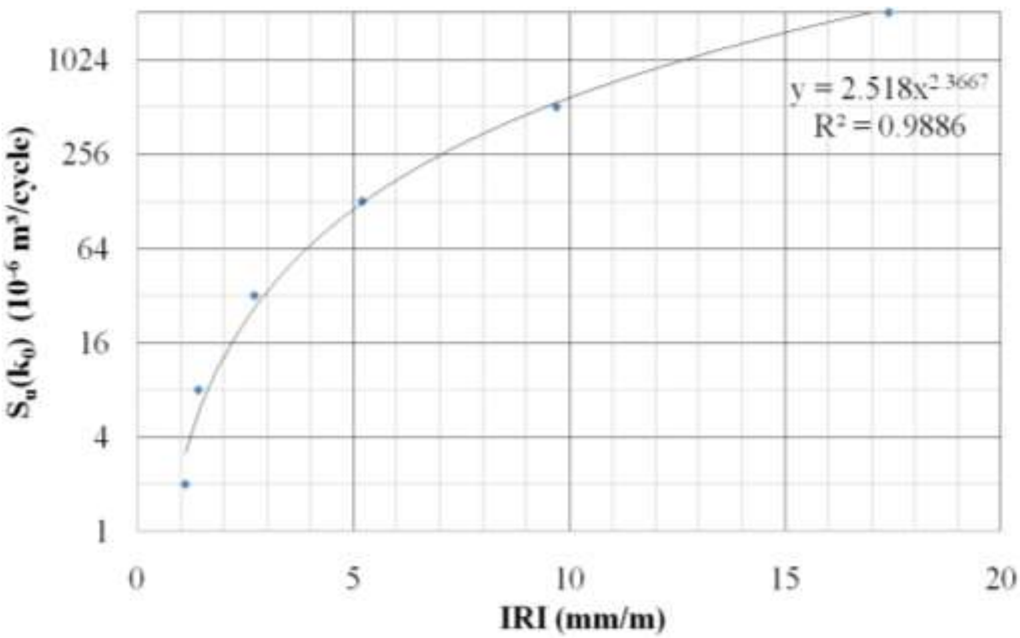

Figure 3.7 – Correlation between $S_u(\kappa_0)$ and IRI

Table 3.3 – Variation in $S_u(\kappa_0)$ with IRI

IRI (mm/m)	IRI (in/mile)	$S_u(\kappa_0)$ (10^{-6}m³/cycle)
1	63	2
2	126	13
3	190	34
4	253	67
5	316	114
6	380	176

CHAPTER 4: ESTIMATION OF DYNAMIC LOAD COEFFICIENT

In this chapter the process followed to estimate the dynamic load coefficient (DLC) is discussed. As reflected in Equation 2.1, the standard deviation of the dynamic loads applied to the pavement due to the variation in the roughness of the road is needed for estimating the DLC. This implies that the dynamic forces exerted to the pavement have to be calculated. To achieve this goal, the first step is to model a suspension system with a number of masses (m_i's), springs (k_i's) and viscous dampers (c_i's, see Figure 4.1). The second step is to estimate the displacement (u_i) that the roughness profile of the road exerts to each tire of the suspension system. The final step is to determine the dynamic forces (F_i's) exerted to the pavement due to the vibration of the suspension system.

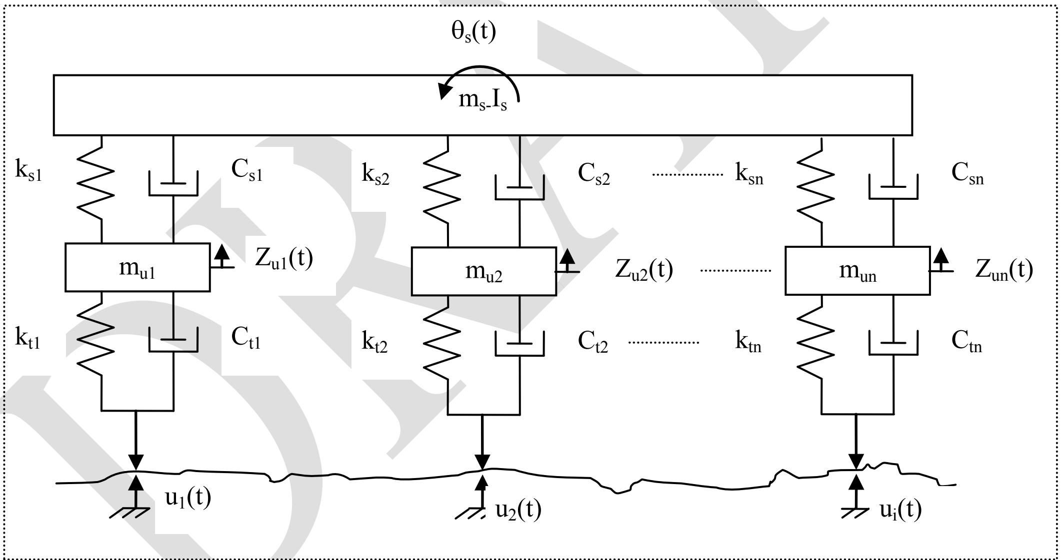

Figure 4.1– General Model for Estimating Dynamic Loads

Two different approaches for solving a model excited by a rough pavement can be pursued. This problem can be either solved in the time-domain or the frequency-domain (Cebon, 1999). The time-domain simulations are particularly attractive for nonlinear dynamic systems. The main concern with this type of solution is the computation time because of the intense numerical integration algorithms necessary. For complex dynamic systems that can be approximated as linear systems, the frequency domain solutions are preferred. In this study a frequency domain solution, based on the frequency response model, is implemented as discussed below. The flowchart associated with this task is shown in Figure 4.2.

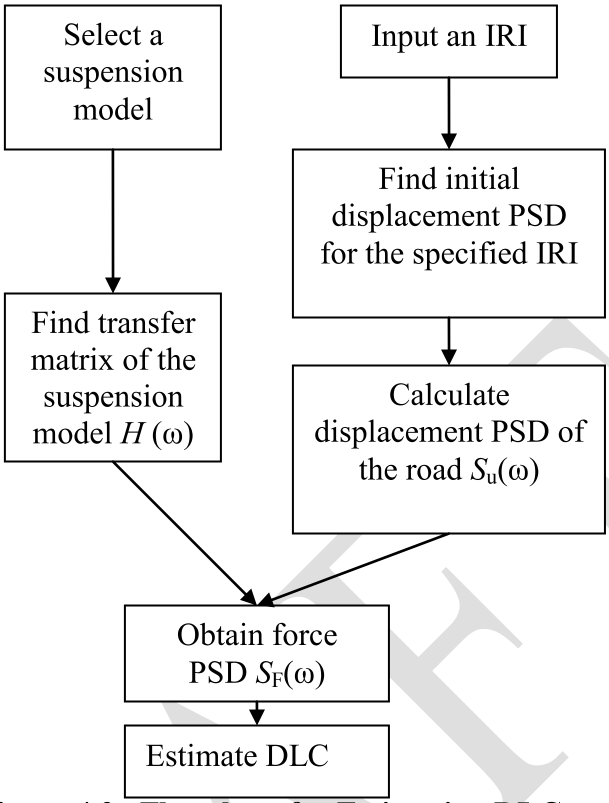

Figure 4.2 –Flowchart for Estimating DLC

FREQUENCY RESPONSE MODEL

Frequency response model is an input/output linear model with the applied force being the input and displacement being the output. For a given frequency, ω, the input and output are related according to:

$$U(\omega)=H(\omega).F(\omega) \quad \textbf{(4.1)}$$

where $U(\omega)$ is a vector of displacements at frequency ω, $F(\omega)$ is the vector of resulting forces at frequency ω and $H(\omega)$ is called the frequency response function (FRF) or transfer function. The FRF is a matrix whose elements are related to the masses, spring constants and damping characteristic of the suspension system. Since the goal is to obtain the forces from known displacements, Equation 4.1 can be rearranged to:

$$F(\omega)=H(\omega)^{*}.U(\omega).\ H(\omega)^{T} \quad \textbf{(4.2)}$$

where symbols * and ^{T} signify the complex conjugate and the transpose of matrix H(ω).

For the problem at hand where the displacement and forces at multiple frequencies are known, Equation 4.2 can be generalized to (from Cebon, 1999):

$$[S_F(\omega)]= [H\ (\omega)]^{*}\ [S_u(\omega)]\ [H\ (\omega)]^{T} \quad \textbf{(4.3)}$$

where $S_F(\omega)$ is a matrix of the spectral densities of tire forces, $S_u(\omega)$ is a matrix of road profile displacement spectral densities. Element H(i,j) of the matrix $H(\omega)$ is the dynamic force generated by tire i due to a unit harmonic displacement input at tire j.

ESTABLISHING ROAD PROFILE DISPLACEMENT SPECTRAL DENSITY, $S_U(\Omega)$

The process of calculation of S_u(k), where k was the wavenumber, was discussed in detail in Chapter 3 (see Equation 3.1). S_u(k) can be readily converted to $S_u(\omega)$ by simply dividing S_u(k) by $2\pi V$, where V is the vehicle speed. As an example, the $S_u(\omega)$ associated with the S_u(k) in Figure 3.3 is shown in Figure 4.3 for a vehicle speed of 80 km/hr.

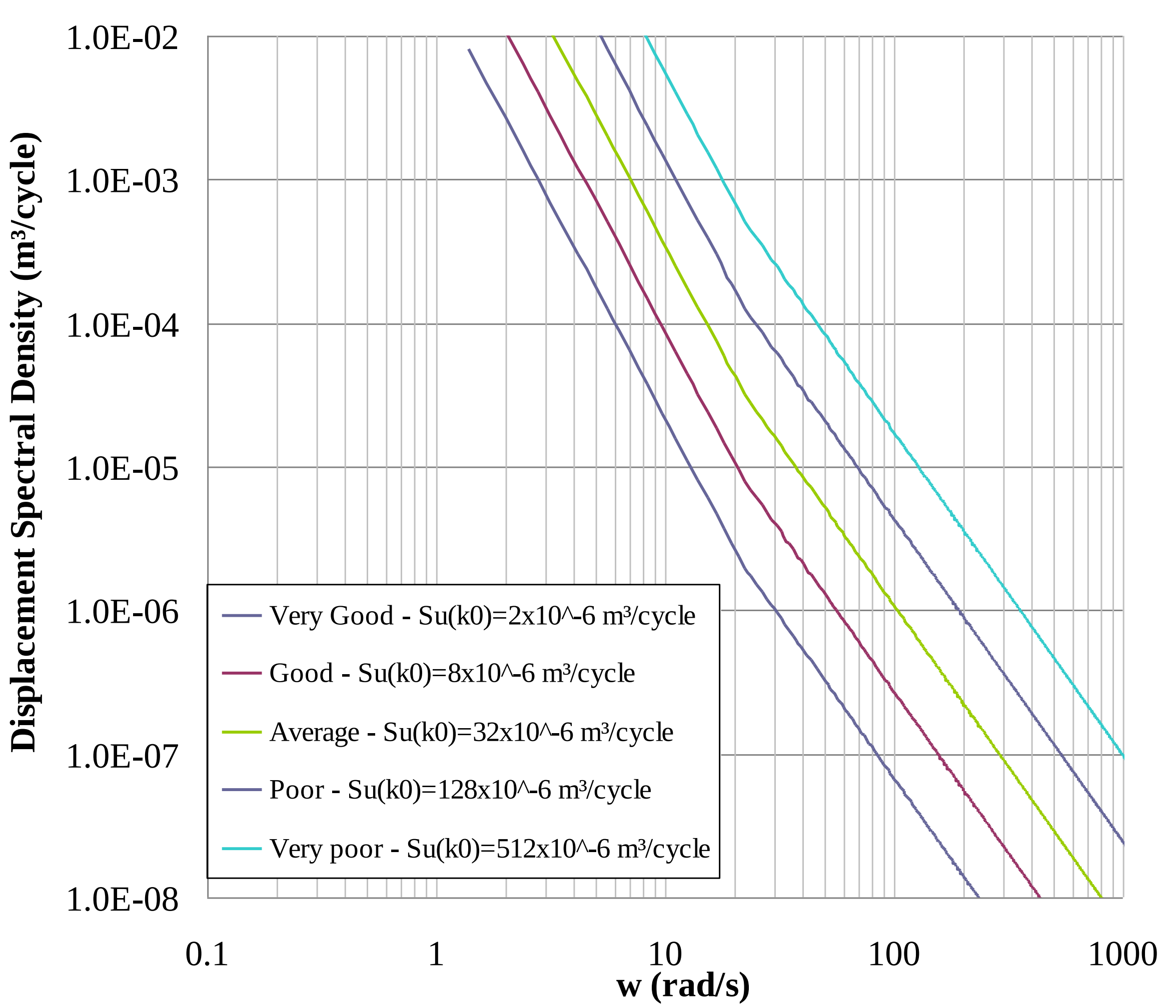

Figure 4.3 – Displacement PSD vs. Angular Frequency at Speed of 80 km/m

ESTABLISHING TRANSFER FUNCTION MATRIX $H(\Omega)$

Transfer matrix [H (ω)] is related to response of the system. If a road roughness displacement spectral density is assumed as $u(t) = \bar{u}e^{i\omega t}$, the vector of generalized force follows $Q(t) = \bar{Q}e^{i\omega t}$ (Cebon, 1999), where parameter $\bar{Q}$ can be obtained from:

$$\bar{Q} = [D][R]\bar{u} \quad \textbf{(4.4)}$$

with [R] = [diag(k_t+iωc_t)] and [D] = linear transformation matrix, and k_t and c_t are the spring ratio and damping coefficient of the tire. Linear transformation matrix, which is based on geometry of the model, describes how much force applied is transferred to each wheel.

Generally, the equation of motion for a linear vehicle model can be written in matrix form as follows:

$$[M]\ddot{q}+[C]\dot{q}+[K]q=Q \tag{4.5}$$

where [M] is the mass matrix, [C] is the damping matrix, and [K] is the stiffness matrix. Combining Equations 4.4 and 4.5, one obtains:

$$[B]\overline{q}=[D][R]\overline{u} \tag{4.6}$$

where

$$[B]=-\omega^2[M]+i\omega[C]+[K] \tag{4.7}$$

The vector of dynamic tire amplitude $\overline{F}_t$ is given by

$$\overline{F}_t=[R]([D]^T q-\overline{u}) \tag{4.8}$$

Substitution Equations 4.6 and 4.7 into Equation 4.8 one obtains:

$$\overline{F}_t=[H(\omega)]\overline{u} \tag{4.9}$$

where

$$[H(\omega)]=[R]([D]^T[B]^{-1}[D][R]-[I]) \tag{4.10}$$

For n tires, matrices [R] and [D] can be defined as:

$$R_{n\times n}=\begin{bmatrix} k_{t_1}+i\omega c_{t_1} & 0 & \cdots & 0 \\ 0 & k_{t2}+i\omega c_{t_2} & 0 & \vdots \\ \vdots & 0 & \ddots & 0 \\ 0 & \cdots & 0 & k_{tn}+i\omega c_{t_n} \end{bmatrix} \tag{4.11}$$

$$D_{n+2\times n}=\begin{bmatrix} 0 & 0 & 0 & \cdots & 0 \\ 0 & 0 & 0 & \cdots & 0 \\ 1 & 0 & 0 & \cdots & 0 \\ 0 & 1 & 0 & \cdots & 0 \\ 0 & 0 & 1 & \cdots & 0 \\ 0 & 0 & 0 & \ddots & 0 \\ 0 & 0 & 0 & \cdots & 1 \end{bmatrix} \quad \text{linear transformation matrix} \tag{4.12}$$

Matrix [B], as defined in Equation 4.7, contains three matrices. Matrix [M] can be shown as:

$$M_{n+2\times n+2} = \begin{bmatrix} m_s & 0 & 0 & 0 & 0 \\ 0 & I_u & 0 & 0 & 0 \\ 0 & 0 & m_{u_1} & 0 & 0 \\ 0 & 0 & 0 & \ddots & 0 \\ 0 & 0 & 0 & 0 & m_{u_n} \end{bmatrix} \quad \text{mass matrix} \qquad \textbf{(4.13)}$$

Matrix [C] is presented in Equation 4.14. Matrix [K] is the same as C matrix; except that c_s and c_t are replaced by k_s and k_t.

As an example, a simple model that represents one axle of a truck with a single wheel (a.k.a. quarter car) is shown in Figure 4.4. The quarter car can be modeled as a two-degree of freedom system where the top part represents forces applied from body to the axle and the bottom part represents tire connecting to the pavement.

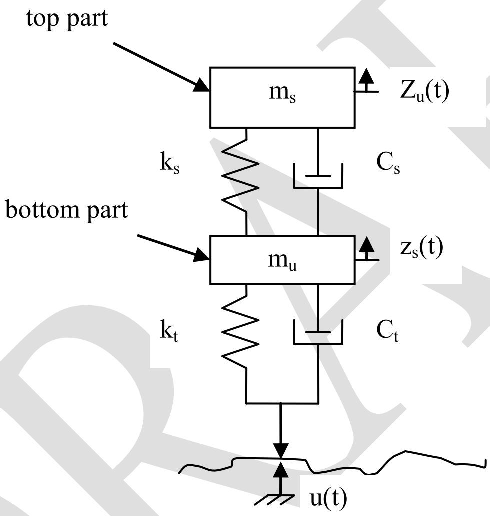

Figure 4.4 – Quarter Car Model

The top mass, denoted as m_s, is the sprung mass which represents the portion of the total weight applied to this suspension system. The second mass, denoted as m_u, is the so-called unsprung mass which consists of the weight of the wheel bearings, tire, axle and a portion of spring and shock absorber. The spring constant and damping coefficient of the suspension system are defined as k_s and C_s. Since every tire is designed to work as a spring-damper system, parameters, k_t and C_t, define the spring constant and damping coefficient of a tire.

$$C_{n+2\times n+2}=\begin{bmatrix}
\sum_{i=1}^{n} c_{s_i} & \sum_{i=1}^{\frac{n-1}{2}}(-c_{s_i}+c_{s_{n+1-i}})(n-2i+1)a & -c_{s_1} & -c_{s_2} & \cdots & -c_{s_{\frac{n+1}{2}}} & -c_{s_{\frac{n+3}{2}}} & \cdots & -c_{s_n} \\
\sum_{i=1}^{\frac{n-1}{2}}(-c_{s_i}+c_{s_{n+1-i}})(n-2i+1)a & \sum_{i=1}^{\frac{n-1}{2}}(c_{s_i}+c_{s_{n+1-i}})a^2(n-2i+1)^2 & c_{s_1}(n-1)a & c_{s_2}(n-3)a & \cdots & 0 & -c_{s_{\frac{n+3}{2}}}\times 2a & \cdots & -c_{s_n}(n-1)a \\
-c_{s_1} & c_{s_1}(n-1)a & c_{s_1}+c_{t_1} & 0 & \cdots & 0 & 0 & \cdots & 0 \\
-c_{s_2} & c_{s_2}(n-3)a & 0 & c_{s_2}+c_{t_2} & 0 & \cdots & 0 & \cdots & 0 \\
\vdots & \vdots & \vdots & 0 & \ddots & \vdots & \vdots & \cdots & \vdots \\
-c_{s_{\frac{n+1}{2}}} & 0 & 0 & \vdots & 0 & c_{s_{\frac{n+1}{2}}}+c_{t_{\frac{n+1}{2}}} & 0 & \cdots & 0 \\
-c_{s_{\frac{n+3}{2}}} & -c_{s_{\frac{n+3}{2}}}2a & 0 & 0 & 0 & 0 & c_{s_{\frac{n+3}{2}}}+c_{t_{\frac{n+3}{2}}} & 0 & \vdots \\
\vdots & \vdots & \vdots & \vdots & \vdots & \vdots & \vdots & \ddots & 0 \\
-c_{s_n} & -c_{s_n}(n-1)a & 0 & \cdots & 0 & \cdots & 0 & \cdots & c_{s_n}+c_{t_n}
\end{bmatrix} \quad \textbf{(4.14a)}$$

$$C_{n+2\times n+2}=\begin{bmatrix}
\sum_{i=1}^{n} c_{s_i} & \sum_{i=1}^{\frac{n}{2}}(-c_{s_i}+c_{s_{n+1-i}})(n-2i+1)a & -c_{s_1} & -c_{s_2} & \cdots & -c_{s_{\frac{n}{2}}} & -c_{s_{\frac{n}{2}+1}} & \cdots & -c_{s_n} \\
\sum_{i=1}^{\frac{n}{2}}(-c_{s_i}+c_{s_{n+1-i}})(n-2i+1)a & \sum_{i=1}^{\frac{n}{2}}(c_{s_i}+c_{s_{n+1-i}})(n-2i+1)^2a^2 & c_{s_1}(n-1)a & c_{s2}(n-3)a & \cdots & c_{s_{\frac{n}{2}}}a & -c_{s_{\frac{n}{2}+1}}a & \cdots & -c_{s_n}(n-1)a \\
-c_{s_1} & c_{s_1}a(n-1) & c_{s_1}+c_{t_1} & 0 & \cdots & 0 & 0 & \cdots & 0 \\
-c_{s_2} & c_{s2}a(n-3) & 0 & c_{s_2}+c_{t_2} & 0 & \cdots & 0 & \cdots & 0 \\
\vdots & \vdots & \vdots & 0 & \ddots & \vdots & \vdots & \cdots & \vdots \\
-c_{s_{\frac{n}{2}}} & c_{s_{\frac{n}{2}}}a & 0 & \vdots & 0 & c_{s_{\frac{n}{2}}}+c_{t_{\frac{n}{2}}} & 0 & \cdots & 0 \\
-c_{s_{\frac{n}{2}+1}} & -c_{s_{\frac{n}{2}+1}}a & 0 & 0 & 0 & 0 & c_{s_{\frac{n}{2}+1}}+c_{t_{\frac{n}{2}+1}} & 0 & \vdots \\
\vdots & \vdots & \vdots & \vdots & \vdots & \vdots & \vdots & \ddots & 0 \\
-c_{s_n} & -c_{s_n}(n-1)a & 0 & \cdots & 0 & \cdots & 0 & \cdots & c_{s_n}+c_{t_n}
\end{bmatrix} \quad \textbf{(4.14b)}$$

Each mass in the model is assumed to provide one degree of freedom; therefore the system is considered as a two-degree of freedom system. The linear transformation matrix [D] for this model has two elements as shown in linear transformation matrix. The first row describes the portion of the sprung mass applied to the tire. For a linear model, this element is 0. As such, the tire has to carry the unsprung mass load in totality, meaning that the second element is 1.

$$D = \begin{bmatrix} 0 \\ 1 \end{bmatrix} \qquad \text{linear transformation matrix} \qquad \textbf{(4.15)}$$

For this model, the mass, stiffness and damping matrices are defined as:

$$M = \begin{bmatrix} m_s & 0 \\ 0 & m_u \end{bmatrix} \qquad \text{mass matrix} \qquad \textbf{(4.16)}$$

$$C = \begin{bmatrix} c_s & -c_s \\ -c_s & c_s + c_t \end{bmatrix} \qquad \text{damping matrix} \qquad \textbf{(4.17)}$$

$$K = \begin{bmatrix} k_s & -k_s \\ -k_s & k_s + k_t \end{bmatrix} \qquad \text{stiffness matrix} \qquad \textbf{(4.18)}$$

$$R = \begin{bmatrix} k_t + i\omega c_t & 0 \\ 0 & k_t + i\omega c_t \end{bmatrix} \text{ R matrix} \qquad \textbf{(4.19)}$$

Substituting these matrices in Equation 4.10, the transfer function matrix [H (ω)] shown in Figure 4.5 is obtained for the quarter car model.

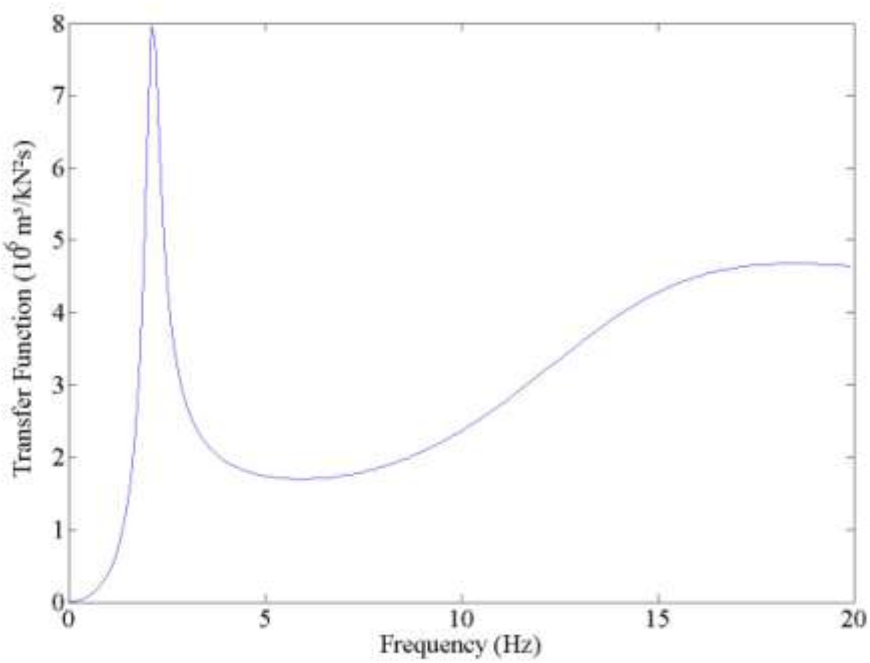

Figure 4.5 – Transfer Function of the Quarter Car Model

Figure 4.6 exhibits the displacement PSD for a $S_u(k_0)$=13x10^{-6} m³/cycle corresponding to an IRI of 2 mm/m.

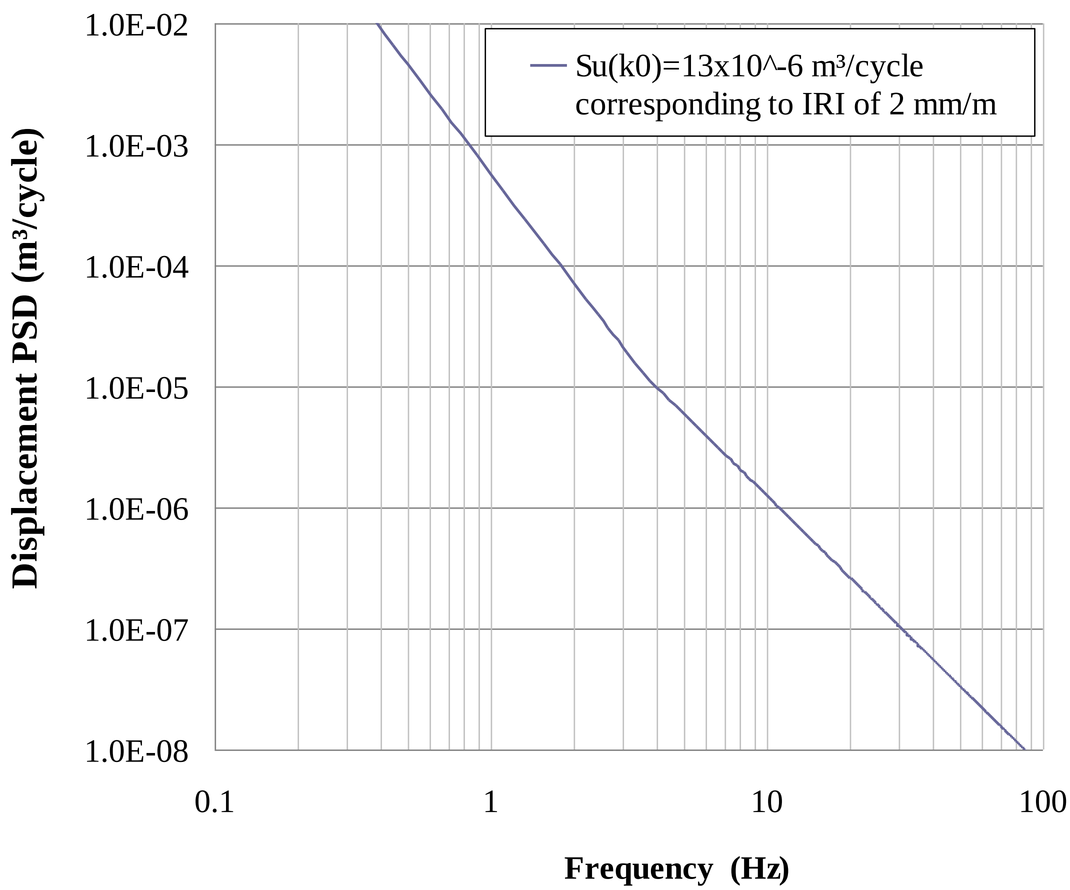

Figure 4.6 – Displacement PSD at Vehicle Speed of 80 km/h

Figure 4.7 demonstrates the force PSD as per Equation 4.3 by using the spectra shown in Figures 4.5 and 4.6. To obtain the DLC according to Equation 2.1 under the *j*th tire in the frequency domain, the following equation is utilized:

$$\sigma_j^2 = \int_0^\infty S_{F_j F_J}(\omega) d\omega \qquad \textbf{(4.20)}$$

The integral corresponds to the area under the curve in Figure 4.7. In the Matlab routine a numerical integration scheme is used for this purpose. After numerical integration, the DLC of this example is 0.15. Assuming that the dynamic load is normally distributed about the static load (see Figure 2.6), the Dynamic Impact Factor (DI) is estimated from:

$$DI=1+Z_r*DLC \qquad \textbf{(4.21)}$$

where Z_r is the reliability index. For a reliability of 95%, Z_r is 2.
For our example, the DI from Equation 4.21 is 1.30. This indicates that the modified static load to be used in IntPave should be increased by 30% to account for the dynamic amplification factor.

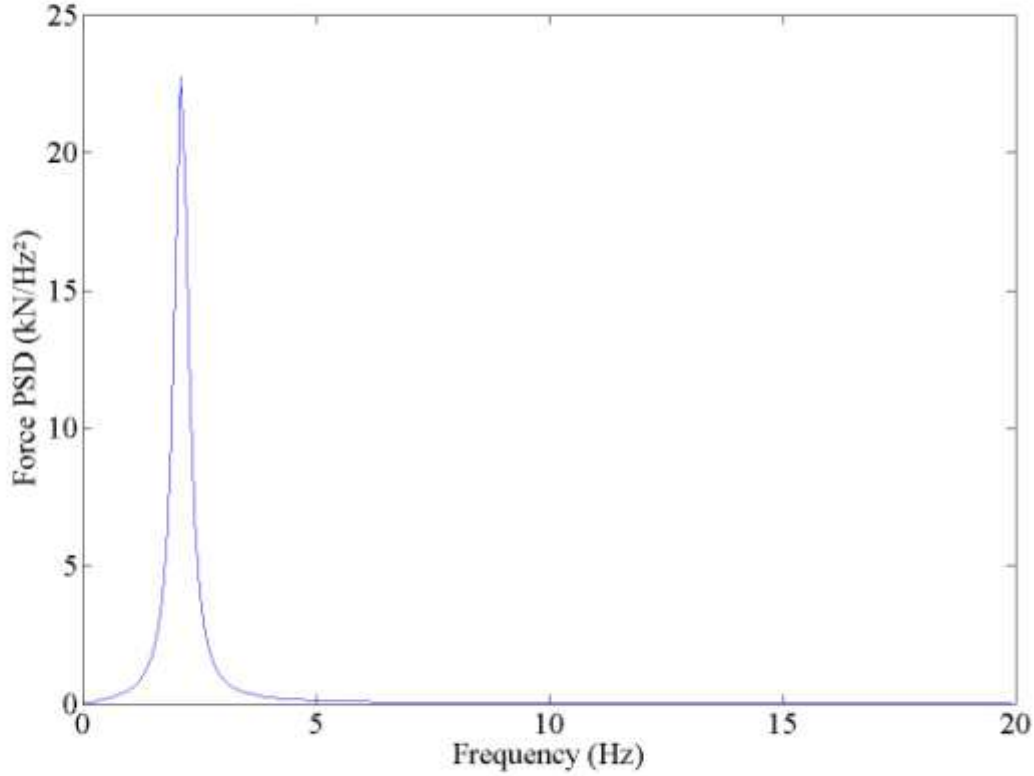

Figure 4.7 – Force PSD under the Wheel at Vehicle Speed of 80 km/h

The detailed information about several types of suspensions is included in Appendices A, B and C. Appendix A focuses on a single tandem leaf spring. Appendix B describes a single tridem leaf spring. Finally, Appendix C contains relevant information about walking beam. The modeling for the walking beam suspension is slightly different that the other two suspension since in the walking beam suspension the unsprung mass rotates. Matrices related to the walking beam model are included in Appendix C as well.

CHAPTER 5: PARAMETRIC STUDY

This chapter contains a parametric study on the impact of different components of each suspension type on the additional load applied to the pavement. The parameters considered for each suspension type are the following:

- stiffness and damping coefficient of suspension system and tire,
- sprung mass and unsprung mass
- pitch inertia, and
- roughness of the road

QUARTER CAR

The baseline parameters considered for this suspension system are shown in Table 5.1. The baseline IRI was assumed to be 2 mm/m corresponding to a road with a reasonably good smoothness. The Dynamic impact factors (DI's) associated with different speeds for the control condition is highlighted in Table 5.2. As the vehicle speed increases, the DI increases as well.

Table 5.1- Baseline Quarter Car Leaf Spring Properties

m_s	sprung mass	7100 kg
m_u	unsprung mass	600 kg
c_s	suspension damping	40 kN·s/m
c_t	tire damping	4 kN·s/m
k_s	suspension stiffness	2 MN/m
k_t	tire stiffness	3.5 MN/m
IRI	road roughness	2 mm/m

The impact of varying the suspension stiffness from 0.5 MN/m to 8 MN/m is also reflected in Table 5.2 and Figure 5.1. As the stiffness increases for a given speed the DI also increases. For a stiffness of 8 MN/m and a speed of 137 km/hr the load applied to the pavement is potentially about 2.25 times the static load. This pattern is reasonable since stiffer springs deflect less and reduce the energy absorbed by the suspension.

Similar exercise but for the tire stiffness is shown in Figure 5.2. The tire stiffness has a minimal effect on the DI and the suspension stiffness dominates the response.

Table 5.2- Impact of Suspension Stiffness on Load Applied to Pavement

Suspension Stiffness, k_s MN/m	Dynamic Impact Factor for a Reliability of 95%				
	8 km/h	40 km/h	72 km/h	105 km /h	137 km/h
0.5	1.02	1.06	1.10	1.14	1.18
1	1.03	1.09	1.14	1.21	1.27
2 (Control)	1.05	1.14	1.24	1.34	1.44
4	1.10	1.26	1.41	1.59	1.77
8	1.16	1.44	1.67	1.96	2.25

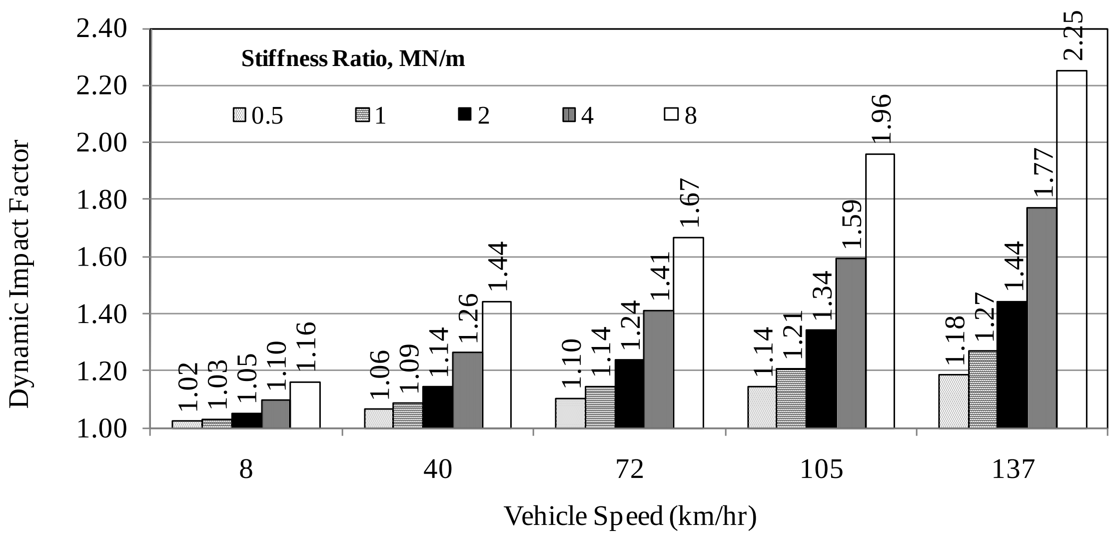

Figure 5.1 – Impact of Suspension Stiffness on Dynamic Impact Factor for Quarter Car

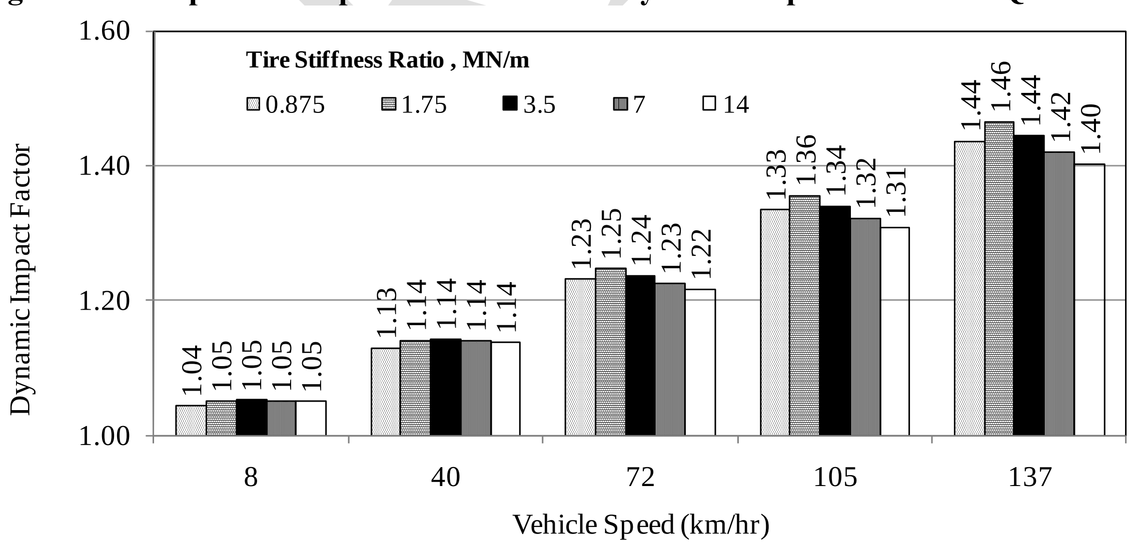

Figure 5.2 – Impact of Tire Stiffness on Dynamic Impact Factor for Quarter Car

The impact of the suspension damping characteristics on DI is shown in Figure 5.3. The suspension damping coefficient significantly impacts the DI. As the vehicular speed increases the impact of the suspension damping coefficient becomes much more pronounced. However, as shown in Appendix D, the damping coefficient of the tire has a minimal effect on the DI.

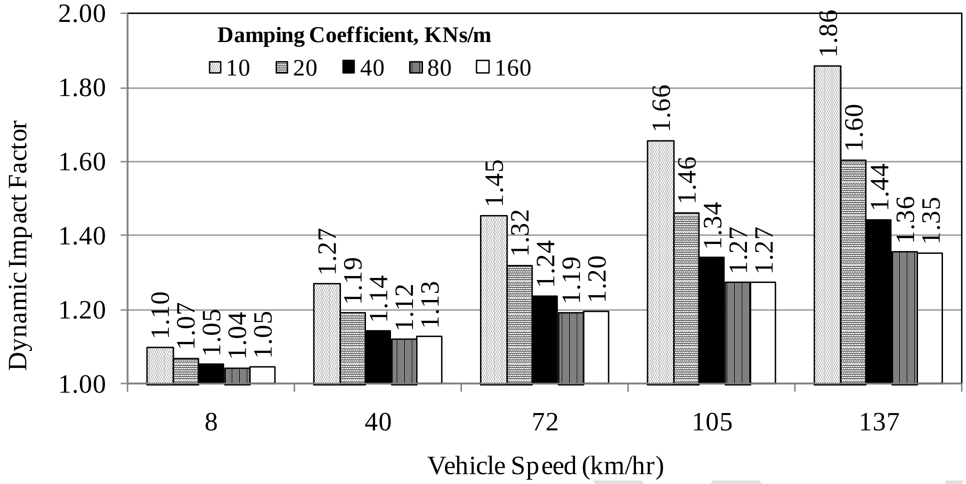

Figure 5.3 – Impact of Suspension Damping Coefficient on Dynamic Impact Factor for Quarter Car

The impact of the load applied to the suspension (from 20% under to 20% over legal limit) is shown in Figure 5.4. As the load increases, the DI slightly decreases. This pattern should not be interpreted as the overloading is beneficial in reducing the dynamic loads applied to the pavement since the decrease in DI is significantly less than the increase in the payload. This decrease is more pronounced at higher speeds. The reason for this pattern is in the fact that when the truck is overloaded, the suspension spring is compressed more under the static load and as such, less movement is transmitted to the tire. As reflected in Figure 5.5, the change in the unsprung mass has negligible impact on the DI.

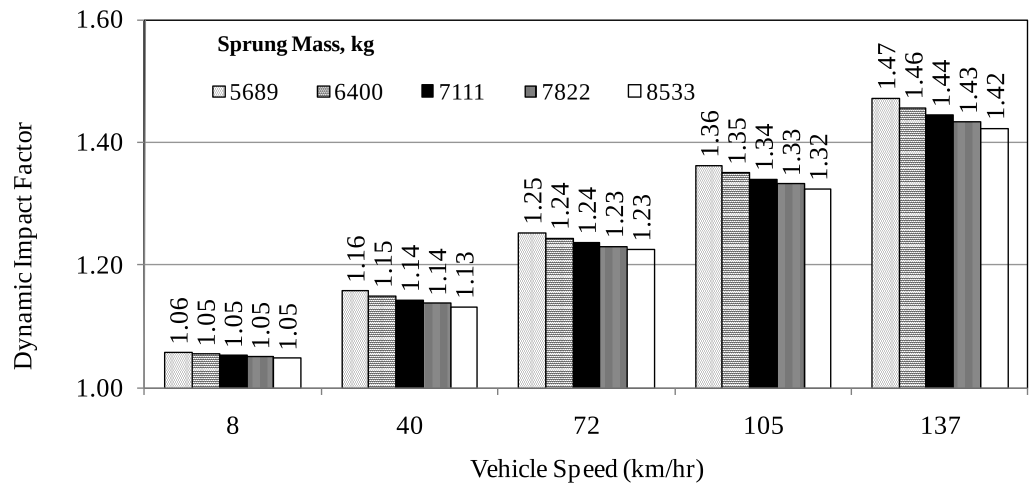

Figure 5.4 – Impact of Sprung Mass on DI for Quarter Car

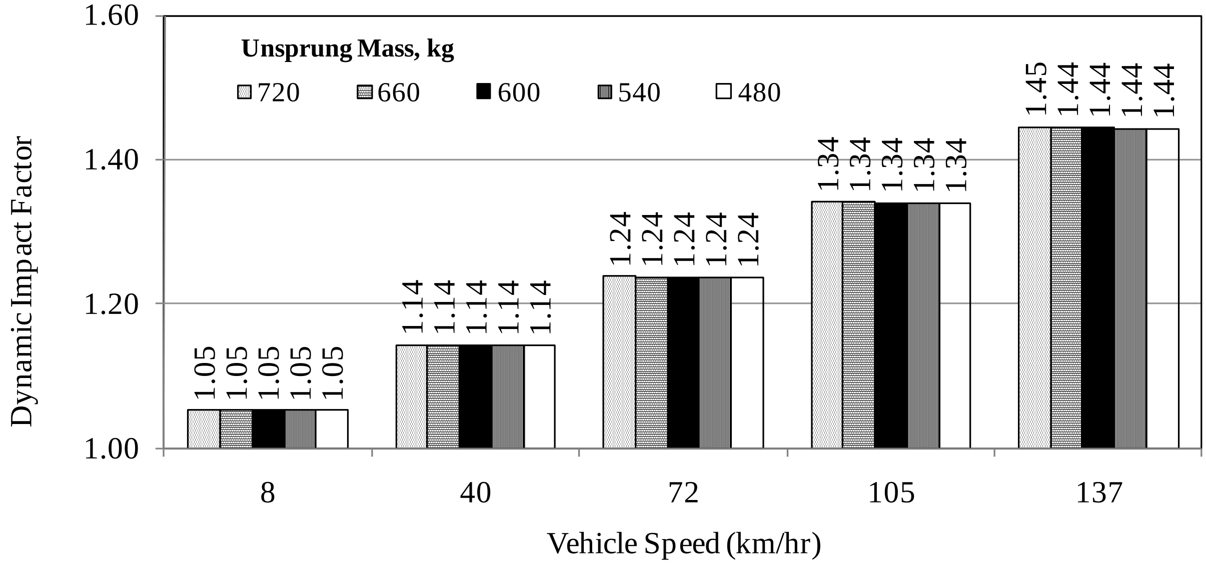

Figure 5.5 – Impact of Unsprung Mass on DI for Quarter Car

The IRI for the parametric studies shown above was maintained at 2 mm/m. The impact of the change in IRI on DI is shown in Figure 5.6. At low speeds (say 8 km/hr) the change in dynamic load is small as the IRI increases. However, as the speed increases, the DI is significantly impacted by the IRI.

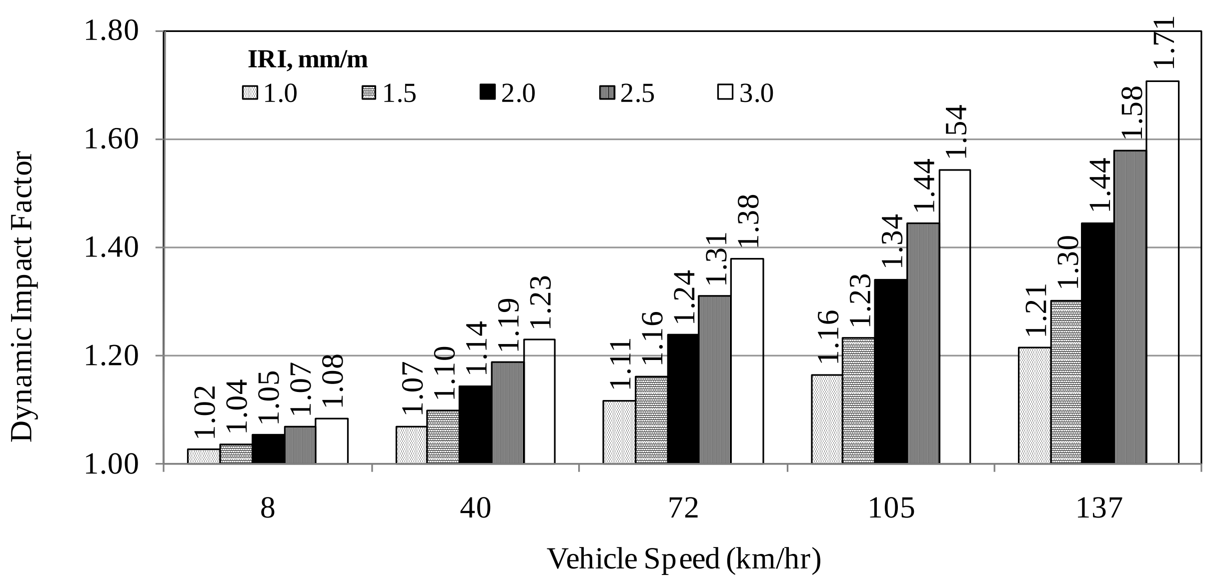

Figure 5.6- Impact of Pavement Roughness on DI for Quarter Car

SINGLE TANDEM LEAF SPRING

The baseline parameters considered for this suspension system are shown in Table 5.3. As shown in Figure 5.7 in solid black, again as the vehicle speed increases, the DI increases as well.

Table 5.3 –Specifications Assumed for Single Tandem Leaf Spring Baseline

m_s	sprung mass	6700 kg
$m_{u1}= m_{u2}$	unsprung mass	500 kg
I_s	pitch inertia	930 kg.m²
$c_{s1}=c_{s2}$	suspension damping	80 kN·s/m
$c_{t1}=c_{t2}$	tire damping	4 kN·s/m
$k_{s1}= k_{s2}$	suspension stiffness	4 MN/m
$k_{t1}= k_{t2}$	tire stiffness	3.5 MN/m
IRI	road roughness	2 mm/m

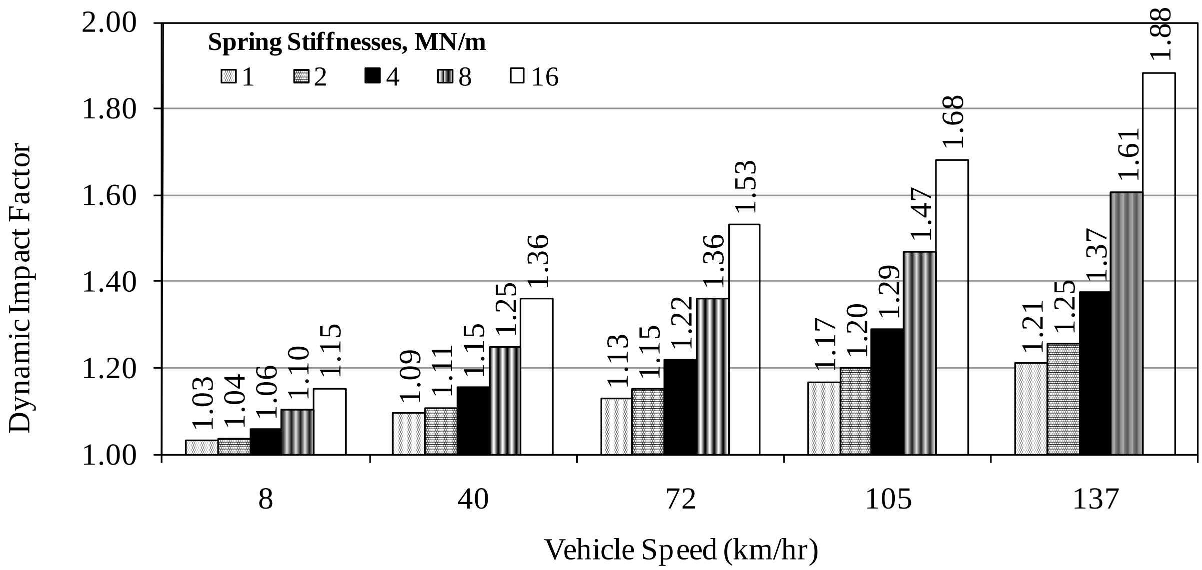

Figure 5.7 – Impact of Suspension Spring Stiffnesses on DI for Single Tandem Leaf Spring

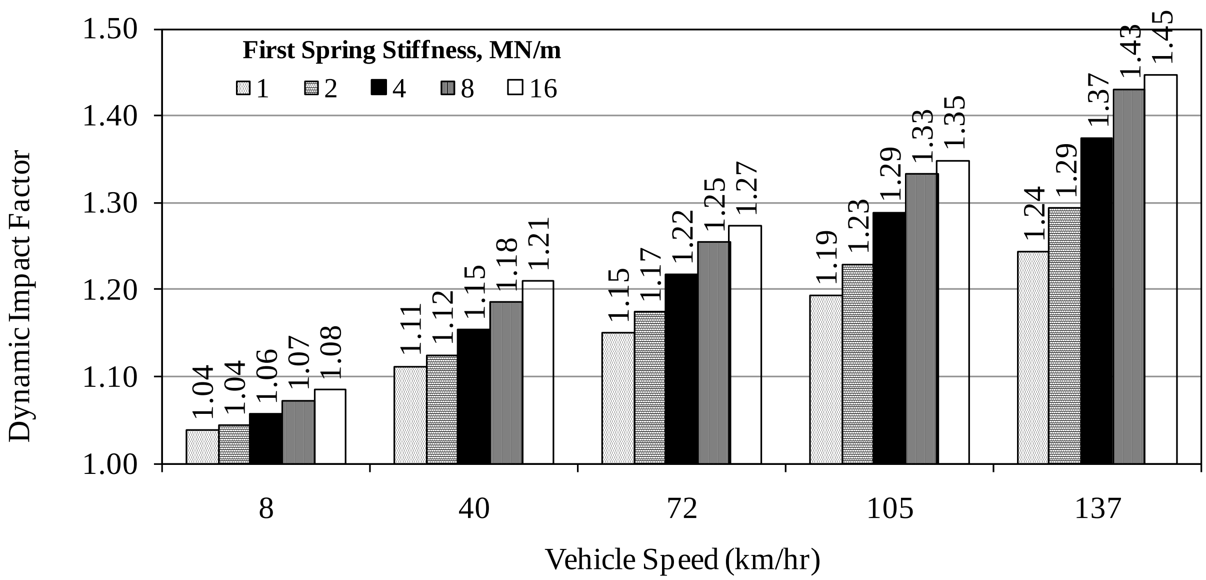

Figure 5.8 – Impact of Varying one Suspension Spring Stiffness on DI for Single Tandem Leaf Spring

The impacts of simultaneously varying the first and second suspension stiffnesses from 1 MN/m to 16 MN/m are reflected in Figures 5.7. As the stiffness increases for a given speed the DI also increases. For a stiffness of 16 MN/m and a speed of 137 km/hr the load applied to the pavement is about 1.88 times the static load. However, if only one suspension stiffness is varied while the second one is maintained at 4 MN/m the trend is slightly different as shown in Figure 5.8. In this case, the dynamic load is only 1.45 times the static load for a stiffness of 16 MN/m and a speed of 137 km/hr. As shown in Figure 5.9, the tire stiffness does not have much of an impact on DI.

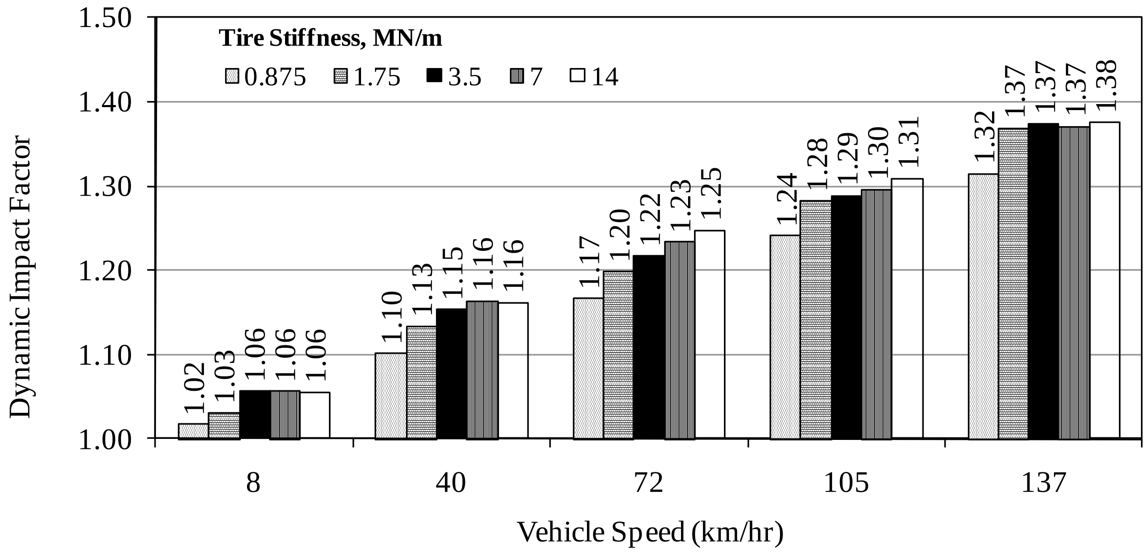

Figure 5.9 – Impact of the Tire Stiffness on DI for Single Tandem Leaf Spring

The impact of the suspension damping characteristics on DI are shown in Figure 5.10. The suspension damping coefficient significantly impacts the DI, especially as the vehicular speed increases

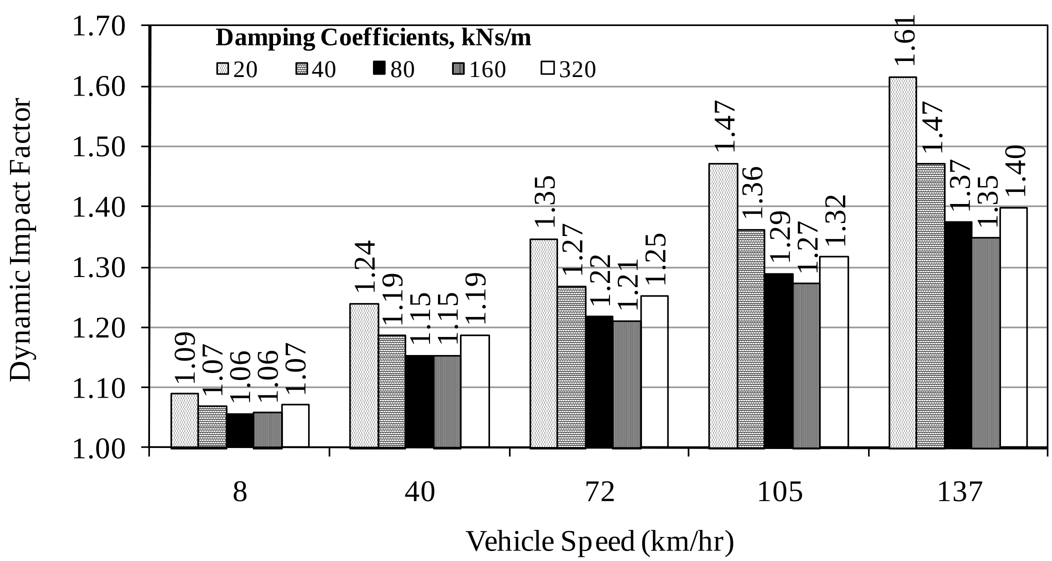

Figure 5.10 –Impact of Damping Coefficients on DI for Single Tandem Leaf Spring

At a given speed the DI decreases with the increase in the suspension damping coefficient. However, for a very high damping coefficient (320 kN.s/m) the DI slightly increases. As shown in Appendix E, the damping coefficient of the tire has a minimal effect on the DI.

The impact of the load applied to the suspension (from 20% under to 20% over legal limit) is shown in Figure 5.11. Similar to the previous case, as the load increases, the DI slightly decreases. This decrease is more pronounced at higher speeds. However, as shown in Appendix E, the damping coefficient of the tire has negligible effect on the DI.

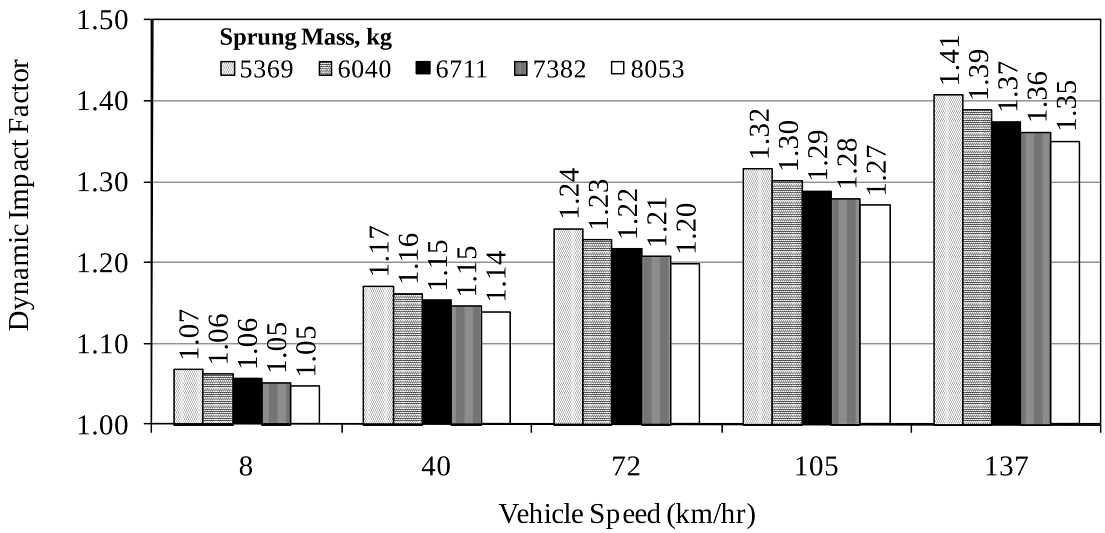

Figure 5.11 –Impact of Sprung Mass on DI for Single Tandem Leaf Spring

The impact of the pitch inertia characteristics on DI is shown in Figure 5.12. The pitch inertia impacts the DI. As the vehicular speed increases the impact of the pitch inertia significantly increases.

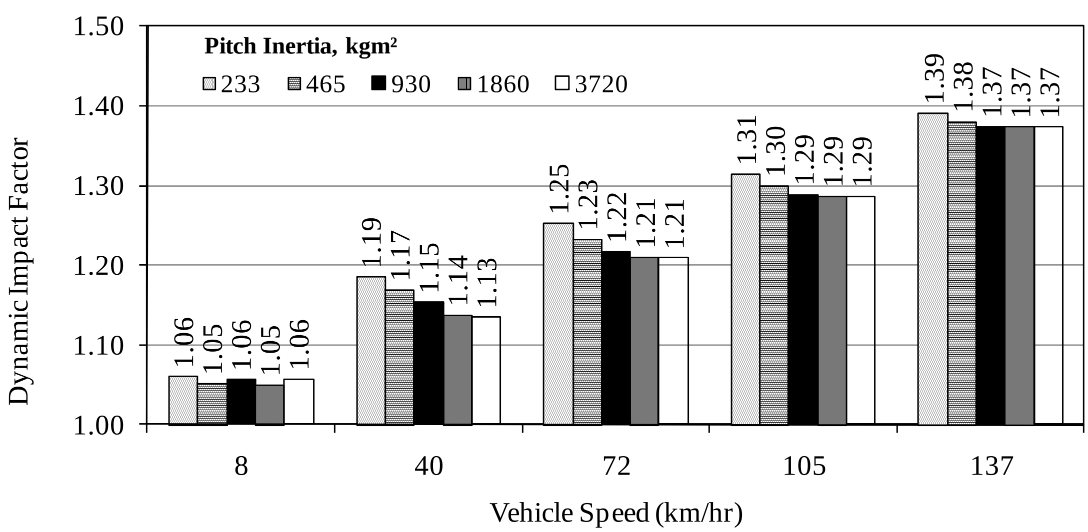

Figure 5.12 –Impact of Pitch Inertia on DI for Single Tandem Leaf Spring

Finally, the impact of the change in IRI on DI is shown in Figure 5.13. At low speeds the change in dynamic load is small as the IRI increases. However, as the speed increases, the DI is significantly impacted by the IRI.

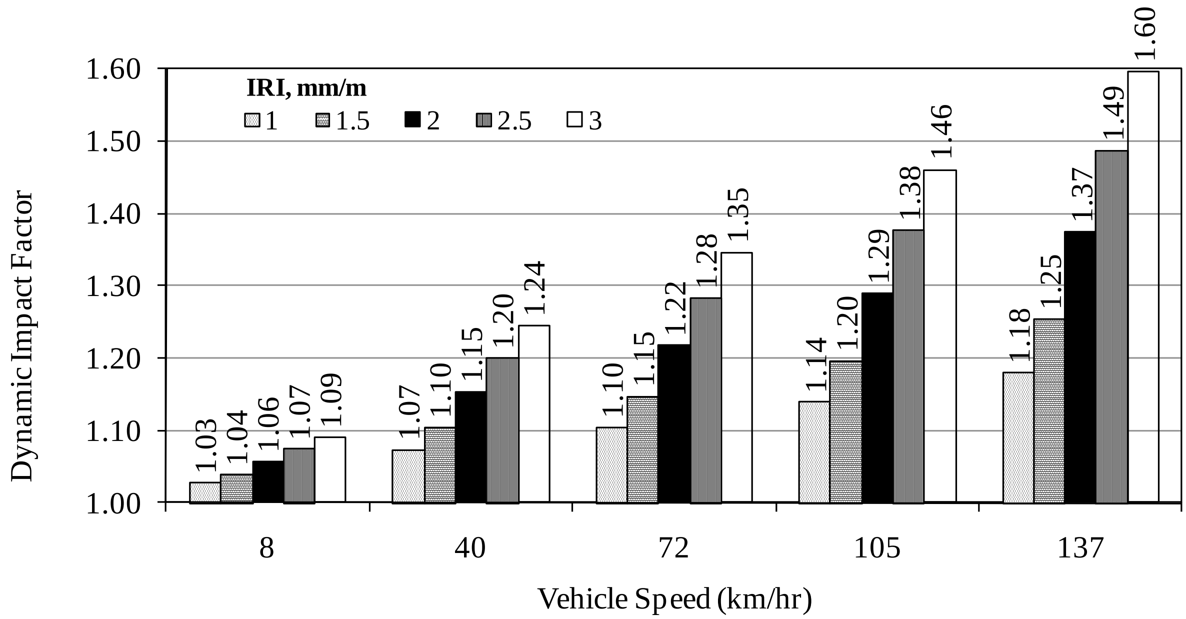

Figure 5.13 –Impact of IRI on DI for Single Tandem Leaf Spring

SINGLE TRIDEM LEAF SPRING

The baseline parameters considered for this suspension system are shown in Table 5.4. The results from this parametric study are documented in Appendix G. As shown in Figure 5.14, the impact of varying the suspension stiffness is similar to the other two cases. As such, only the parameters that exhibit different trends from the previous two cases are discussed.

The tire stiffness impacts the DI differently as compared to the other two cases as shown in Figure 5.15. In this case, the tire stiffness plays a major role on the DI especially at higher speeds because the suspension system has two resonant frequencies between 0 through 20Hz. A critical tire stiffness of 7 MN/m is also observed where the DI's are maximum at all speeds.

The impact of the tire damping characteristics on DI is also shown in Figure 5.16 because, unlike the other cases, it impacts the DI significantly at higher speeds. Like tire stiffness impact, two frequency resonant appears between 0 to 20Hz.

Table 5.4 –Specifications Assumed for Single Leaf Spring Baseline

m_s	sprung mass	6200 kg
$m_{u1}= m_{u2}= m_{u2}$	unsprung mass	500 kg
I_s	pitch inertia	930 kg.m²
$c_{s1}=c_{s2}=c_{s2}$	suspension damping	80 kN·s/m
$c_{t1}=c_{t2}=c_{t2}$	tire damping	4 kN·s/m
$k_{s1}= k_{s2}= k_{s2}$	suspension stiffness	4 MN/m
$k_{t1}= k_{t2}= k_{t2}$	tire stiffness	3.5 MN/m
IRI	road roughness	2 mm/m

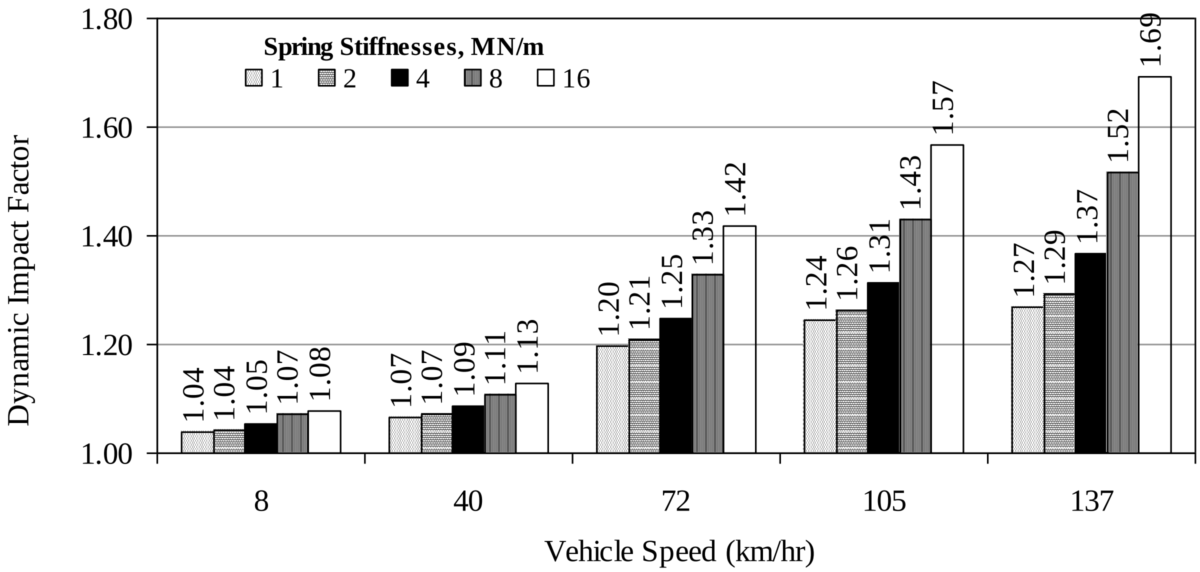

Figure 5.14 – Impact of the Suspension Spring Stiffnesses on DI for Single Tridem Leaf Spring

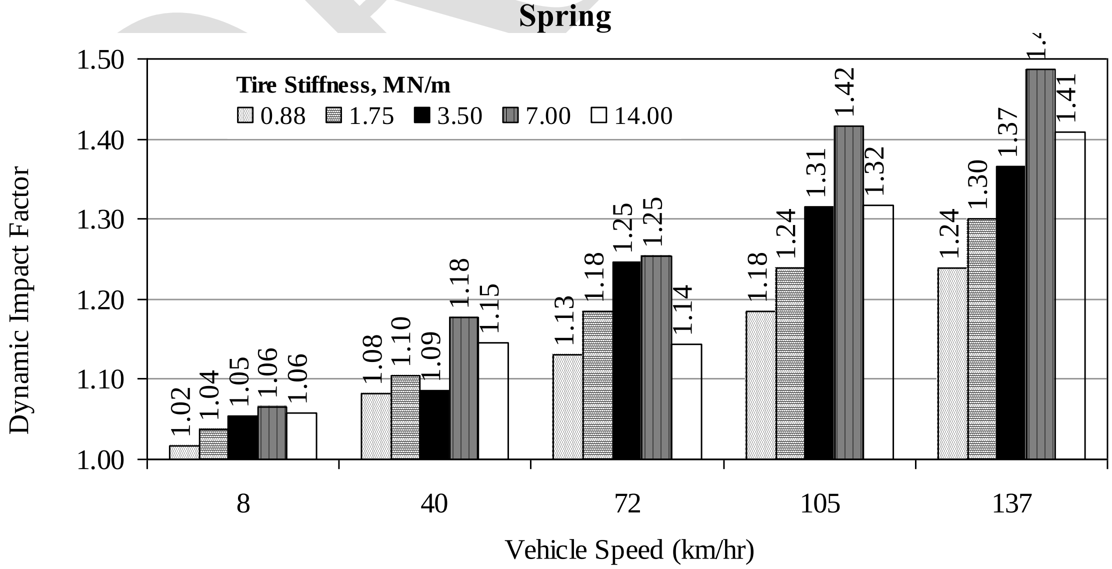

Figure 5.15 – Impact of the Tire Stiffness on DI for Single Tridem Leaf Spring

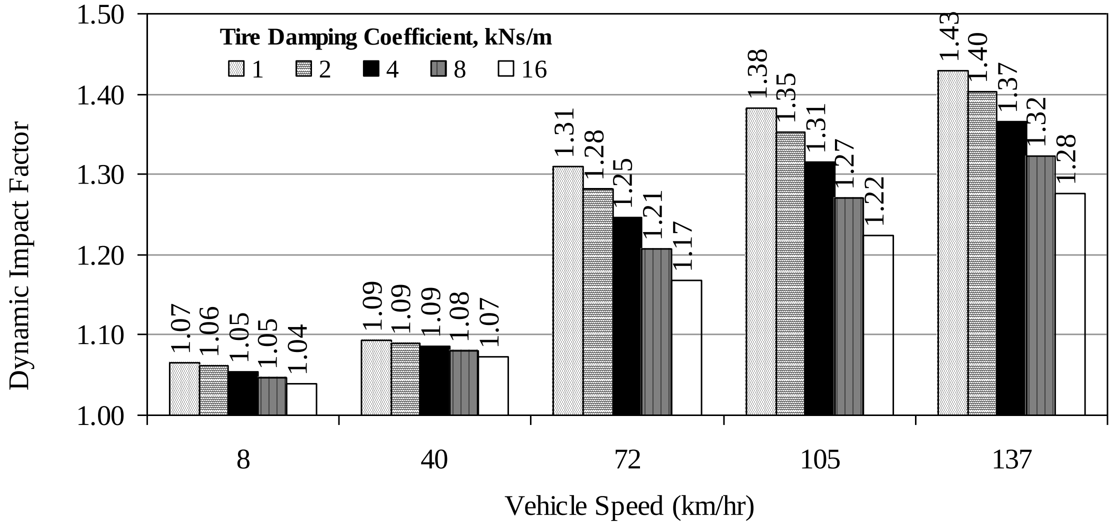

Figure 5.16 –Impact of Tire Damping Coefficient on DI for Single Tridem Leaf Spring

Also, the impact of the pitch inertia characteristics on DI is significantly different than the case of the tandem leaf spring as shown in Figure 5.17. In this case, the pitch inertia plays a major role on the magnitude of the DI at higher speeds, which was not apparent in the previous case.

Overall, the impact of the IRI for the control case is similar to the other cases as shown in Figure 5.18. The IRI for the parametric studies shown above was maintained at 2 mm/m. The impact of the change in IRI on DI is shown in Figure 5.18.

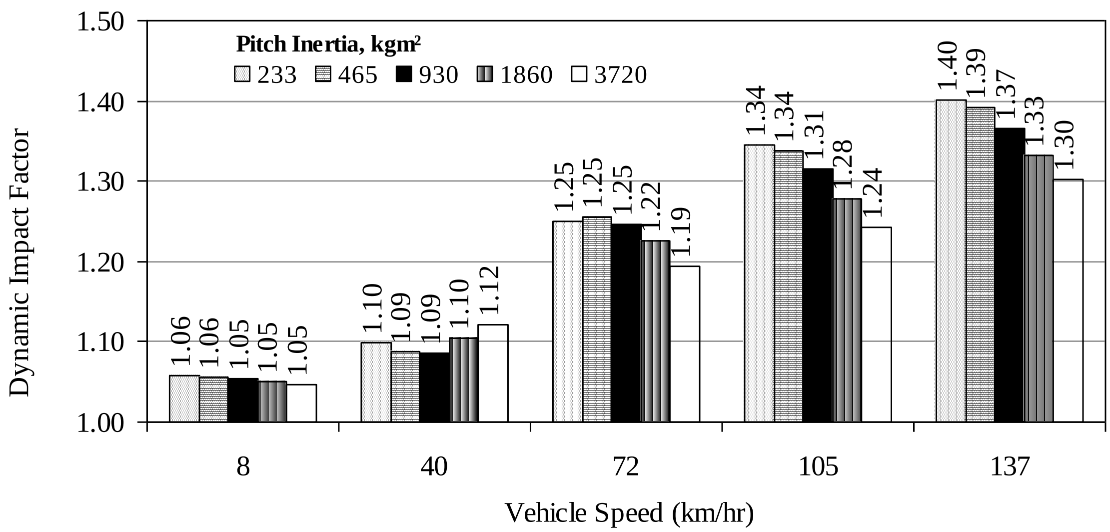

Figure 5.17 –Impact of Pitch Inertia on DI for Single Tridem Leaf Spring

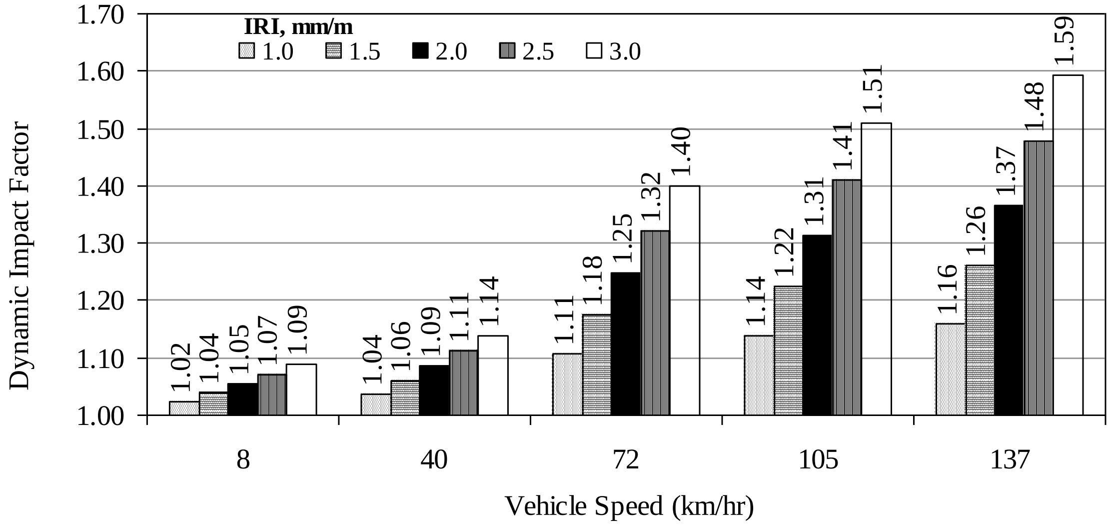

Figure 5.18 –Impact of IRI on DI for Single Tridem Leaf Spring

WALKING BEAM

The baseline parameters considered for this suspension system are shown in Table 5.5. The detailed results are provided in Appendix G. The impacts of the suspension stiffness (Figure 5.19) and tire stiffness (Figure 5.20) on DI are more pronounced that the other cases. Also some differences in the impact of the pitch inertia (Figure 5.21) and the IRI (Figure 5.22) are observed.

Table 5.5- Baseline Walking Beam Properties

m_s	sprung mass	6600 kg
m_u	unsprung mass	1100 kg
I_u	pitch inertia	930 kgm²
c_s	suspension damping	80 kN·s/m
c_t	tire damping	4 kN·s/m
k_s	suspension stiffness	4 MN/m
k_t	tire stiffness	3.5 MN/m
IRI	road roughness	2 mm/m

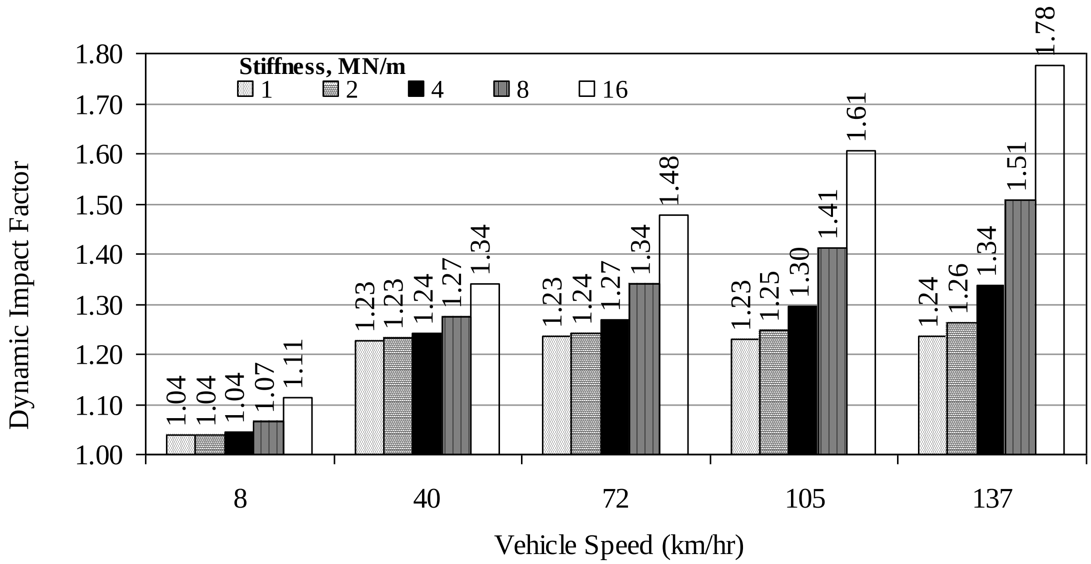

Figure 5.19 – Impact of Suspension Stiffness on Dynamic Impact Factor for Walking Beam

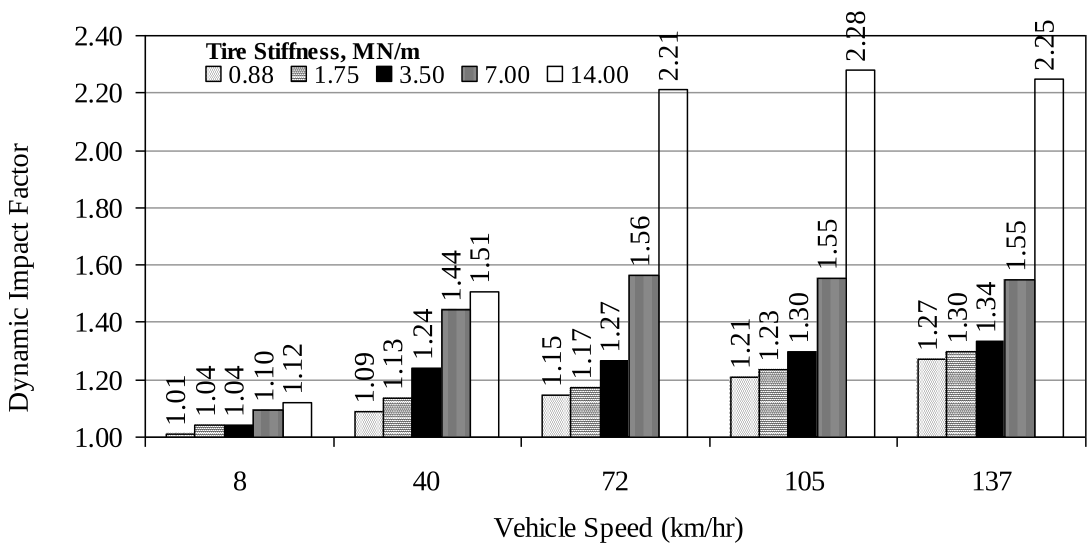

Figure 5.20 – Impact of Tire Stiffness on Dynamic Impact Factor for Walking Beam

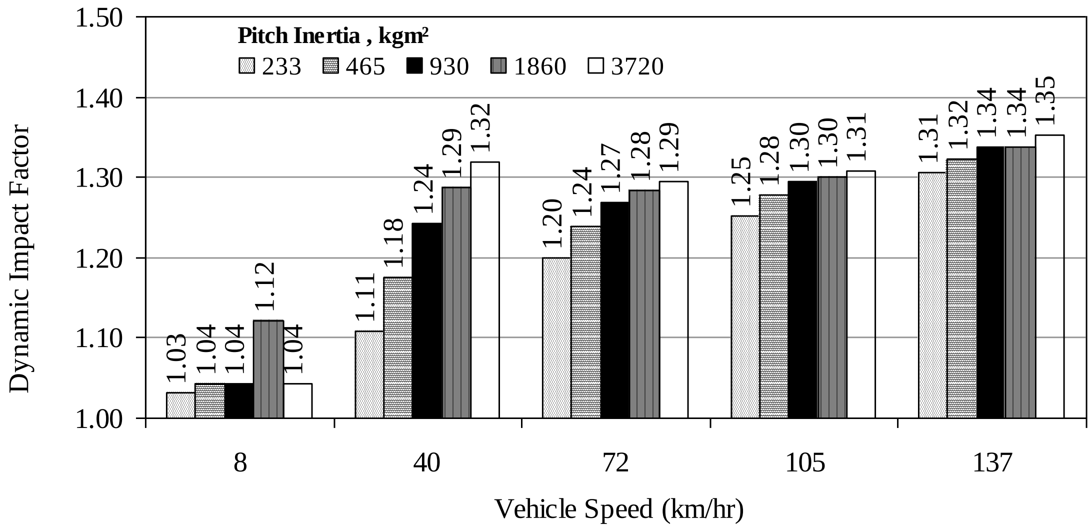

Figure 5.21 – Impact of Pitch Inertia on DI for Walking Beam

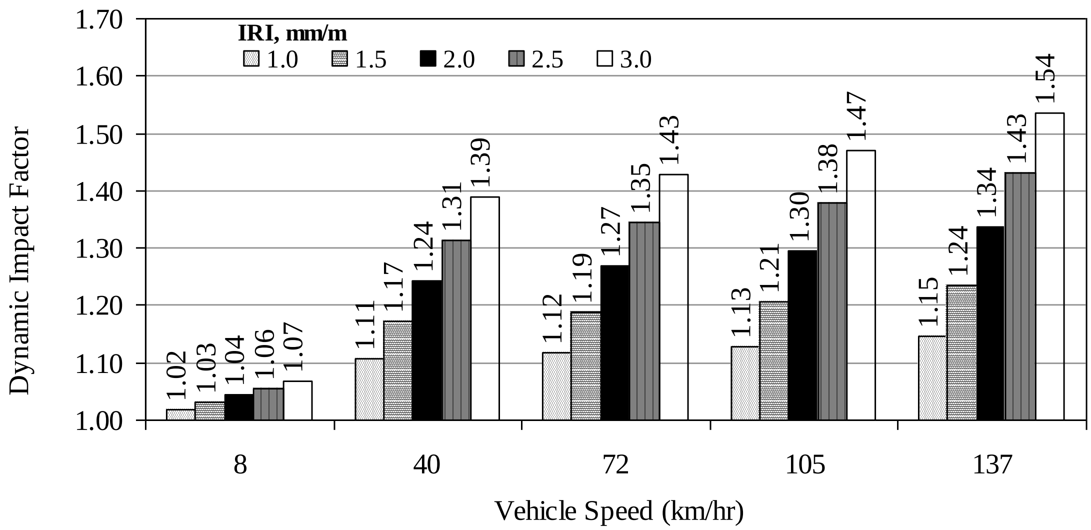

Figure 5.22 - Impact of Pavement Roughness on DI for Walking Beam

COMPARISON OF DIFFERENT MODELS

To compare dynamic load applied on pavement from four different models studied, suspension component properties are considered similar to achieve the best comparison. All results are reflected to Figure 5.23. The models are assumed traveling along the pavement with IRI of 2 mm/m representing good road condition. Regarding to Figure 5.32 the following conclusions are listed:

- Vehicle speed significantly impacts the additional dynamic load applied to pavements.
- Quarter car suspension exerts more loads to a pavement at vehicle speeds of 105 km/h and greater.

- A walking beam suspension exhibits the highest DI for speeds less than 72 km/h and the lowest at 137 km/h.
- Tridem model exhibits slightly higher DI than tandem model at higher speeds (greater than 72 km/h). This trend reverses for the lower speeds.
- The IRI impact of each model is reflected in Figures 5.6, 5.14, 5.25 and 5.31. Among the models studied, walking beam has the least sensitivity to road roughness.

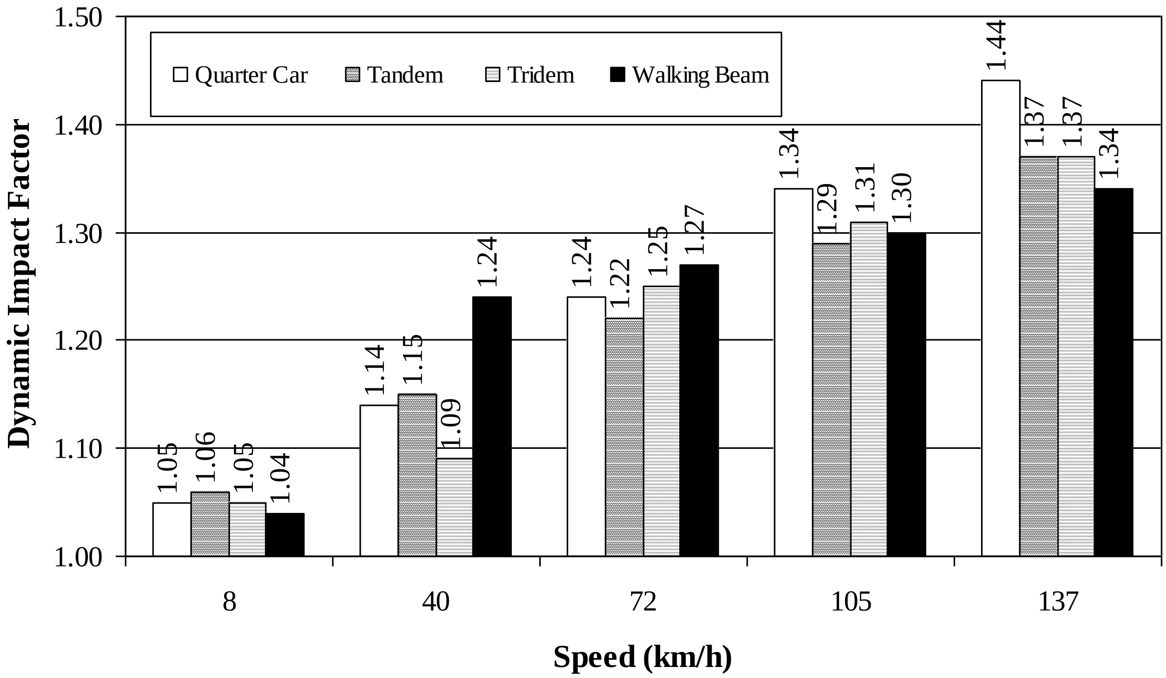

Figure 5.23- Comparison of Dynamic Factor among Different Suspensions

IMPACT OF VEHICLE SPEED AND IRI ON DI

An attempt was made to relate the variation in the DI with the IRI and vehicle speed (V) (see Figures 5.6, 5.13, 5.18 and 5.22) for the standard properties indicated for the four types of suspensions. It was found that Equation 5.1 can be readily utilized for all suspensions except walking beam.

$$DI = 1 + a \times V \times IRI \quad \textbf{(5.1)}$$

Parameter '*a*' for different suspensions and the goodness of the fit are reflected in Table 5.6. As judged by the coefficients of determination (R^2 values) and the standard errors of estimate (SEE), these relationships describe the results quite well.

Walking beam suspension follows a linear model as shown in Equation 5.2 with the parameters reflected in Table 5.7

$$DI = 1 + a \times V + b \times IRI \quad \textbf{(5.2)}$$

Table 5.6- Model Coefficients for Equation 5.1

Suspension Type	Fit Parameter	R^2	SEE
	a		
Quarter Car	0.0017	0.99	0.01
Tandem	0.0015	0.96	0.02
Tridem	0.0015	0.95	0.03

Table 5.7- Model Coefficients for Walking Beam

Vehicular Speed	Fit Parameter		R^2	SEE
	a	b		
>40 km/h	0.0008	0.2258	0.94	0.033
≤40 km/h	0.0053	0.0000	0.99	0.00

COMPARISON OF DAMAGE FACTOR FOR HEAVY TRUCKS

According to the procedure developed in the report two trucks have been compared. The first one is a 36200 kg (80 kips) standard truck that consists of a 5400 kg (12 kips) steering axle modeled as a quarter car and two 15400 kg (34 kips) trailing axle groups modeled as tandem leaf springs. The other truck is a 54400 kg (120 kips) heavy truck consisting of a 5400 kg (12 kips) steering axle modeled as a quarter car, 17200 kg (38 kips) tandem axle groups modeled as leaf spring and 31800 kg (70 kips) quad axle groups modeled as leaf spring. Two typical pavement structures were considered: an Interstate Highway (IH) pavement that includes a 250 mm (10 in.) thick HMA, a 300 mm (12. in.) thick granular base material and a subgrade and a State Highway (SH) pavement that includes a 75 mm (3 in.) thick HMA, a 300 mm (12. in.) thick granular base material and a subgrade damage factors for six road condition were obtained. A perfectly smooth pavement has an IRI of zero with a DI of unity. Given that the initial IRI, i.e. road opening condition, has an impact on DI, five initial IRIs were studied (initial IRI of 0.5, 1.0, 1.5, 2.0, 2.5 mm/m) to compare damage to each pavement condition. A vehicular speed of 96 km/hr (60 mph) was assumed.

Damage Factor is defined as the ratio of the number of standard truck passes required to reach failure by the number of heavy truck passes required to reach the same failure. Damage factors can be developed based on different distress types, i.e. rutting or fatigue cracking. To compensate the fact that the 54400 kg (120 kips) truck can carry more cargo with fewer passes, the damage factor was reduced by a payload factor which is the ratio of cargo carried by the heavy truck and standard truck. A payload factor of 1.77 is obtained for a 54400 kg (120 kips) truck, as 1.77 standard truck passes are required to carry the same amount of pay load that the heavy truck carries. Therefore the Damage Factor can be defined as:

$$DF = \frac{N_{f.std}}{N_{f.Heavy}} \times \frac{Payload_{std}}{Payload_{Heavy}} \quad \textbf{(5.3)}$$

where N_f is the total number of truck passes to produce failure in either rutting or fatigue cracking on the wheel tracks.

As the fatigue cracking and rutting increase with the number of truck passes, the IRI of the road changes as well. An extensive literature search for determining a published relationship between IRI and rut depth and percent cracking was carried out. The most appropriate model found was the so-called WesTrack model (Mactutis et al., 2000). That relationship is in the form of

$$IRI = 0.597 IRI_{init} + 0.0094 Fatigue\% + 0.00847 RutDepth + 0.382 \quad \textbf{(5.4)}$$

where IRI is measured in mm/m, RutDepth is in millimeters, and Fatigue% is the percentage of fatigue cracking in total lane area. This or similar relationships allow for an iterative process where as the rut depth and fatigue cracking progress, the IRI and as a result the DI are updated.

After each truck pass more damage is developed and, as a consequence, the pavement becomes rougher. The effect of initial IRI on Damage Factors was studied using two different criteria based on a constant IRI and progressive IRI. Constant IRI is influenced only by initial IRI and the DI remains unchanged regardless on the number of truck passes. On the other hand, a progressive IRI requires a recalculation of DI after each truck pass resulting in an increasing rate of rutting and fatigue cracking distresses. Progressive IRI is calculated by implementing pavement damage parameters after *n* truck passes.

The variations in Damage Factor due to rutting and fatigue cracking with the initial IRI of the road are shown in Figures 5.24 through 5.25. Considering a perfectly smooth pavement (with initial IRI =0 and DI =1), the heavy truck causes more damage in rutting to both pavements as the DF is greater than unity. For the case of fatigue cracking, the pavement with 10 in. ACP experiences less damage from the heavy truck than the standard truck, and slightly more for the pavement with 3 in. ACP.

According to Figures 5.24 and 5.25, as the pavement becomes rougher, the damage factors on both pavement types and for both modes of distress tend to become smaller. Since the heavy truck has a quad trailing axle as opposed to the dual tandem for the standard truck, the DI from the heavy truck is smaller than the standard truck. Consequently, the quad axle exerts less dynamic load to the rougher pavements than a dual tandem axle.

The same analyses were carried out when the DI's were kept constant based on the initial IRIs, ignoring the gradual change in IRI and DI during the life of the pavement. As shown in Figure 5.26, ignoring the progressive increase in IRI will consistently yield higher damage factors independent of the ACP thickness or the mode of failure.

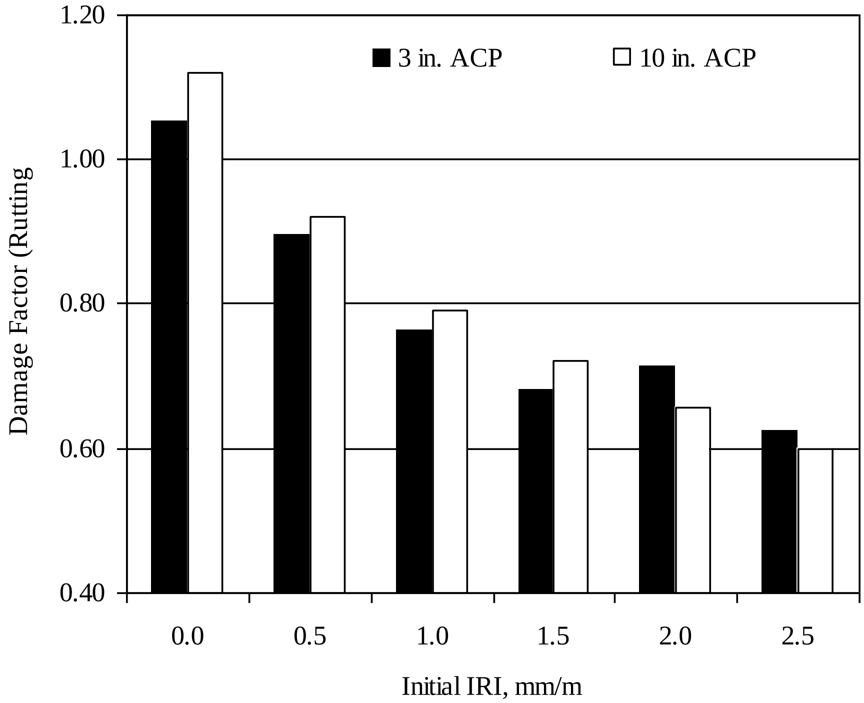

Figure 5.24- Damage Factor Based on Rutting with Progressive IRI.

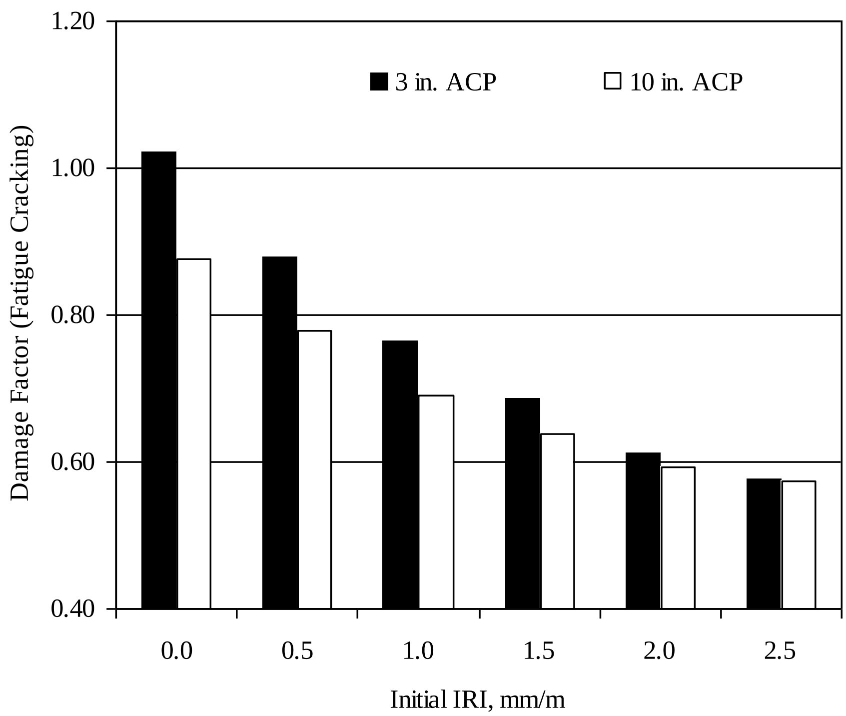

Figure 5.25- Damage Factor Based on Fatigue Cracking with Constant IRI

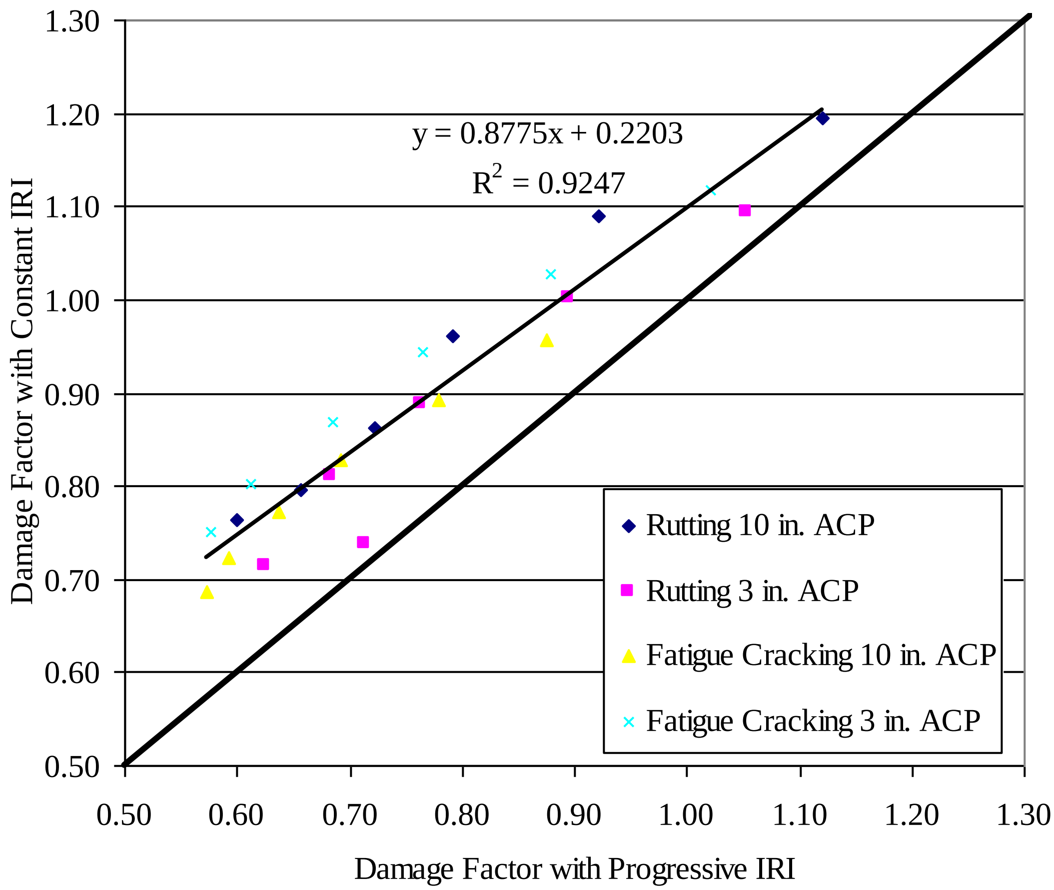

Figure 5.26- Comparisons of Damage Factors with Constant IRI and Progressive IRI

CHAPTER 6: CONCLUSION

Trucking accounts for about 80% of freight transportation in the United States. The use of heavy loads and new vehicle configurations has a major impact on the structural and functional performance of the highway network. An analytical tool is needed to predict the additional damage and to quantify the economic impact of allowing such trucks to use the highway system. A software package called Integrated Pavement Damage Analyzer (IntPave) has been developed at The University of Texas at El Paso (UTEP) for this purpose. IntPave structural model is a finite element program that calculates pavement responses and estimates the progression of distresses to predict performance and damage to pavements.

IntPave currently conducts the damage analysis and permit fee allocation assuming the loads are exerted statically. The interaction of truck suspension system with the roughness of the road surface may exert additional forces to the pavement. The aim of this study was to quantify the impact of truck suspension system and road surface condition on the damage exerted to the road. Common suspension systems were modeled. The International Roughness Index (IRI) was used to simulate the road roughness. Based on these two parameters, the truck-pavement interaction was modeled to estimate the dynamic load applied to the pavement. These analyses were incorporated in a new module of IntPave to modify the static load amplitudes to dynamic ones.

Four types of suspension systems were described in the report. The frequency response function for each type was calculated. Also frequency response for n-tire leaf spring was generalized. Force spectral density was derived from frequency response function of system and displacement spectral density of any road. Impact of truck suspension and roughness reflected to force spectral density. Dynamic Impact factor was calculated from force spectral density which the factor modifying static load per axle group. The modified static load considers impact of truck suspension and road roughness. Four parametric studies based on each model were developed and the report includes the results of them. Stiffness of any suspension system considerably increased the amount the modified static load; also the road roughness impact was severe. An optimal damping coefficient is observed in tridem and tandem suspension system. which the damping coefficient minimizes the DI. Sprung mass is able to handle the amplitude of the vibration, therefore as sprung mass increase DI reduces. Pitch inertia impacts on magnitude of DI of single tridem model.

Vehicle Speed significantly impacts the additional dynamic load applied to pavements. Quarter car suspension exerts more loads to a pavement at vehicle speeds of 105 km/h and greater. A walking beam suspension exhibits the highest DI for speeds less than 72 km/h and the lowest at 137 km/h. Tridem model exhibits slightly higher DI than tandem model at higher speeds (greater than 72 km/h). This trend reverses for the lower speeds. Studying all models at certain condition showed increase of speed led implementing walking beam rather others. Walking beam has the least sensitivity to road roughness. As vehicular increase dynamic Impact of both tandem and tridem model is almost the same.

Vehicle speed and road roughness (IRI) relate to DI for default suspension properties Quarter car, Tandem and Tridem follows the same model. The model developed works for walking beam with vehicle speed less than 40 km/h. for vehicle speed greater than 40 km/h the linear model was developed.

References

Aruell, J., *The Influence of Different Suspension Parameters on Dynamic Wheel Loads*, IMechE Conference on Road Wear: The Interaction between Vehicle Suspensions and the Road. London, 1991.

Cebon, D. and. Winkler,C., *A Study of Roaddamage Due to Dynamic Wheel Loads Using a Load Measuring Mat Volume 1,* April, 1990.

Cebon, D., *Handbook of Vehicle-Road Interaction*, Swets & Zeitlinger, 1999.

Cebon, D., *Heavy Vehicle Vibration - a Case Study*, 9th IAVSD Symposium on the Dynamic of Vehicles on Roads and Tracks. Swets and Zeitlinger, 1985.

Cebon, D, *Interaction between Heavy Vehicles and Roads,* SAE 1993. 1993.

Cole, D.J. and Cebon D., *Influence of Tractor-Trailer Interaction on Assessment*, Automobile Engineering (July 1996).

Cole, D.J. and Cebon, D., *Truck Tires, Suspension Design and Road Damage*, International Rubber Conference IRC'96, 17-21 June, 1996, Manchester, UK.

Davis, L., *Heavy Vehicle Suspension Testing and Analysis – Dynamic Load Sharing*, March 2009.

de Pont, J., Pidwerbesky, B. and Steven, B.,*The Influence of Vehicle Dynamics on Pavement Life,* 1996.

Organization for Economic Cooperation & Devel, *Dynamic Interaction between Vehicles and Infrastructures Experiment (DIVINE),* 1998.

Gillespie, T.D., Karamihas, S. M., Sayers, M. W., Nasim, M. A., Hansen, W., Ehsan, N., Cebon, D.., *Effects of Heavy Vehicle Characteristics on Pavement Response and Performance*, August 1992.

Heath, A.N., *Heavy Vehicle Design Affecting Road Loading*, ARRB/FORS Symposium on Heavy Vehicle Suspension Characteristics. Canberra, Australia, 1987.

Morris, J.R., *Effects of Heavy Vehicle Characteristics on Pavement Response - Phase 1*, TRB. 1987.

Mikhail, M Y. and Mamlouk, M. S., *Effect of Vehicle-Pavement Interaction on Pavement Response*, Transportation Research Board of the National Academies, Volume 1570 (1997): 78-88.

Organization for Economic Cooperation & Devel, *Dynamic Interaction between Vehicles and Infrastructure Experiment (DIVINE),* 1998.

Organization for Economic Cooperation & Devel., *Dynamic Loading of Pavements,* 1992.

Potter, T.E.C., Cebon, D., Cole, D.J. and Collop, A.C. *Road Damage Due to Dynamic Tyre Forces, Measured on a Public Road*, 1996.

Kelly, L. et al., *Pavement Smoothness Index Relationships*, FHWA-RD-02-057 OCTOBER 2002.

Sayers, M.W. and Karimihas, S.M. *The Little Book of Profiling,* 1998.

Sun, L. *Simulation of Pavement Roughness and IRI Based on Power Spectral Density*. Mathematics and Computers in Simulation 61 (2003): 77-88.

Sweatman, P.F. *A Study of Dynamic Wheel Forces in Axle Group Suspensions of Heavy Vehicles*. 1983.

Mactutis, J.A. ,Alavi, S.H. and Ott. W.C *Investigation of Relationship between Roughness and Pavement Surface Distress Based on WesTrack Project,* Transportation Research Record 1699, pp. 107-113, 2000

APPENDIX A: SINGLE TANDEM MODEL

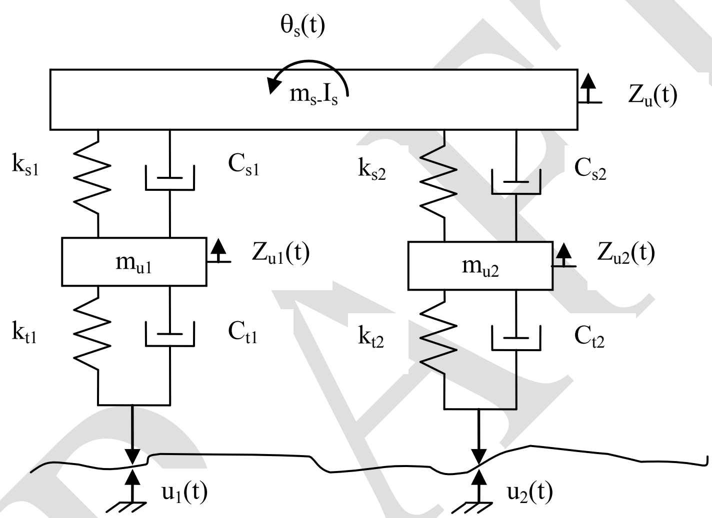

Figure A.1 – Single-Tandem Leaf Spring Model

$$D = \begin{bmatrix} 0 & 0 \\ 0 & 0 \\ 1 & 0 \\ 0 & 1 \end{bmatrix} \quad \text{linear transformation matrix} \qquad \textbf{(A.1)}$$

The Mass, stiffness and damping matrices are defined as following:

$$M = \begin{bmatrix} m_s & 0 & 0 & 0 \\ 0 & I_s & 0 & 0 \\ 0 & 0 & m_{u1} & 0 \\ 0 & 0 & 0 & m_{u2} \end{bmatrix} \text{mass matrix} \qquad \textbf{(A.2)}$$

$$C = \begin{bmatrix} c_{s1} + c_{s2} & (-c_{s1} + c_{s2}) \times a & -c_{s1} & -c_{s2} \\ (-c_{s1} + c_{s2}) \times a & (c_{s1} + c_{s2}) \times a^2 & c_{s1} \times a & -c_{s2} \times a \\ -c_{s1} & c_{s1} \times a & c_{s1} + c_{t1} & 0 \\ -c_{s2} & -c_{s2} \times a & 0 & c_{s2} + c_{t2} \end{bmatrix} \text{damping matrix} \qquad \textbf{(A.3)}$$

$$K = \begin{bmatrix} k_{s1}+k_{s2} & (-k_{s1}+k_{s2})\times a & -k_{s1} & -k_{s2} \\ (-k_{s1}+k_{s2})\times a & (k_{s1}+k_{s2})\times a^2 & k_{s1}\times a & -k_{s2}\times a \\ -k_{s1} & k_{s1}\times a & k_{s1}+k_{t1} & 0 \\ -k_{s2} & -k_{s2}\times a & 0 & k_{s2}+k_{t2} \end{bmatrix} \text{stiffness matrix} \qquad \textbf{(A.4)}$$

Table A.1 – Values of Parameters Assumed for Single Leaf Spring Model

m_s	sprung mass	6711 kg
$m_{u1}= m_{u2}$	unsprung mass	500 kg
I_s	pitch intertia	930 kg.m²
$c_{s1}=c_{s2}$	suspension damping	80 kN·s/m
$c_{t1}=c_{t2}$	tire damping	4 kN·s/m
$k_{s1}= k_{s2}$	suspension stiffness	4 MN/m
$k_{t1}= k_{t2}$	tire stiffness	3.5 MN/m
IRI	road roughness	2 m/km

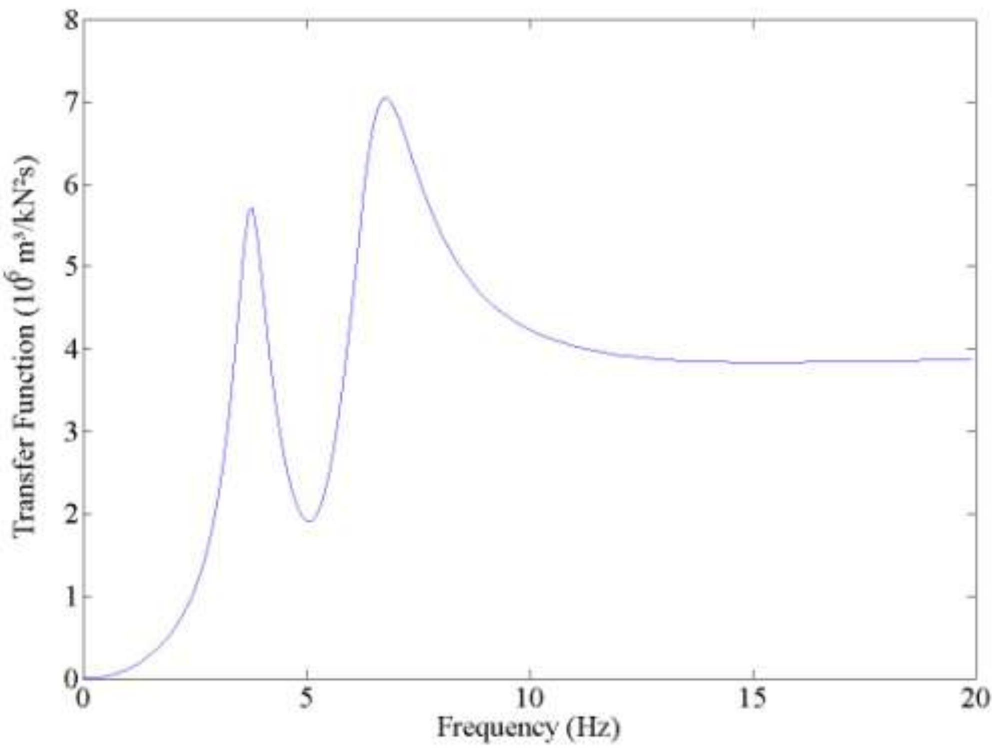

Figure A.2 – Transfer Function H(ω)

Table A.2- DLC at Different Speed

Speed (km/h)	8	40	70	100	140
DLC	0.03	0.08	0.11	0.14	0.19

APPENDIX B: SINGLE TRIDEM MODEL

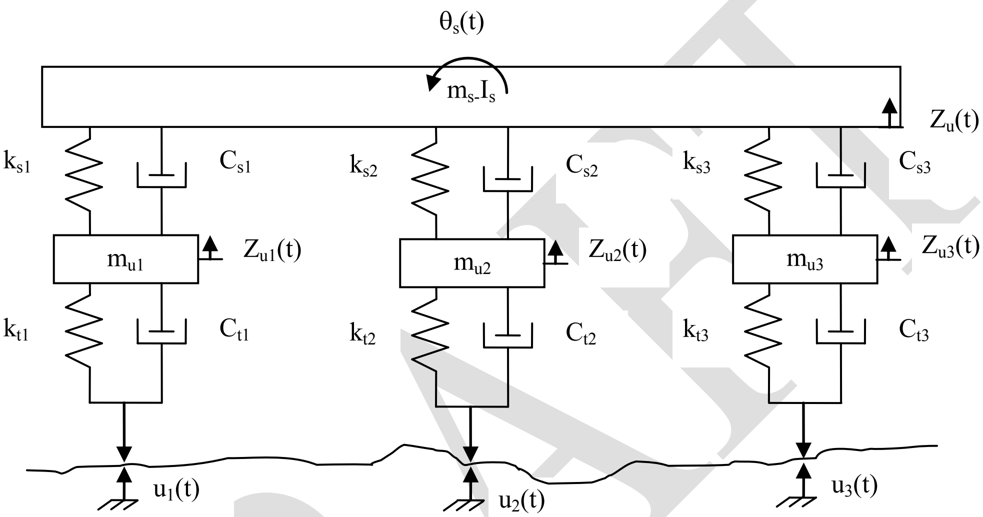

Figure B.1– Single-Tandem Leaf Spring Model

$$D = \begin{bmatrix} 0 & 0 & 0 \\ 0 & 0 & 0 \\ 1 & 0 & 0 \\ 0 & 1 & 0 \\ 0 & 0 & 1 \end{bmatrix} \quad \text{linear transformation matrix} \qquad \textbf{(B.1)}$$

The Mass, stiffness and damping matrices are defined as following:

$$M = \begin{bmatrix} m_s & 0 & 0 & 0 & 0 \\ 0 & I_u & 0 & 0 & 0 \\ 0 & 0 & m_{u1} & 0 & 0 \\ 0 & 0 & 0 & m_{u2} & 0 \\ 0 & 0 & 0 & 0 & m_{u3} \end{bmatrix} \text{mass matrix} \qquad \textbf{(B.2)}$$

$$C = \begin{bmatrix} c_{s1}+c_{s2}+c_{s3} & (-c_{s1}+c_{s3})\times 2a & -c_{s1} & -c_{s2} & -c_{s3} \\ (-c_{s1}+c_{s3})\times 2a & (c_{s1}+c_{s3})\times 4a^2 & c_{s1}\times 2a & 0 & -c_{s3}\times 2a \\ -c_{s1} & c_{s1}\times 2a & c_{s1}+c_{t1} & 0 & 0 \\ -c_{s2} & 0 & 0 & c_{s2}+c_{t2} & 0 \\ -c_{s3} & -c_{s3}\times 2a & 0 & 0 & c_{s3}+c_{t3} \end{bmatrix} \text{damping matrix} \quad \textbf{(B.3)}$$

$$K = \begin{bmatrix} k_{s1}+k_{s2}+k_{s3} & (-k_{s1}+k_{s3})\times 2a & -k_{s1} & -k_{s2} & -k_{s3} \\ (-k_{s1}+k_{s3})\times 2a & (k_{s1}+k_{s3})\times 4a^2 & k_{s1}\times 2a & 0 & -k_{s3}\times 2a \\ -k_{s1} & k_{s1}\times 2a & k_{s1}+c_{t1} & 0 & 0 \\ -k_{s2} & 0 & 0 & k_{s2}+k_{t2} & 0 \\ -k_{s3} & -k_{s3}\times 2a & 0 & 0 & k_{s3}+k_{t3} \end{bmatrix} \text{stiffness matrix}$$

Table B.1 – Values of Parameters Assumed for Single Tridem Leaf Spring

m_s	sprung mass	6711 kg
$m_{u1}= m_{u2}= m_{u3}$	unsprung mass	500 kg
I_s	pitch inertia	930 kg.m²
$c_{s1}= c_{s2}= c_{s3}$	suspension damping	80 kN·s/m
$c_{t1}= c_{t2}= c_{t3}$	tire damping	4 kN·s/m
$k_{s1}= k_{s2}= k_{s3}$	suspension stiffness	4 MN/m
$k_{t1}= k_{t2}= k_{t3}$	tire stiffness	3.5 MN/m
IRI	road roughness	2 m/km

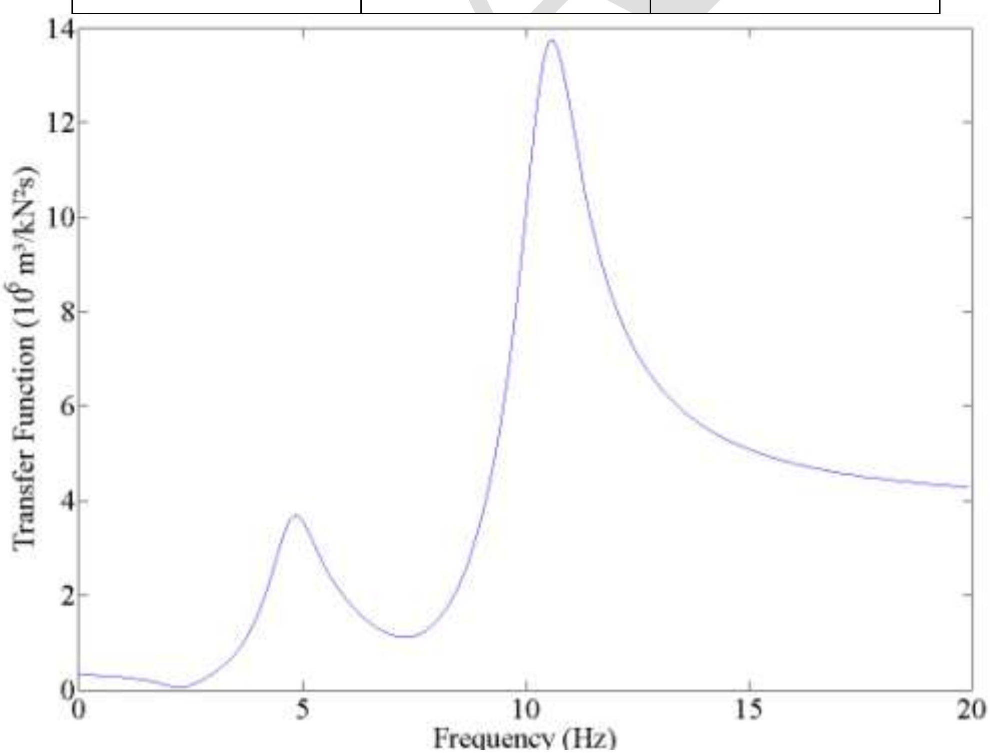

Figure B.2– Transfer Function

Table B.2- DLC at Different Speed

Speed (km/h)	8	40	70	100	140
DLC	0.03	0.04	0.12	0.16	0.18

APPENDIX C: WALKING BEAM MODEL

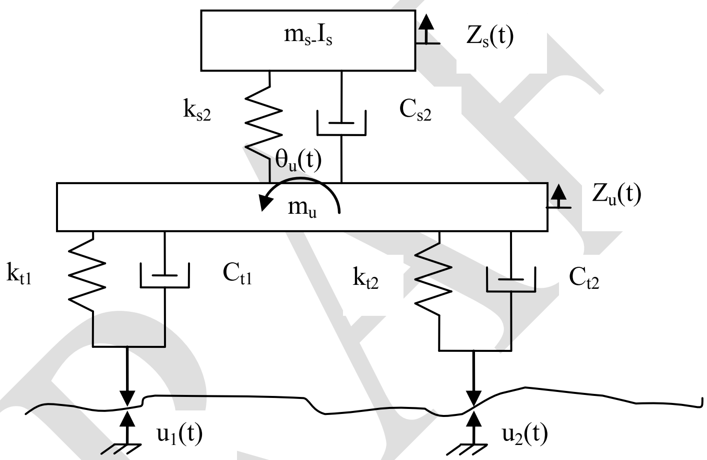

Figure C.1 – Walking-Beam Model

$$D = \begin{bmatrix} 0 & 0 \\ 1 & 1 \\ a & -a \end{bmatrix} \quad \text{linear transformation matrix} \qquad \textbf{(C.1)}$$

The Mass, stiffness and damping matrices are defined as following:

$$M = \begin{bmatrix} m_s & 0 & 0 \\ 0 & m_u & 0 \\ 0 & 0 & I_u \end{bmatrix} \text{mass matrix} \qquad \textbf{(C.2)}$$

Elements of damping and stiffness matrices are derived by developing motion equation of every degree of freedom.

$$C = \begin{bmatrix} c_s & -c_s & 0 \\ -c_s & c_s + c_{t1} + c_{t2} & 0 \\ 0 & 0 & a^2 c_{t1} + a^2 c_{t2} \end{bmatrix} \text{damping matrix} \tag{C.3}$$

$$D = \begin{bmatrix} k_s & -k_s & 0 \\ -k_s & k_s + k_{t1} + k_{t2} & 0 \\ 0 & 0 & a^2 k_{t1} + a^2 k_{t2} \end{bmatrix} \text{stiffness matrix} \tag{C.4}$$

Table C.1 – Values of Parameters Assumed for Walking Beam

m_s	sprung mass	6611 kg
m_u	unsprung mass	1100 kg
c_s	suspension damping	80 kN·s/m
c_t	tire damping	4 kN·s/m
k_s	suspension stiffness	4 MN/m
k_t	tire stiffness	3.5 MN/m
2a	distance between axles	1.3 m
IRI	road roughness	2 m/km

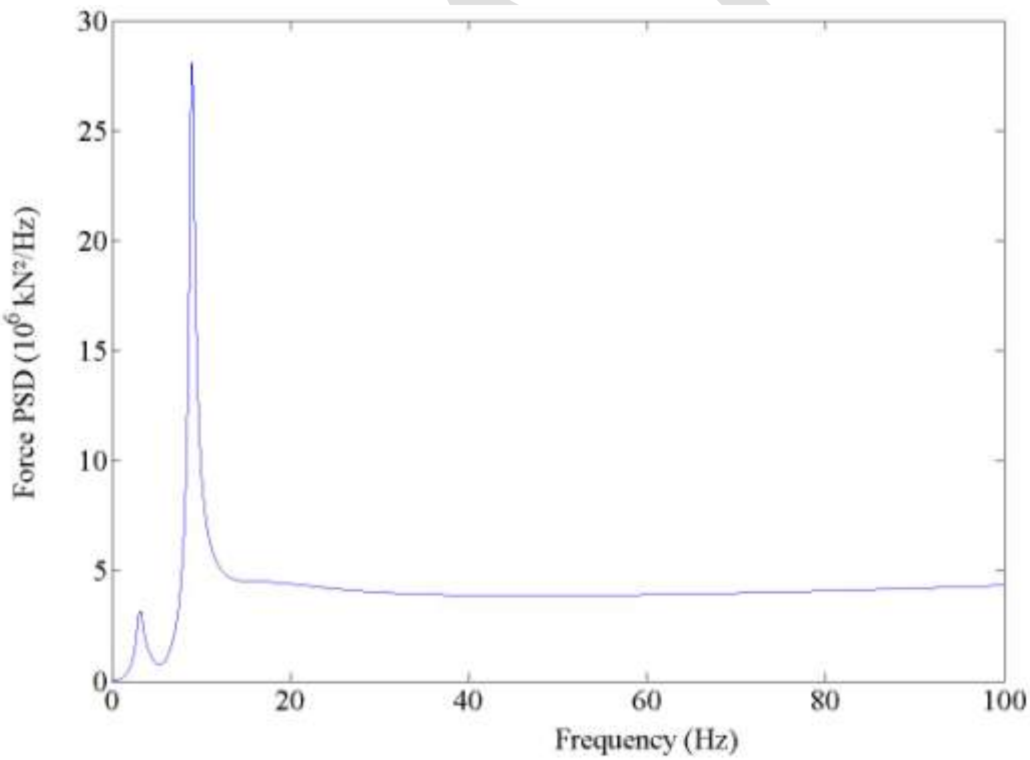

Figure C.2– Walking Beam Model Transfer Function

Table C.2- DLC at Different Speed

Speed (km/h)	8	40	70	105	85
DLC	0.02	0.12	0.13	0.15	0.17

APPENDIX D: QUARTER CAR MODEL PARAMETRIC STUDY

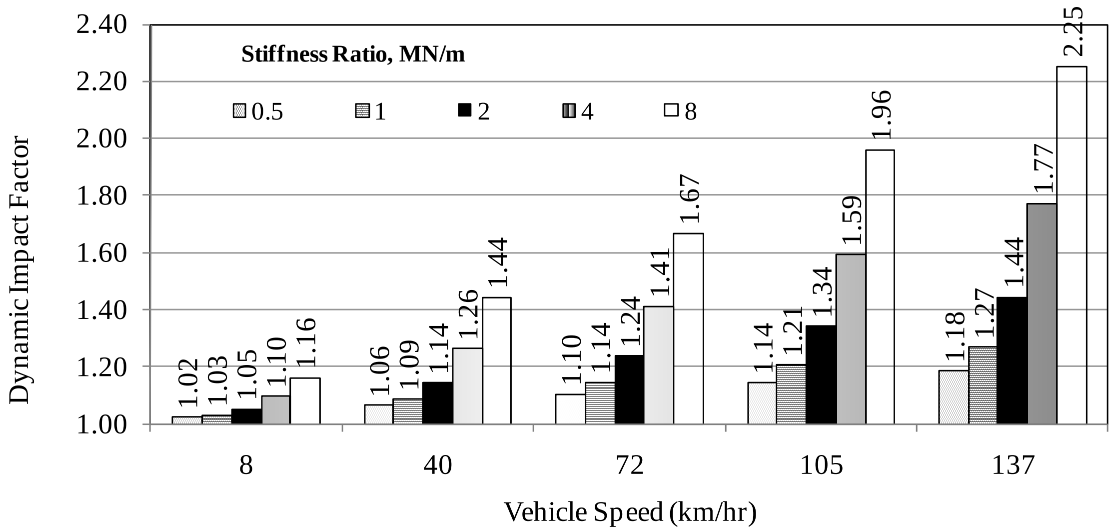

Figure D.1 – Impact of Variation of Stiffness Ratio on DI

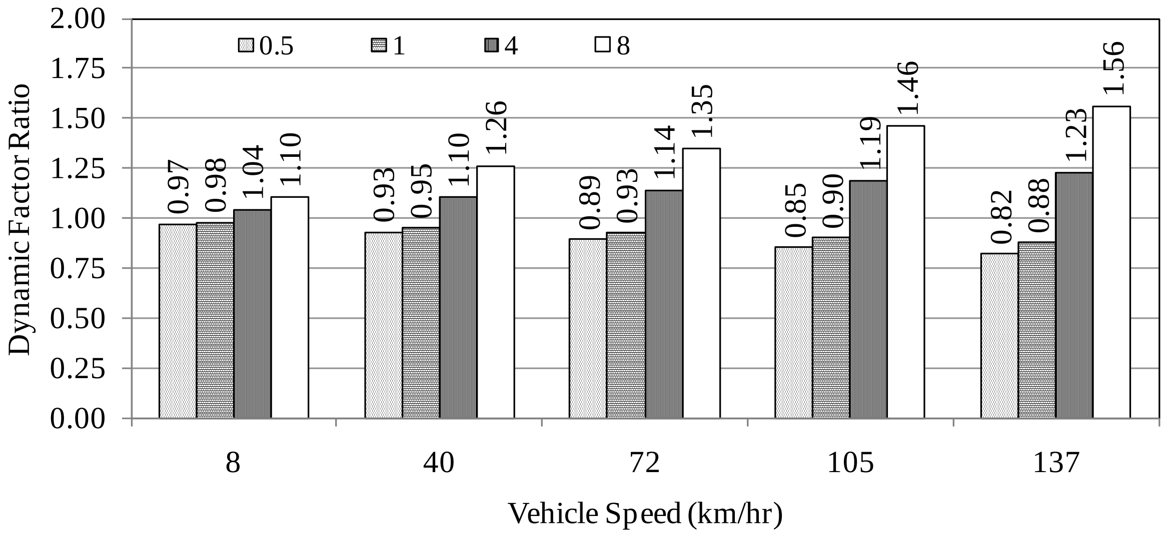

Figure D.2 – Comparison of the Impact of Variation of Stiffness Ratio

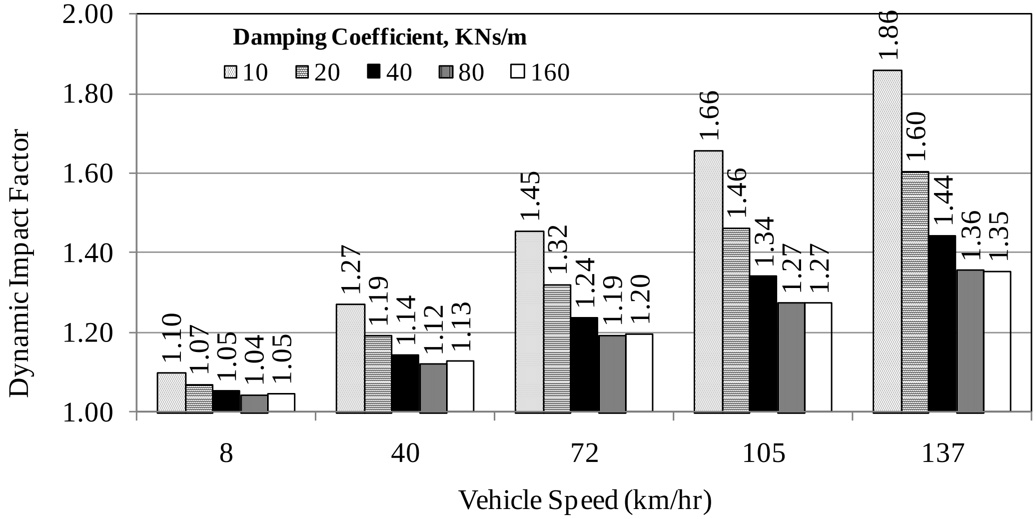

Figure D.3 – Impact of Damping Coefficient on DI

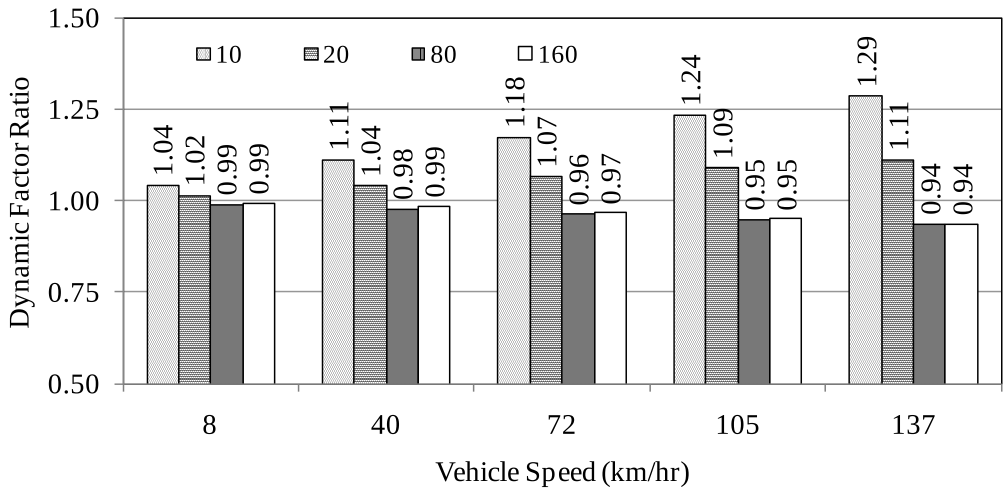

Figure D.4 – Comparison of the Impact of Damping Coefficient

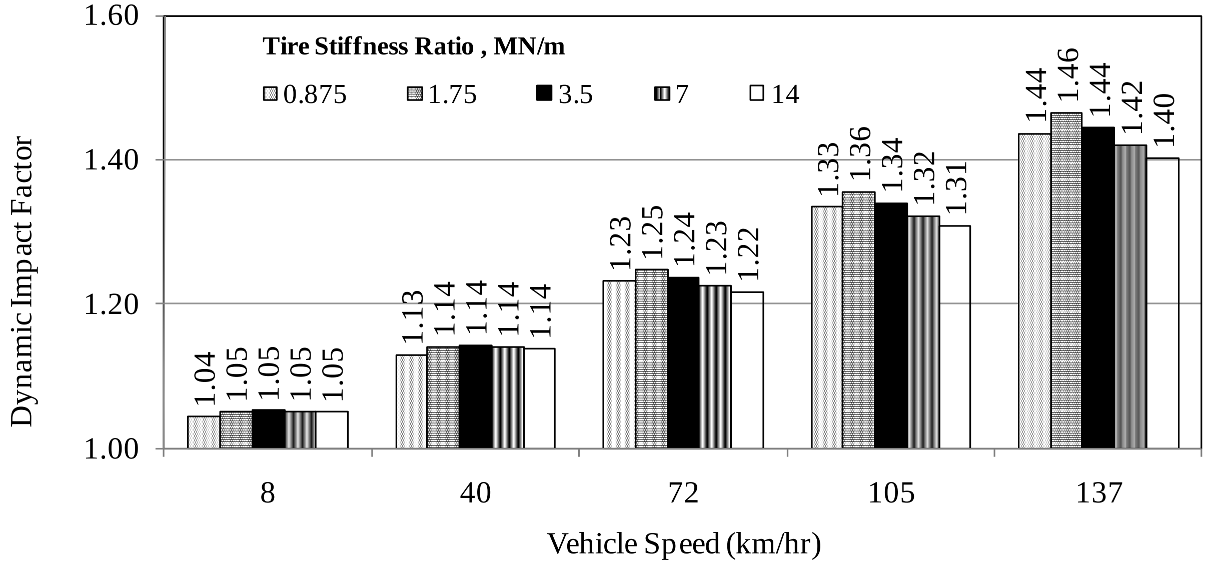

Figure D.5 – Impact of Tire Stiffness on DI

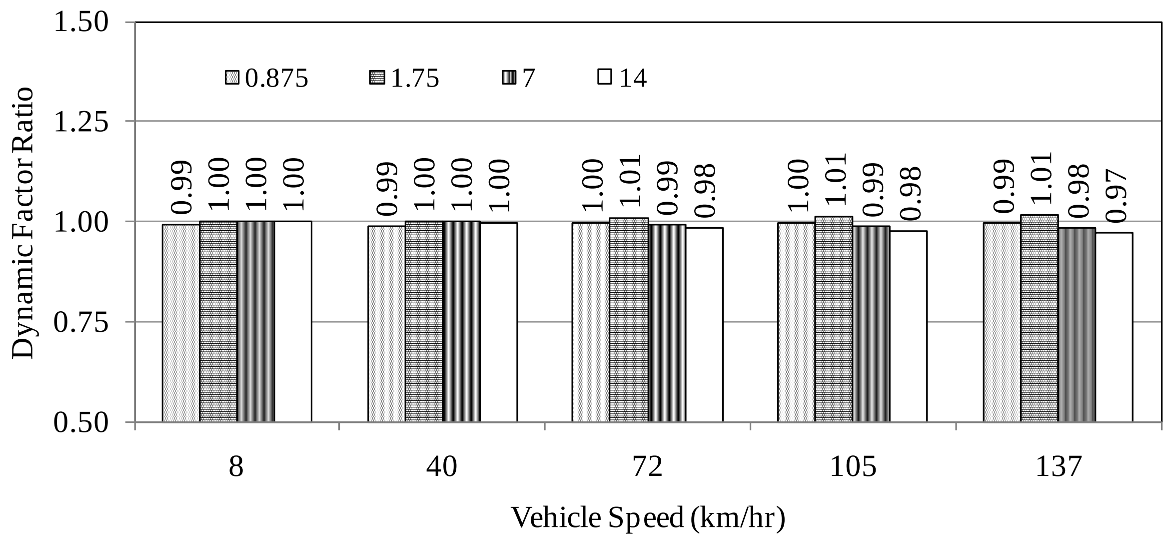

Figure D.6 – Comparison of the Impact of Tire Stiffness

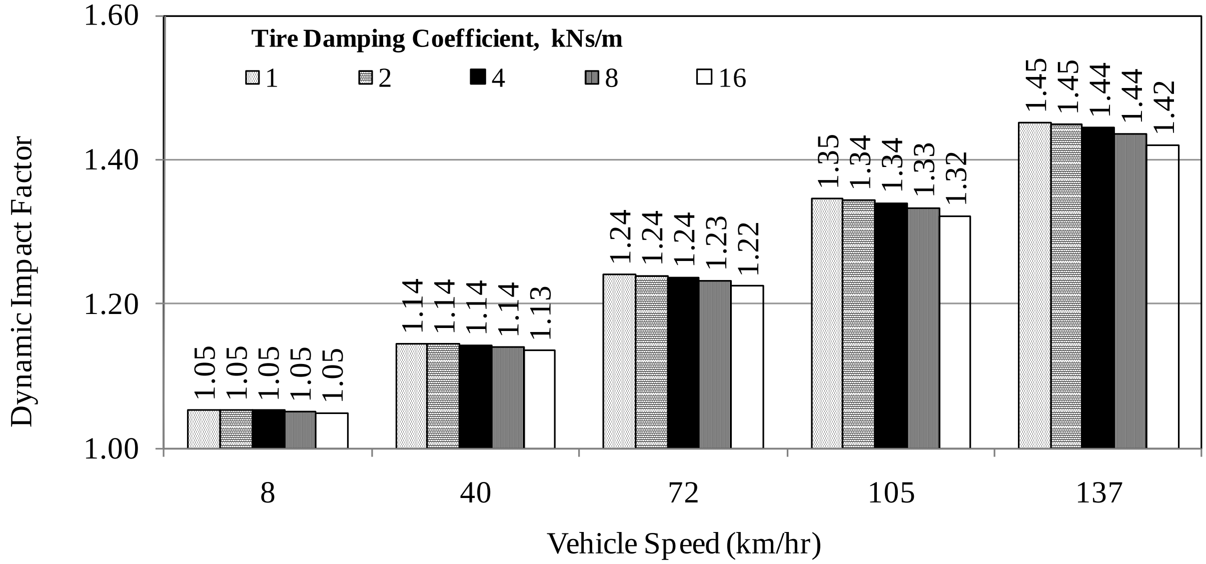

Figure D.7 – Impact of Tire Damping Coefficient on DI

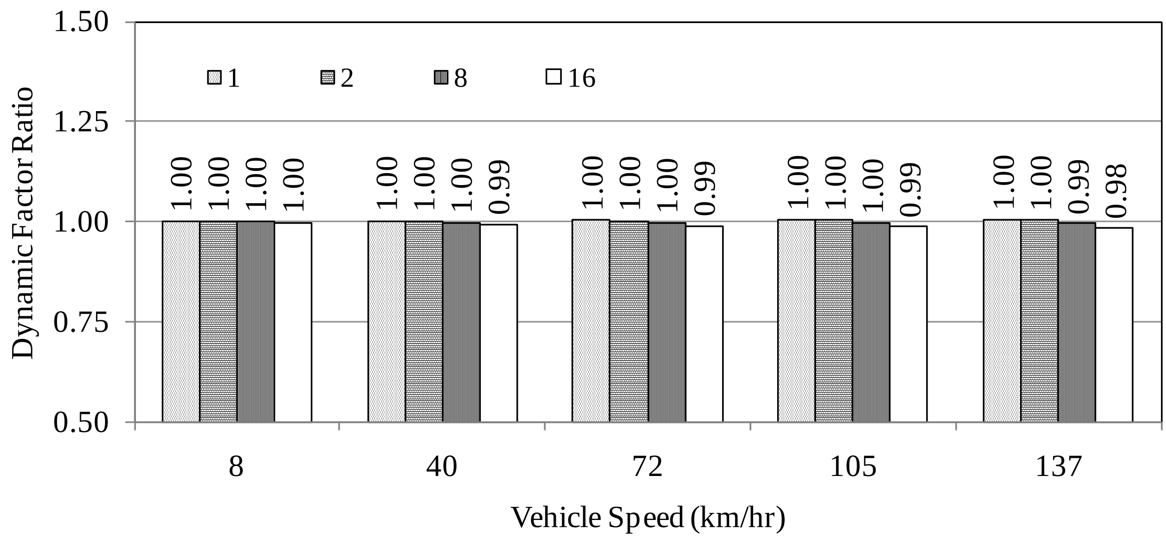

Figure D.8 – Comparison of the Impact of Tire Damping Coefficient

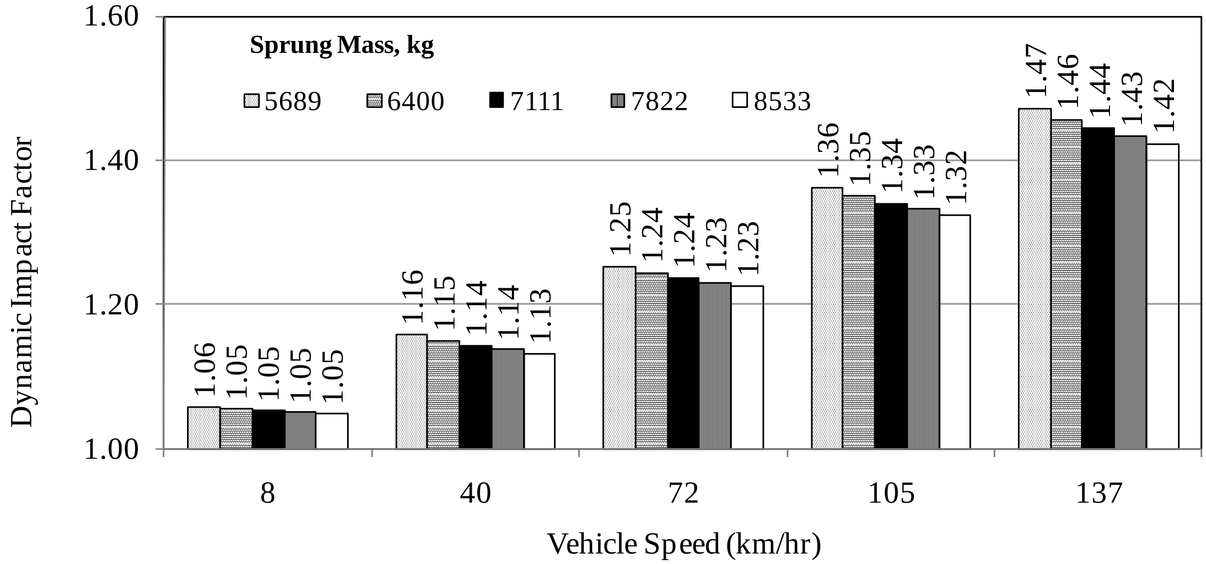

Figure D.9 – Impact of Sprung Mass on DI

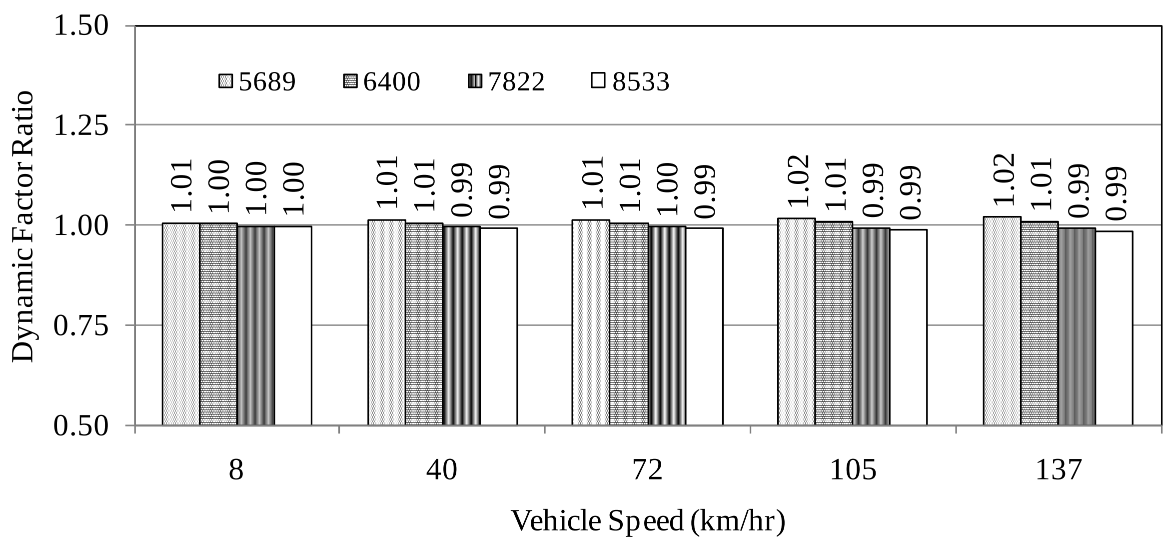

Figure D.10 – Comparision of The Impact of Sprung Mass

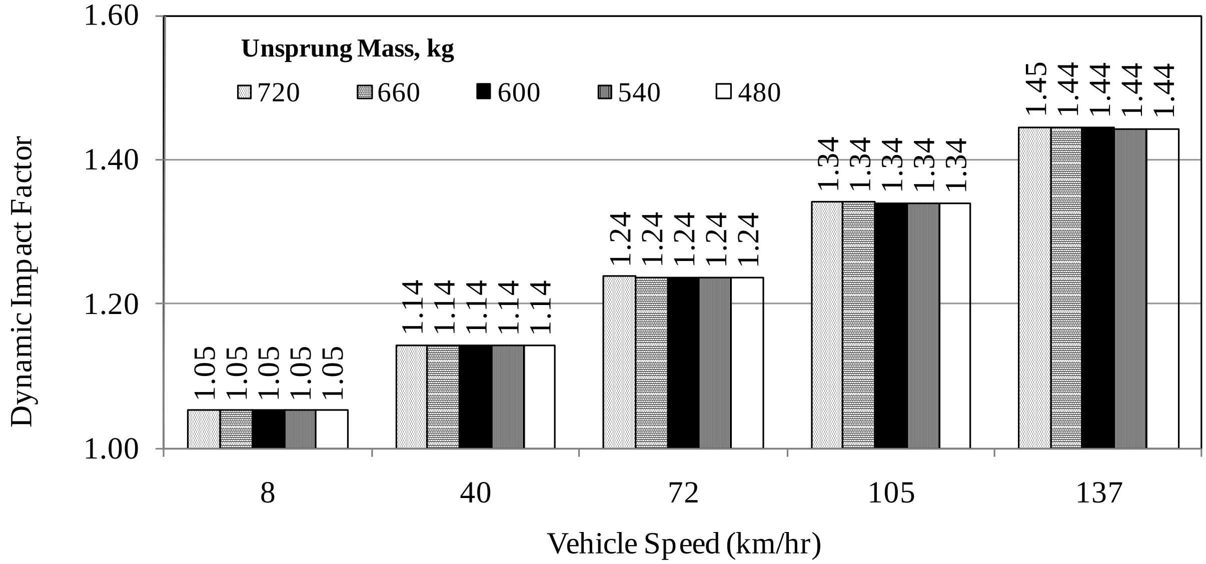

Figure D.11 – Impact of Unsprung Mass on DI

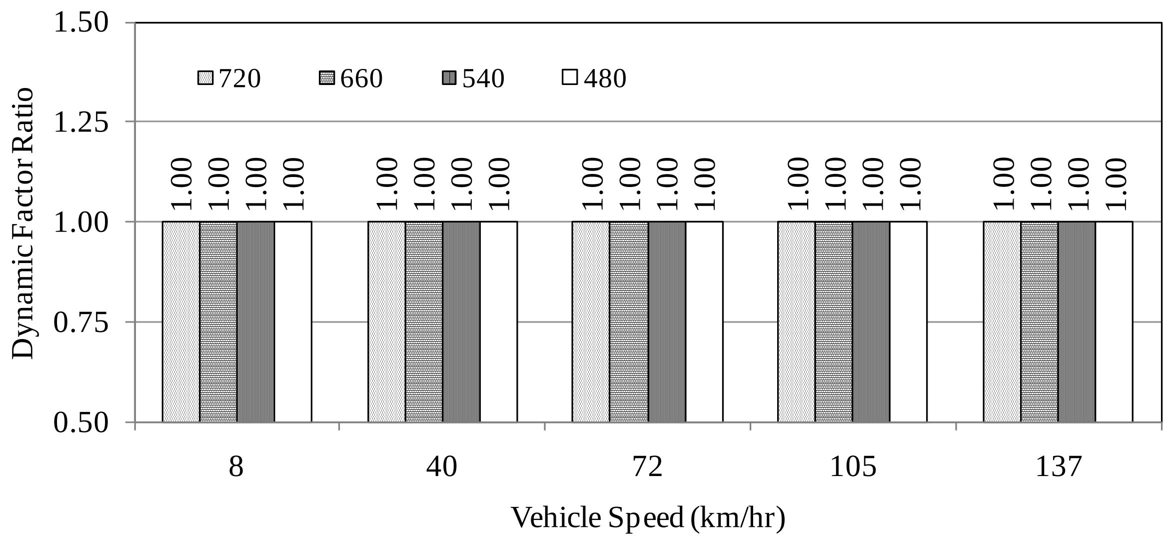

Figure D.12 – Comparison of the Impact of Unsprung Mass

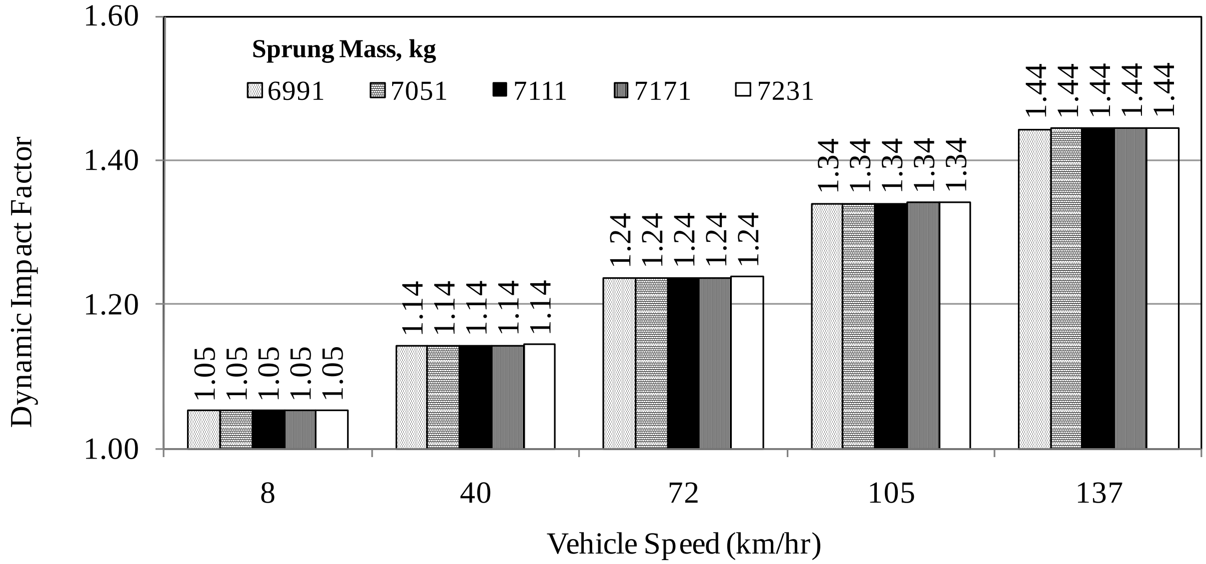

Figure D.13 – Impact of Sprung Mass on DI

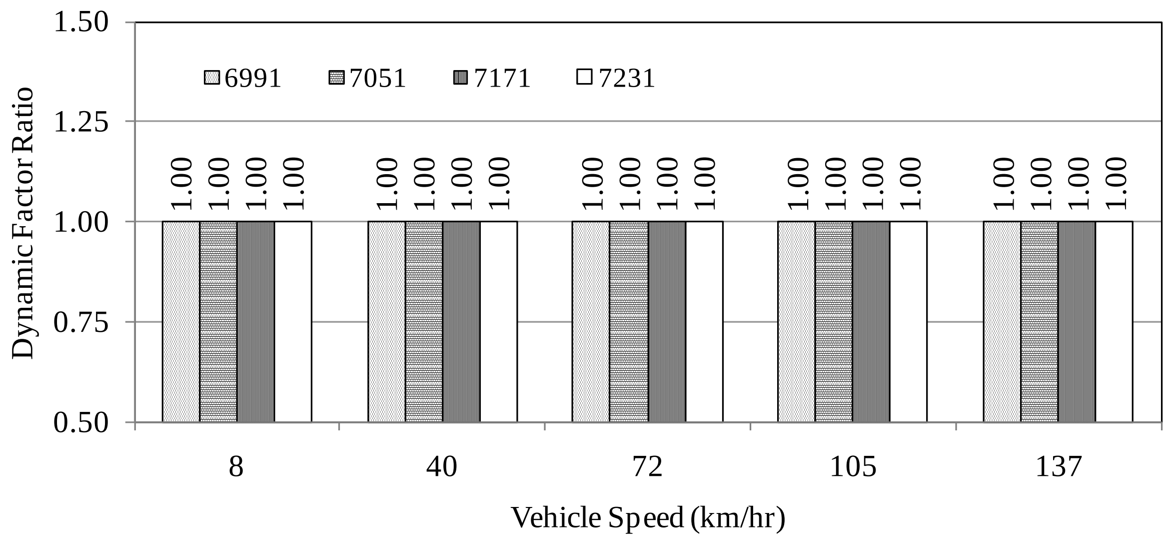

Figure D.14 – Comparison of the Impact of Sprung Mass

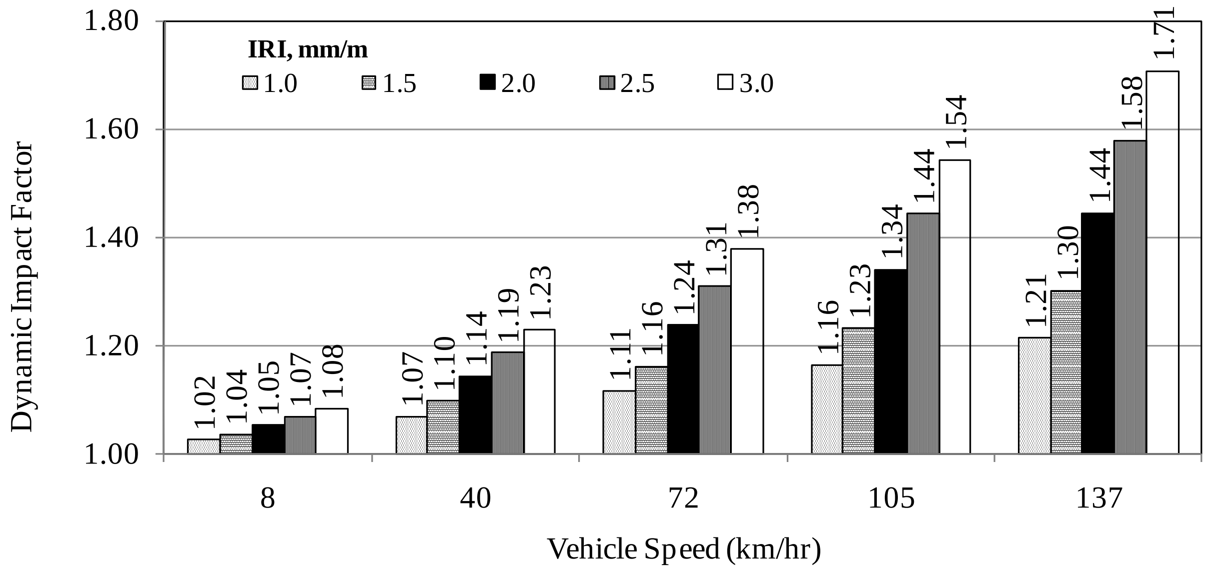

Figure D.15 – Impact of IRI on DI

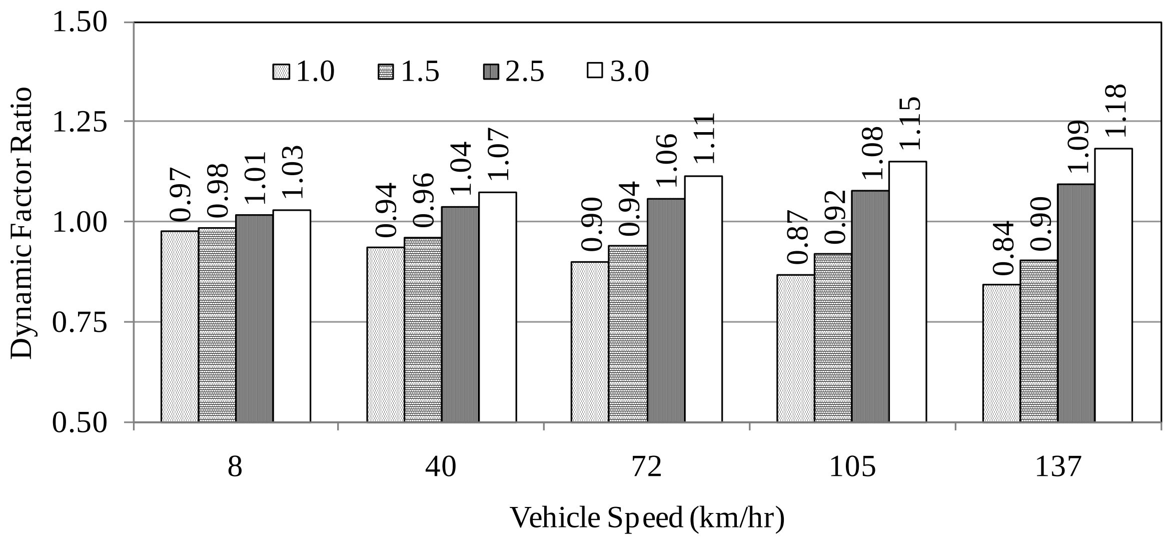

Figure D.16 – Comparison of The Impact of IRI

APPENDIX E: TANDEM LEAF SPRING MODEL PARAMETRIC STUDY

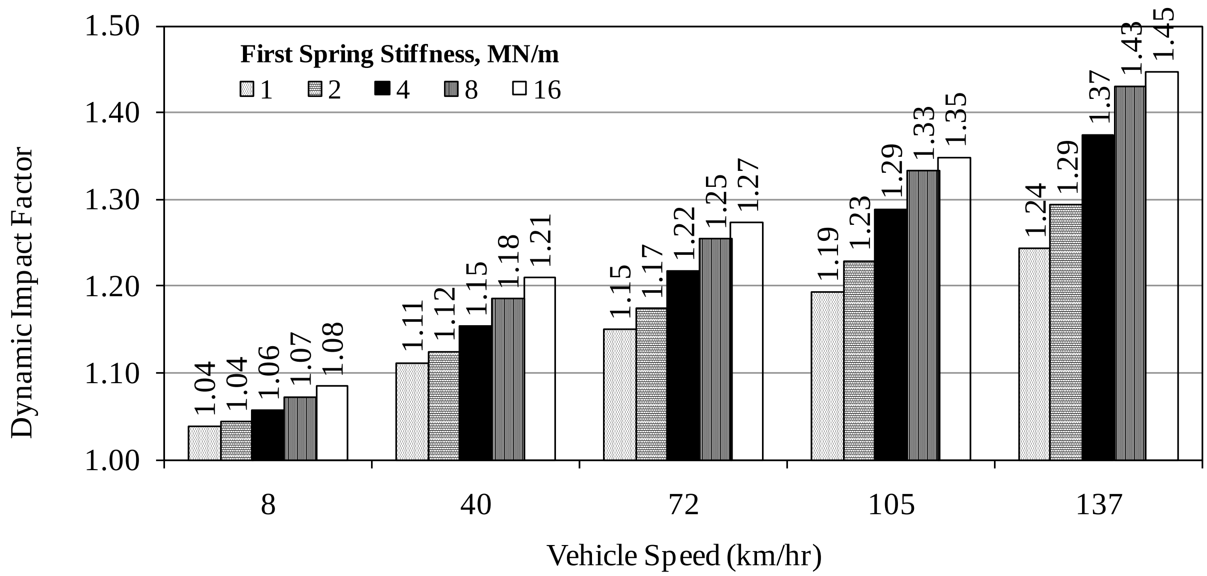

Figure E.1 – Impact of First Spring Stiffness on DI

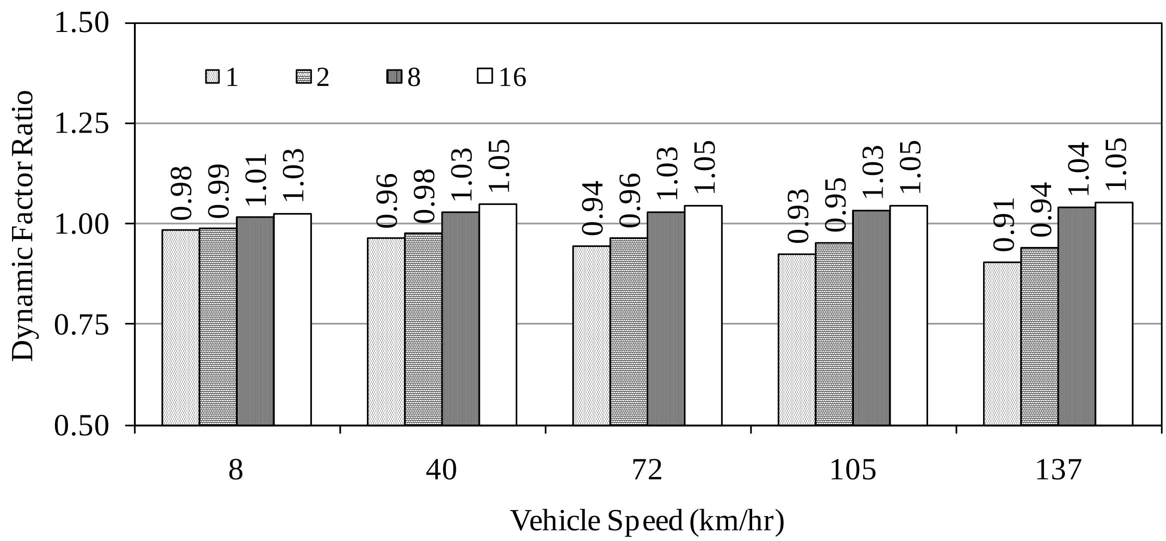

Figure E.2 – Comparison of the Impact of First Spring Stiffness

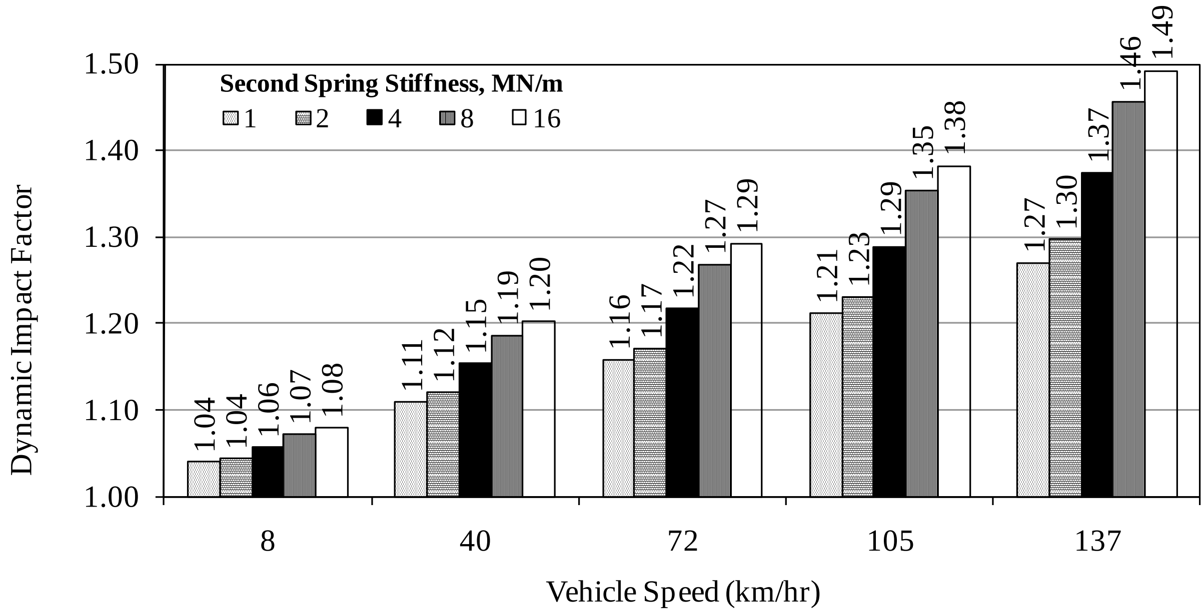

Figure E.3 – Impact of Second Spring Stiffness on DI

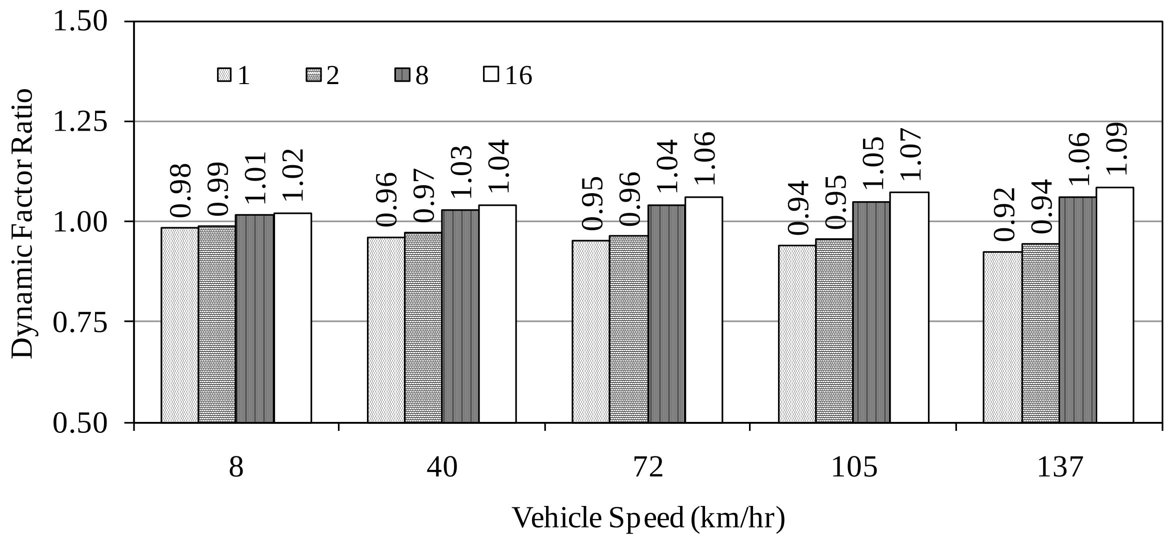

Figure E.4 – Comparison of the Impact of Second Spring Stiffness

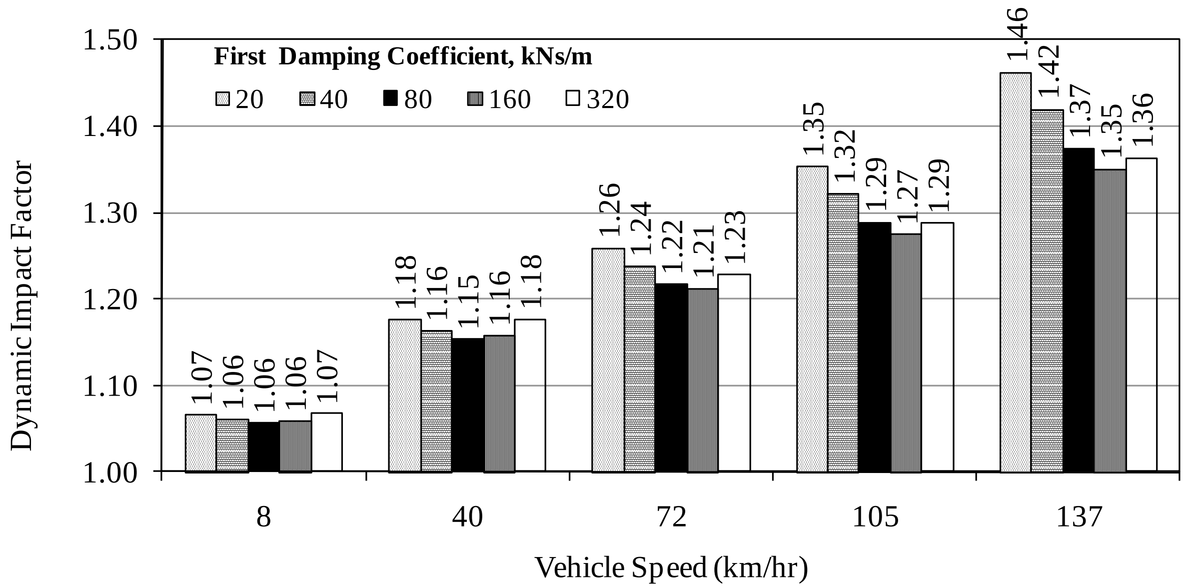

Figure E.5 –Impact of First Damping Coefficient on DI

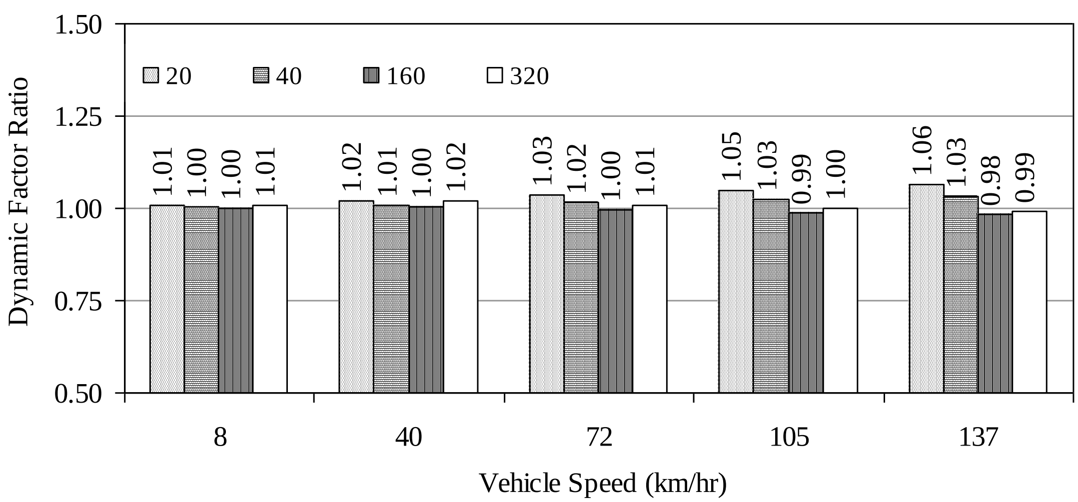

Figure E.6 – Comparison of the Impact of First Damping Coefficient

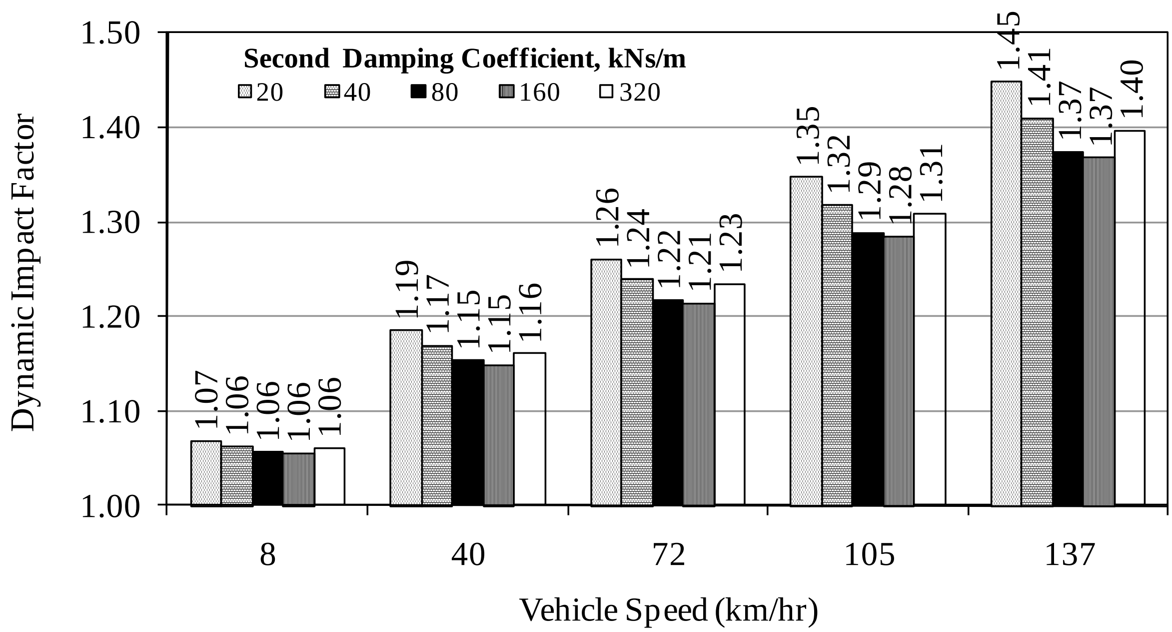

Figure E.7 –Impact of Second Damping Coefficient on DI

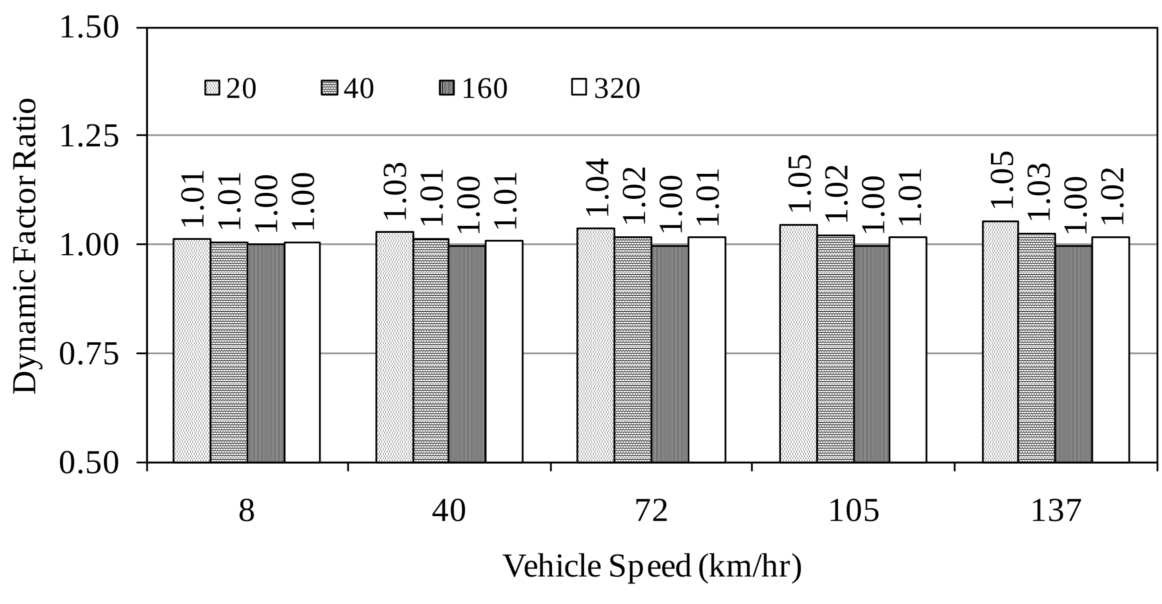

Figure E.8– Comparison of the Impact of Second Damping Coefficient

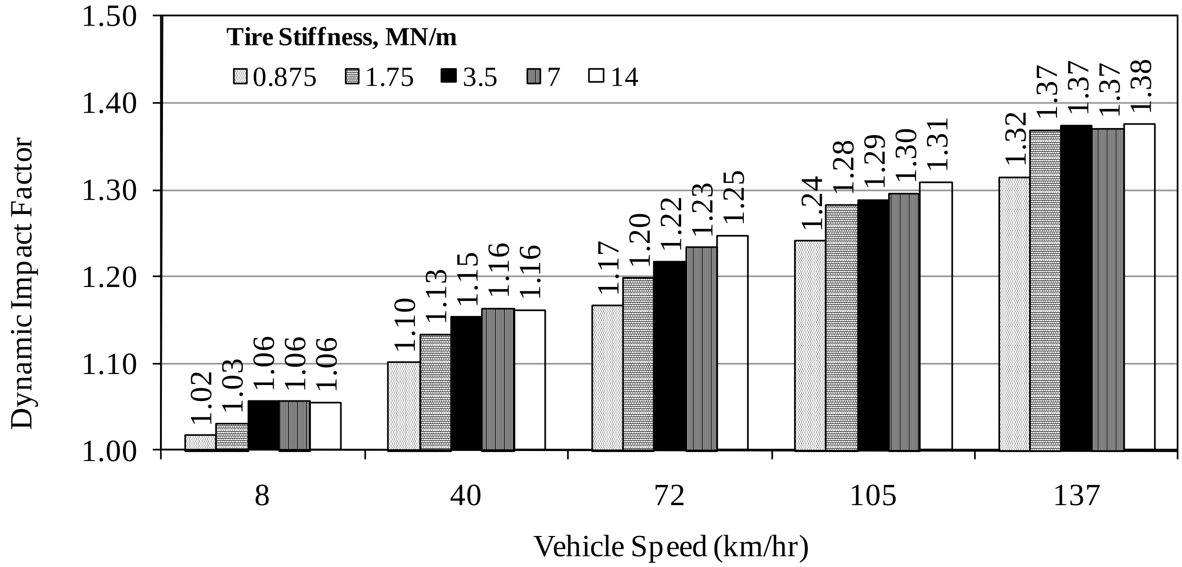

Figure E.9 –Impact of Tire Stiffness on DI

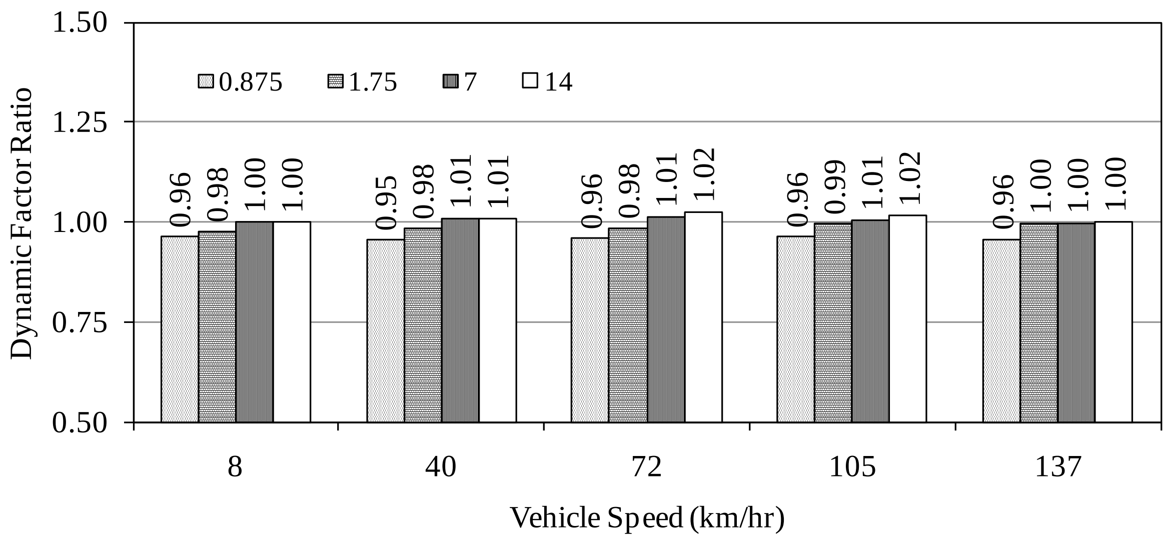

Figure E.10– Comparison of the Impact of Tire Stiffness

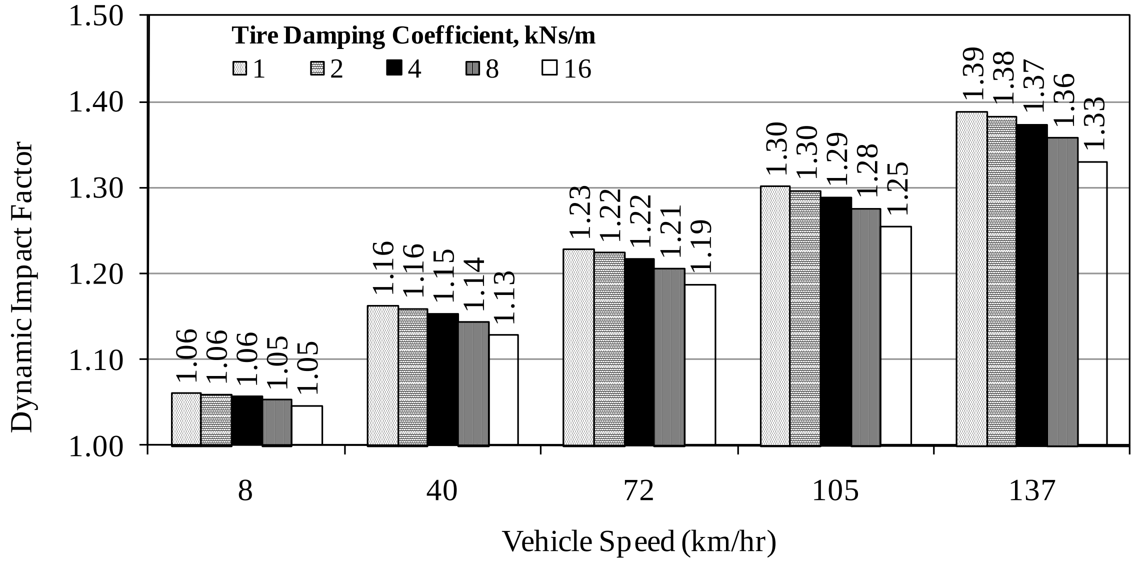

Figure E.11 –Impact of Tire Damping Coefficient on DI

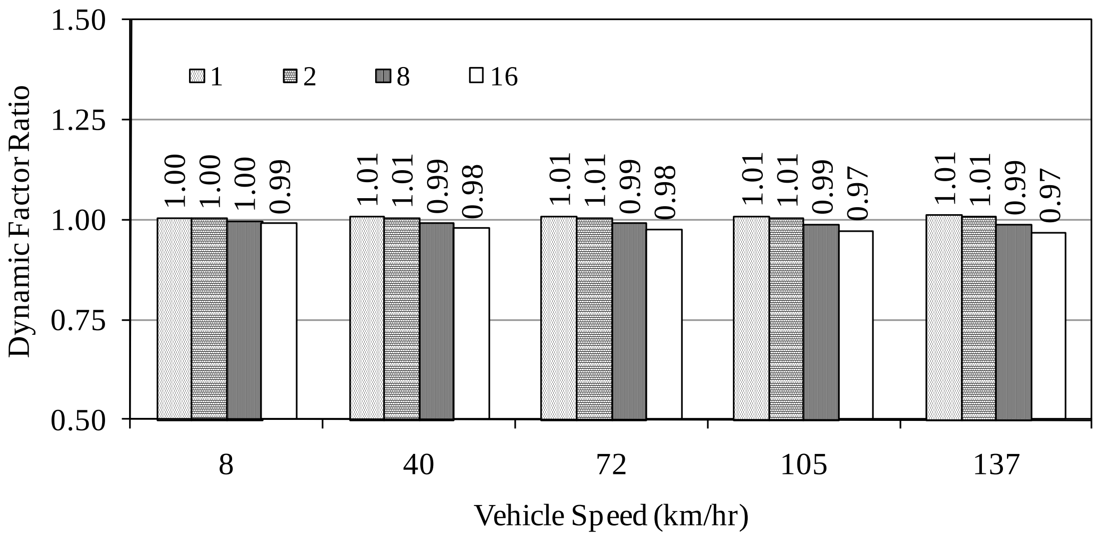

Figure E.12– Comparison of the Impact of Tire Damping Coefficient

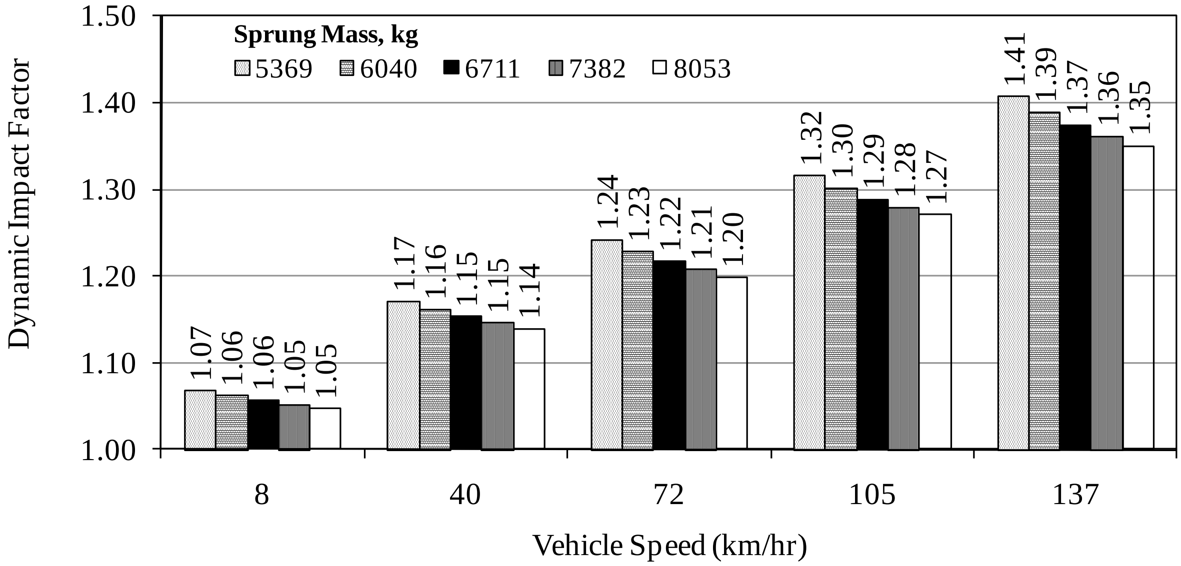

Figure E.13 –Impact of Sprung Mass on DI

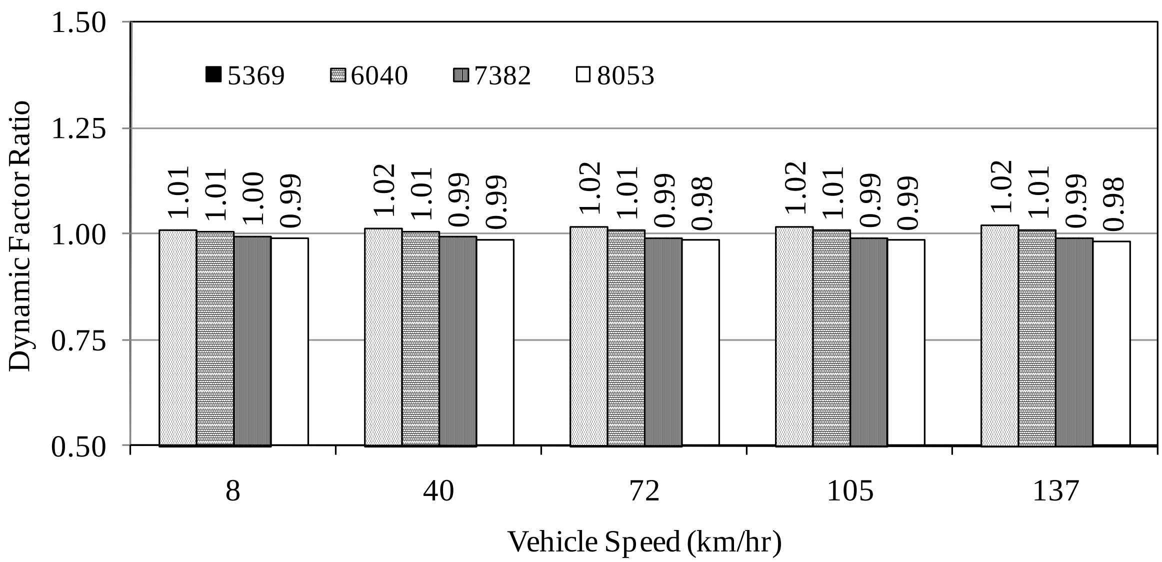

Figure E.14– Comparison of the Impact of Sprung Mass

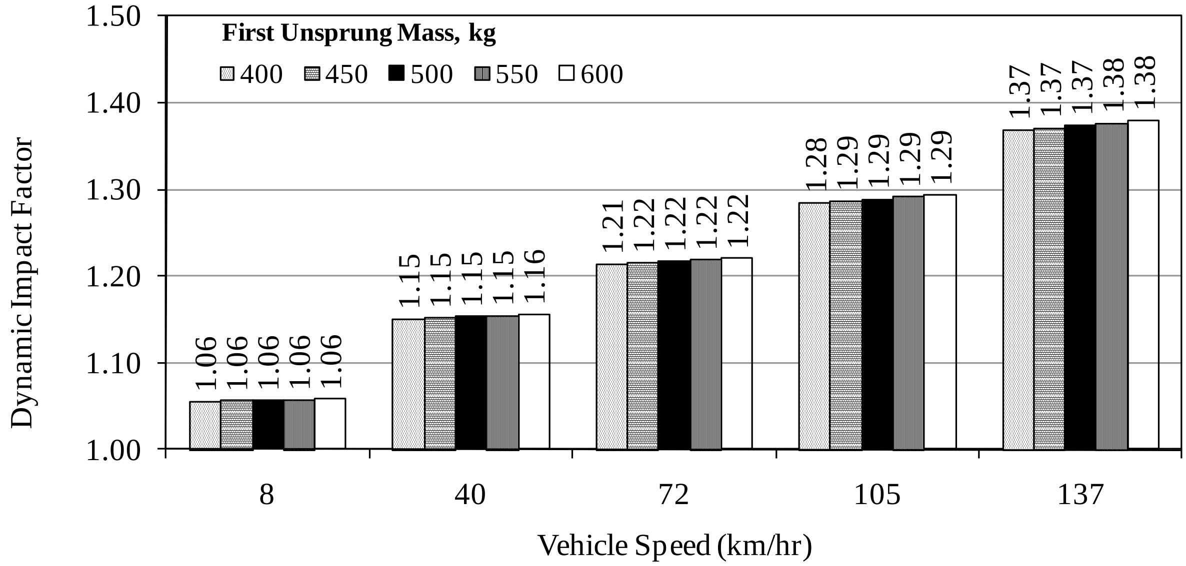

Figure E.15 –Impact of First Unsprung Mass on DI

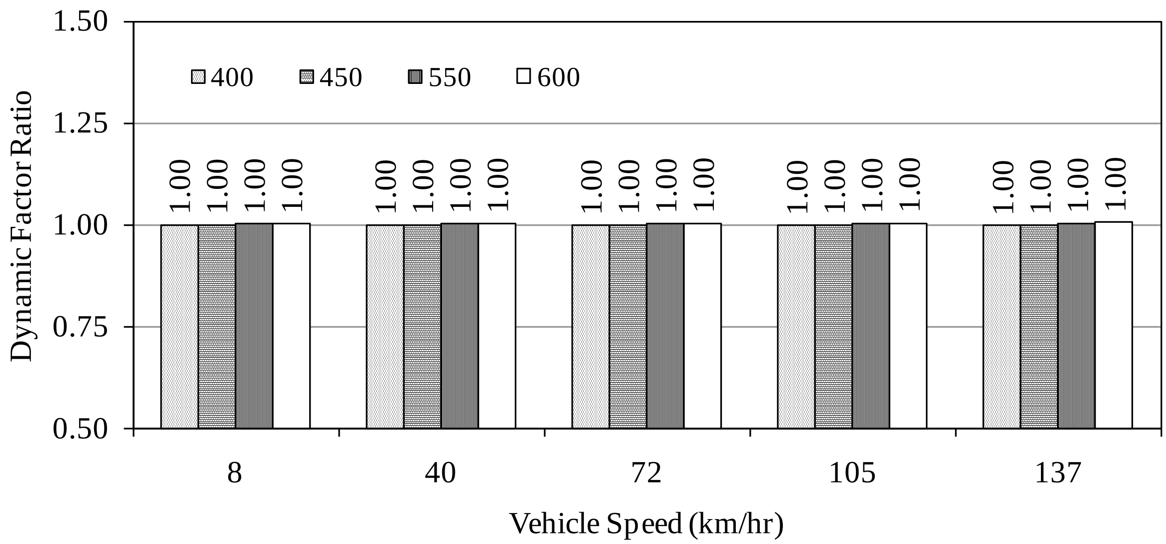

Figure E.16– Comparison of the Impact of First Unsprung Mass

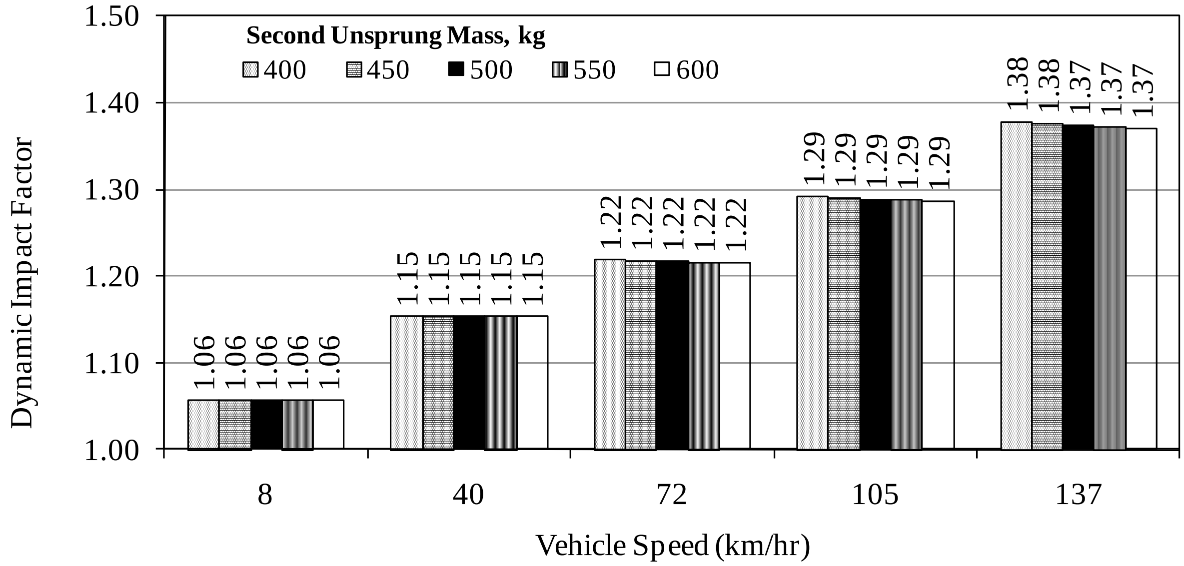

Figure E.17 –Impact of Second Unsprung Mass on DI

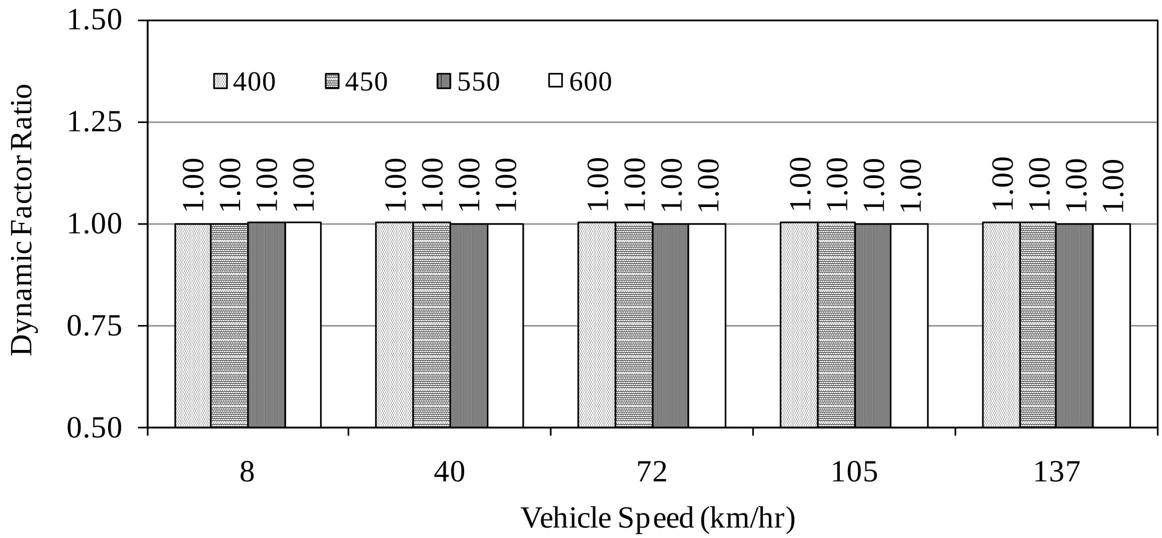

Figure E.18– Comparison of the Impact of Second Unsprung Mass

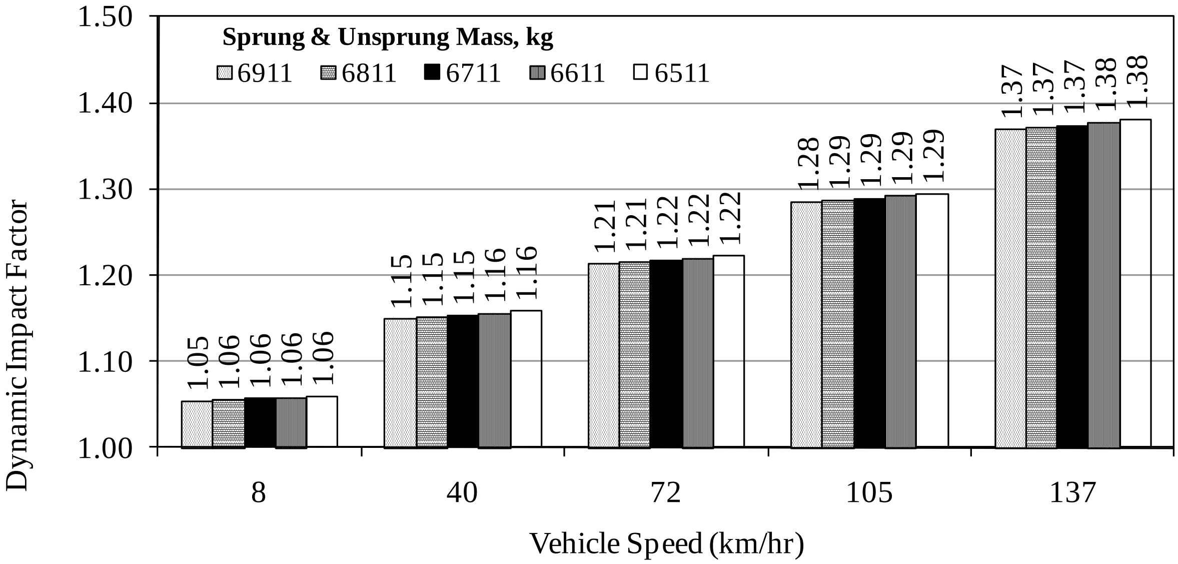

Figure E.19 –Impact of Masses on DI (Standard Truck)

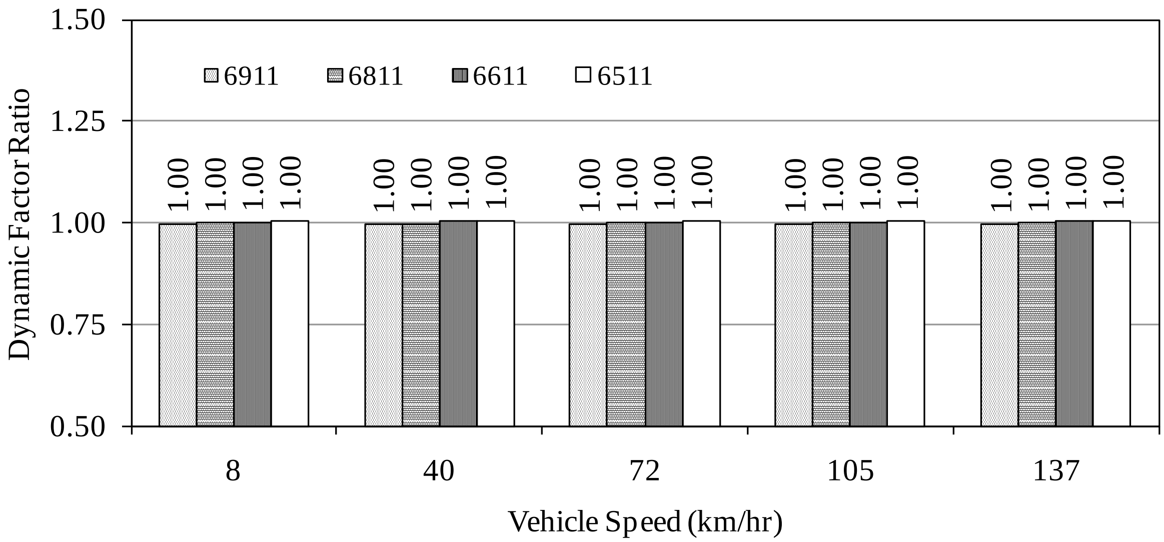

Figure E.20– Comparison of the Impact of Masses

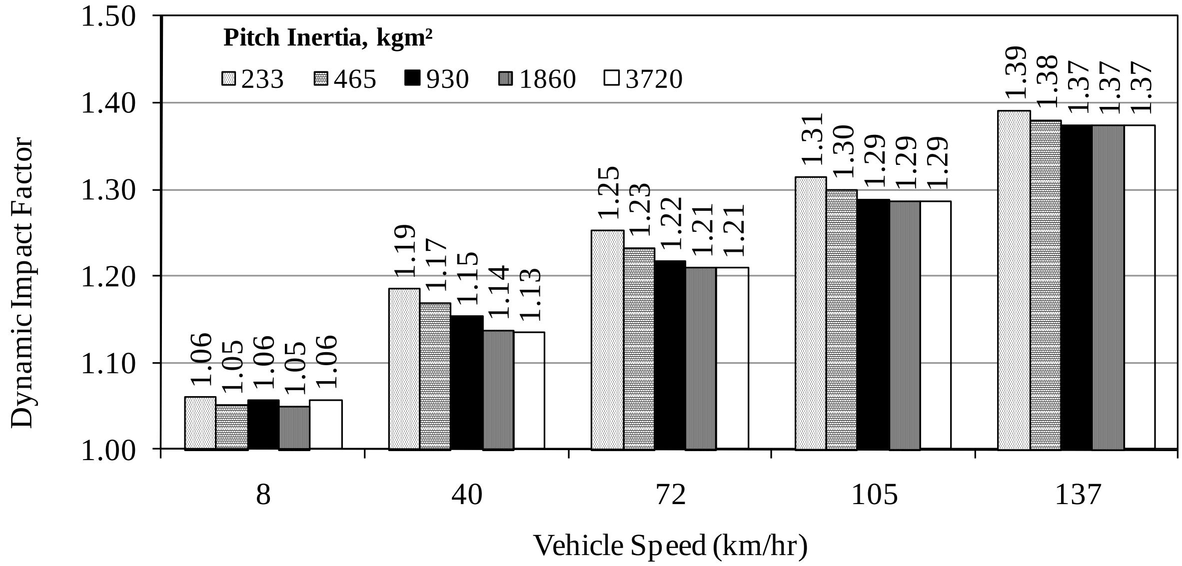

Figure E.21 –Impact of Pitch Inertia on DI

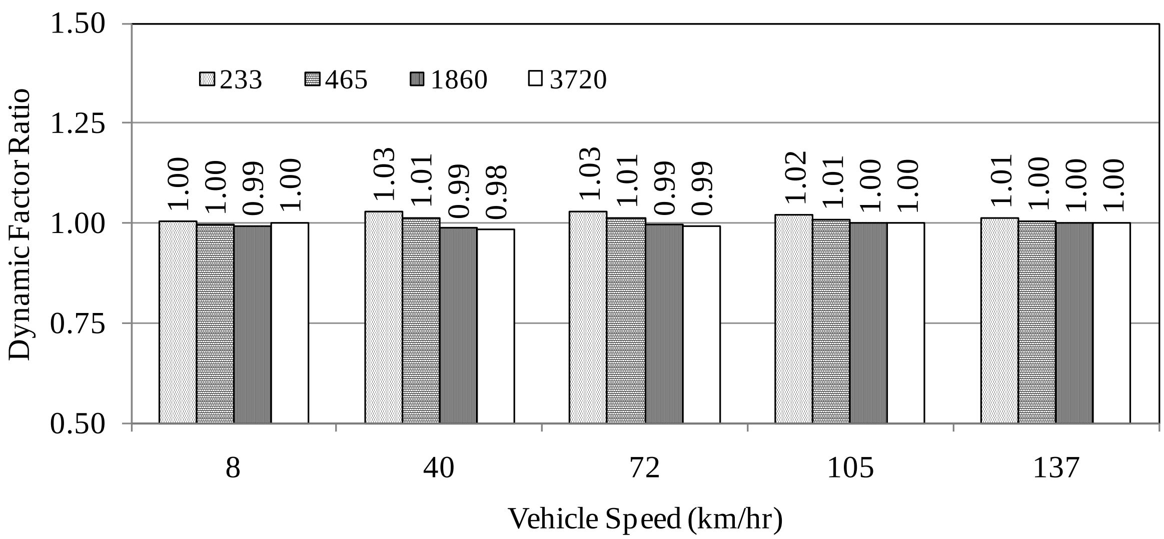

Figure E.22– Comparison of the Impact of Pitch Inertia

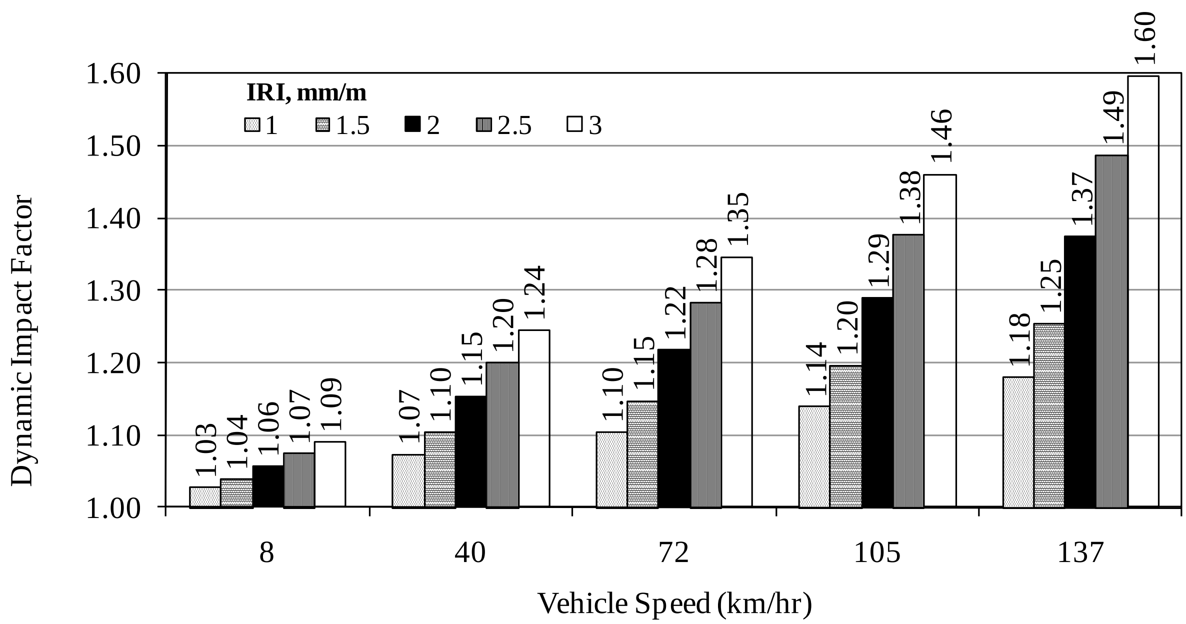

Figure E.23 –Impact of IRI on DI

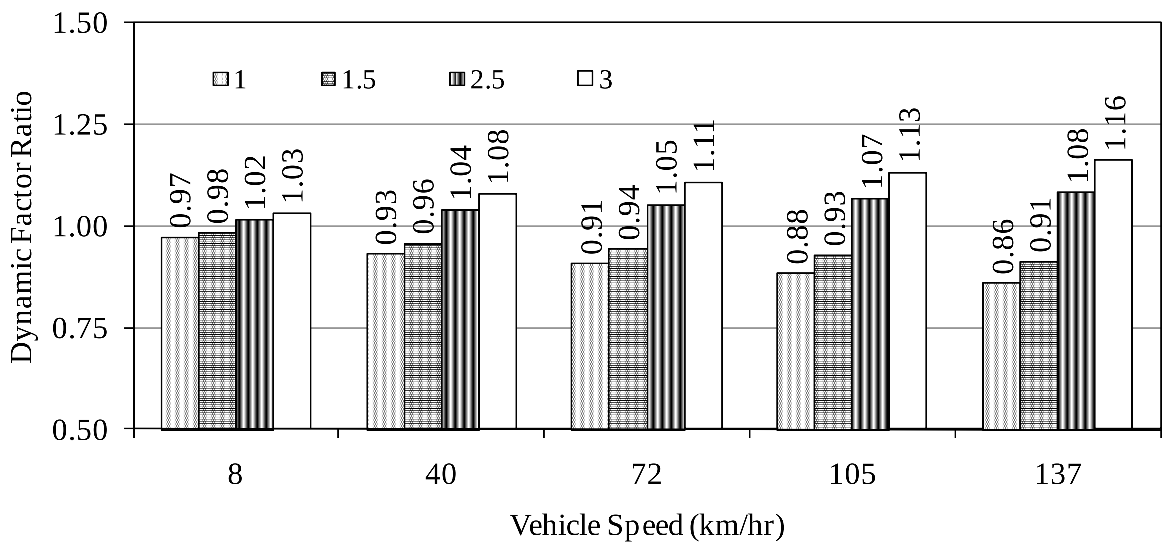

Figure E.24– Comparison of the Impact of IRI

APPENDIX F: TRIDEM LEAF SPRING MODEL PARAMETRIC STUDY

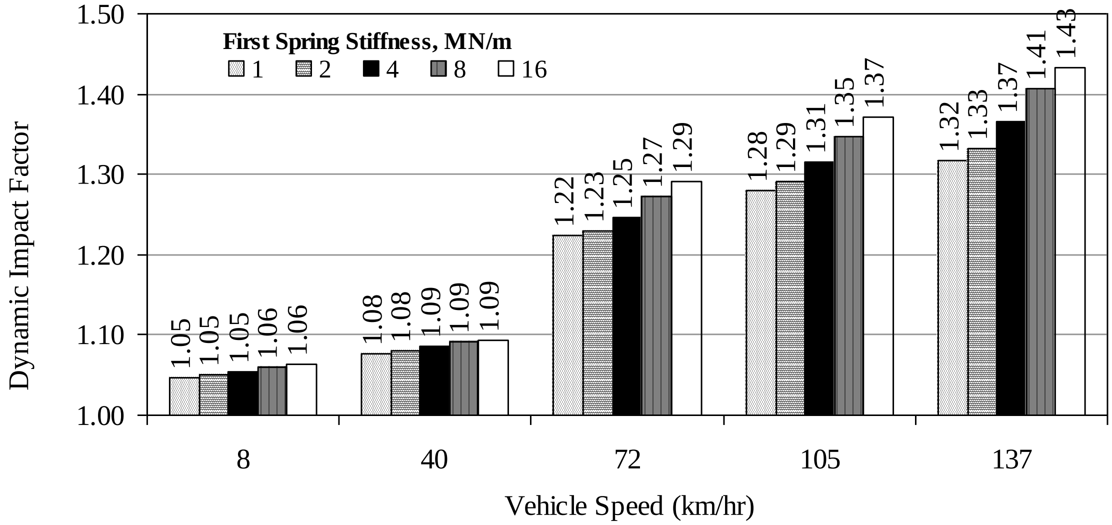

Figure F.1 – Impact of First Spring Stiffness on DI

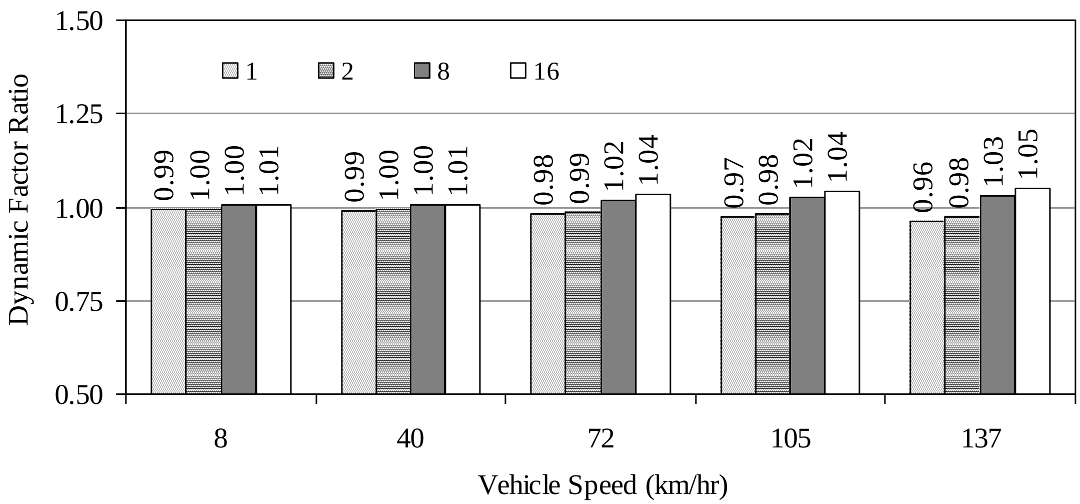

Figure F.2 – Comparison of the Impact of First Spring Stiffness

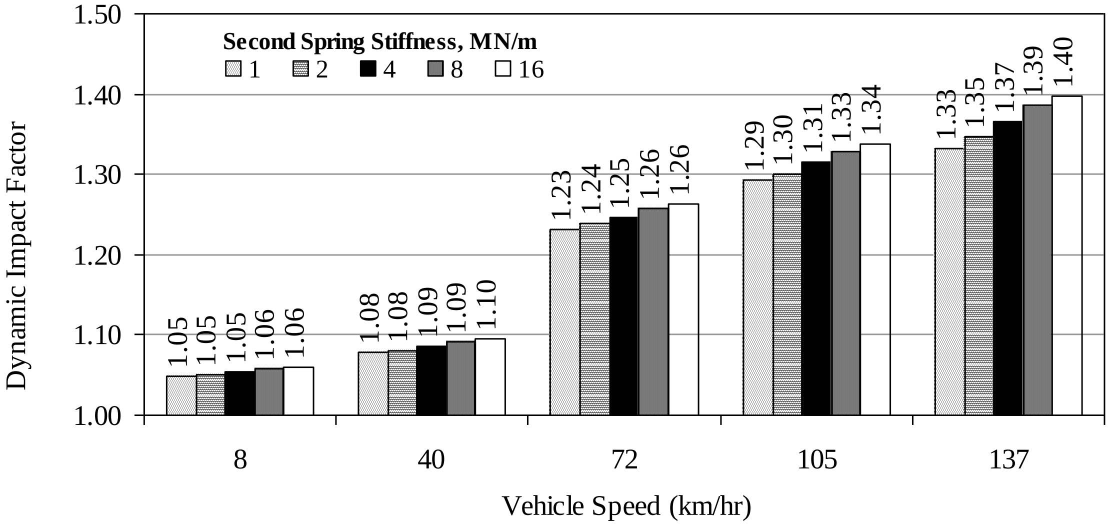

Figure F.3 – Impact of Second Spring Stiffness on DI

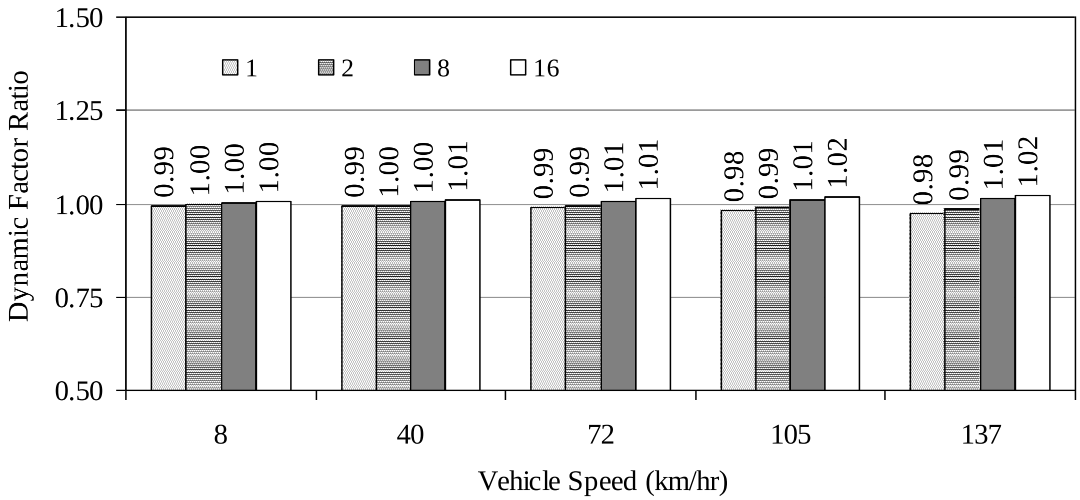

Figure F.4 – Comparison of the Impact of Second Spring Stiffness

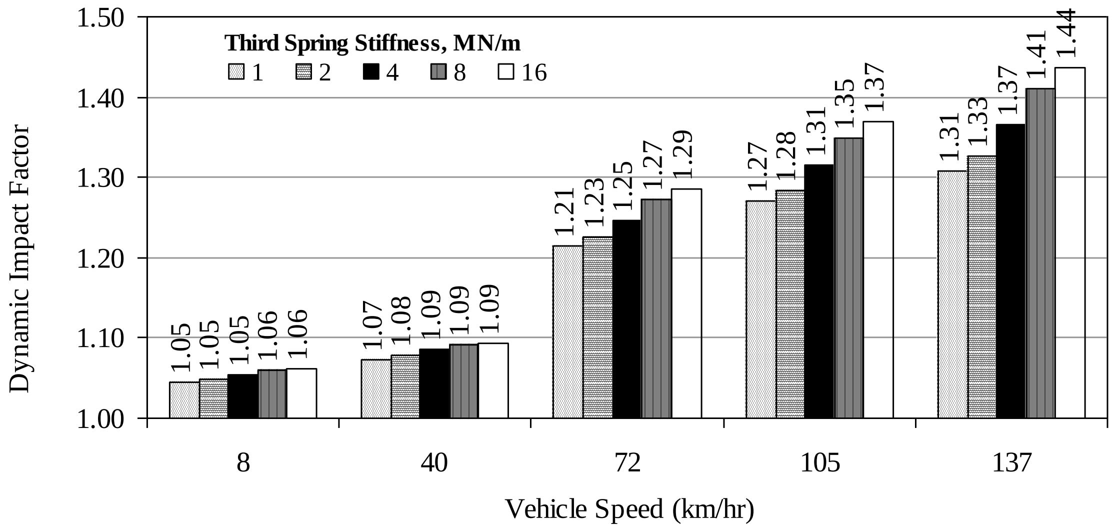

Figure F.5 – Impact of Third Spring Stiffness on DI

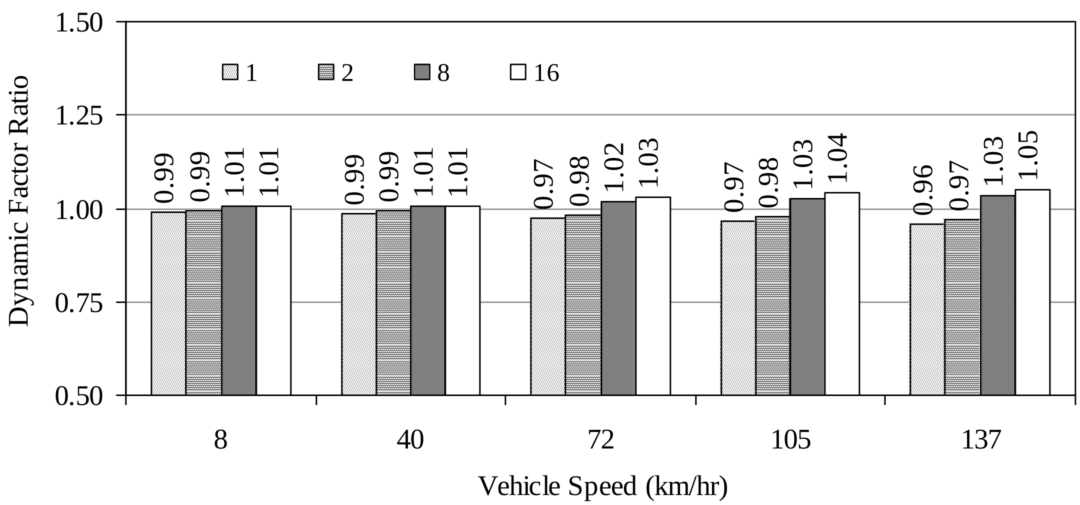

Figure F.6 – Comparison of the Impact of Third Spring Stiffness

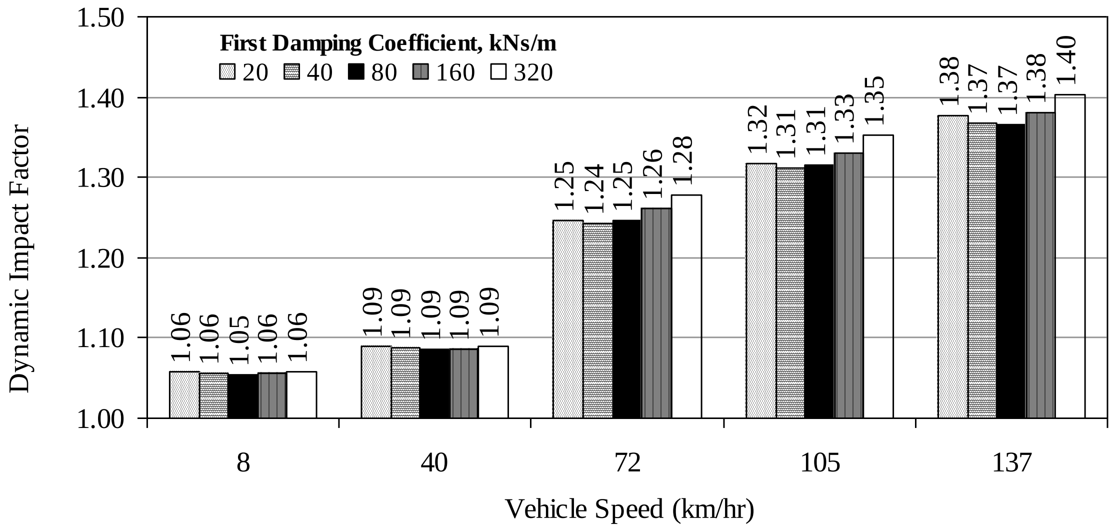

Figure F.7 –Impact of First Damping Coefficient on DI

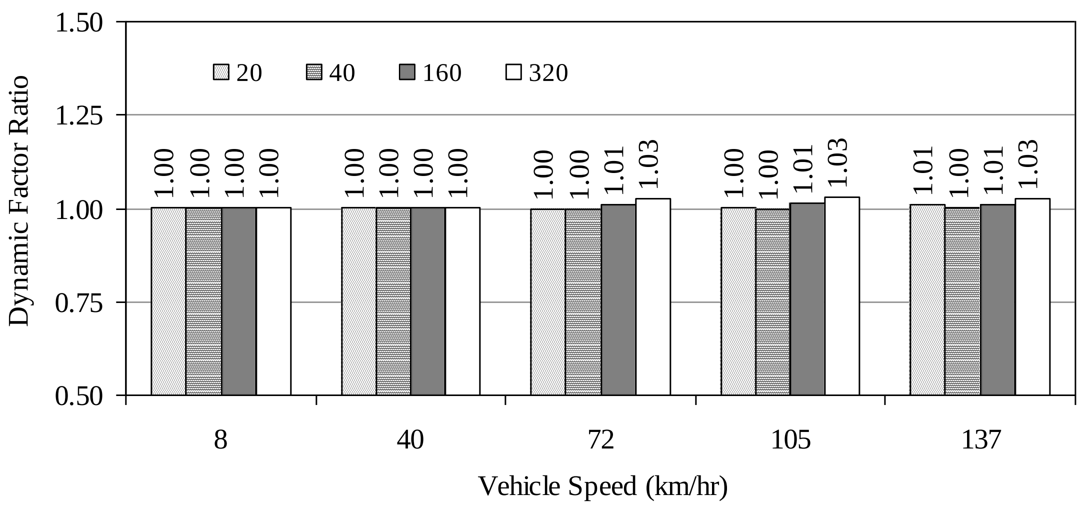

Figure F.8 – Comparison of the Impact of First Damping Coefficient

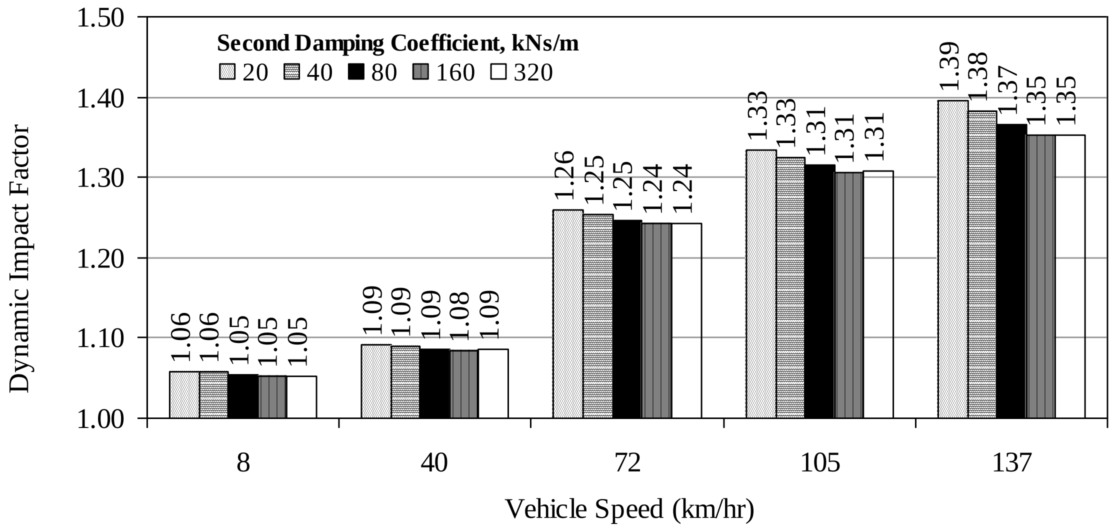

Figure F.9 –Impact of Second Damping Coefficient on DI

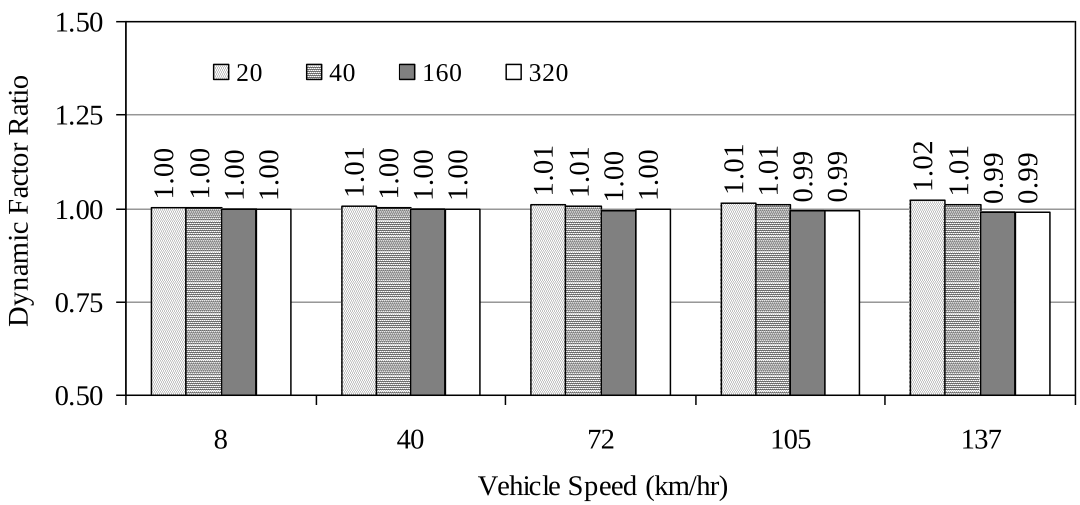

Figure F.10– Comparison of the Impact of Second Damping Coefficient

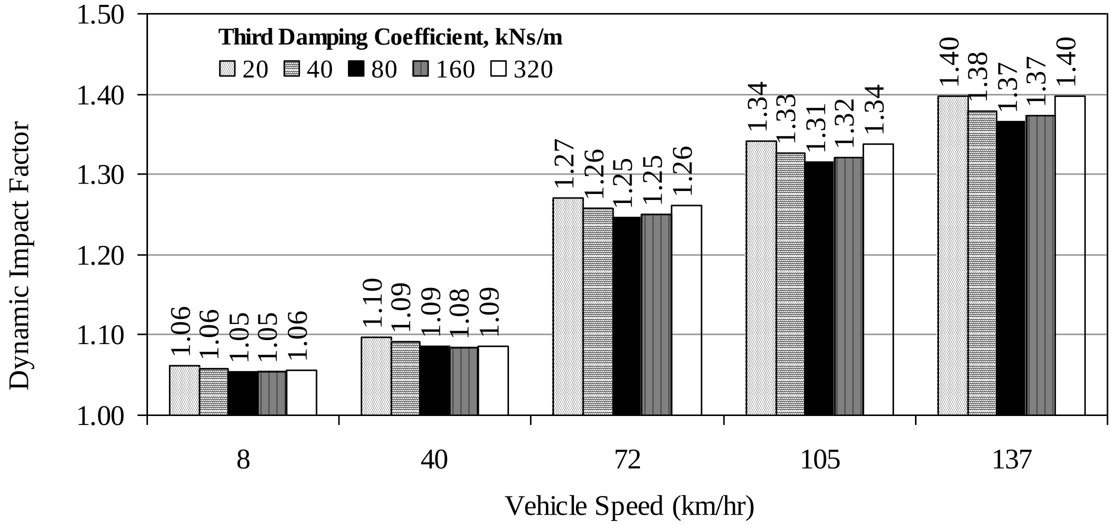

Figure F.11 –Impact of Third Damping Coefficient on DI

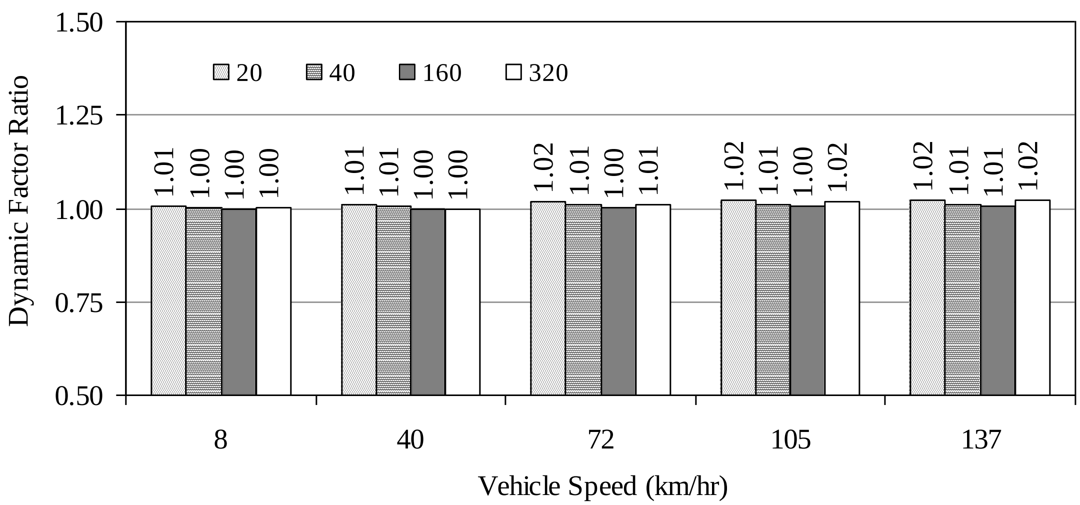

Figure F.12– Comparison of the Impact of Third Damping Coefficient

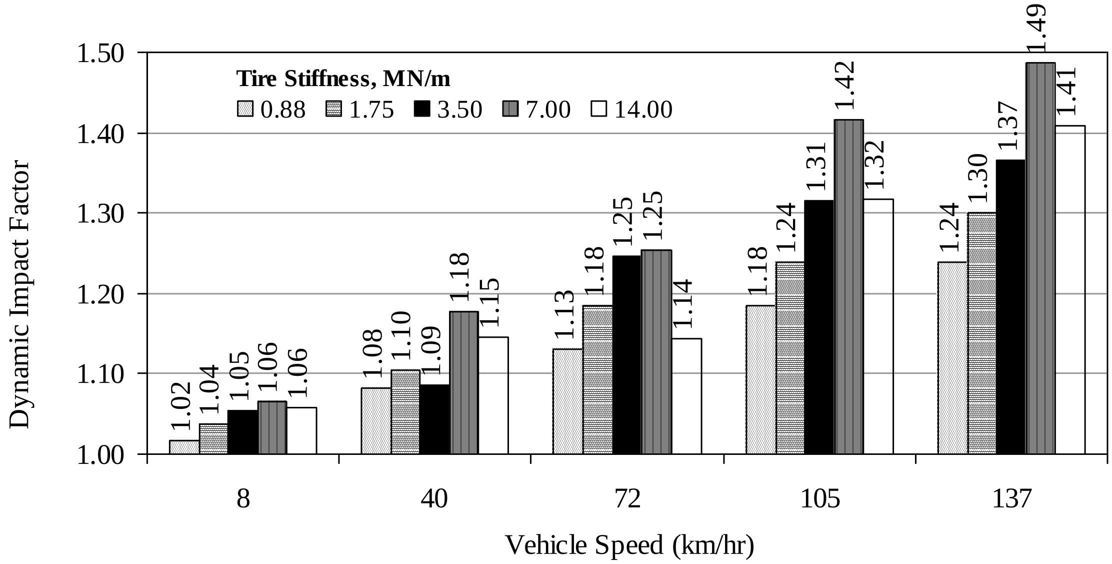

Figure F.13 –Impact of Tire Stiffness on DI

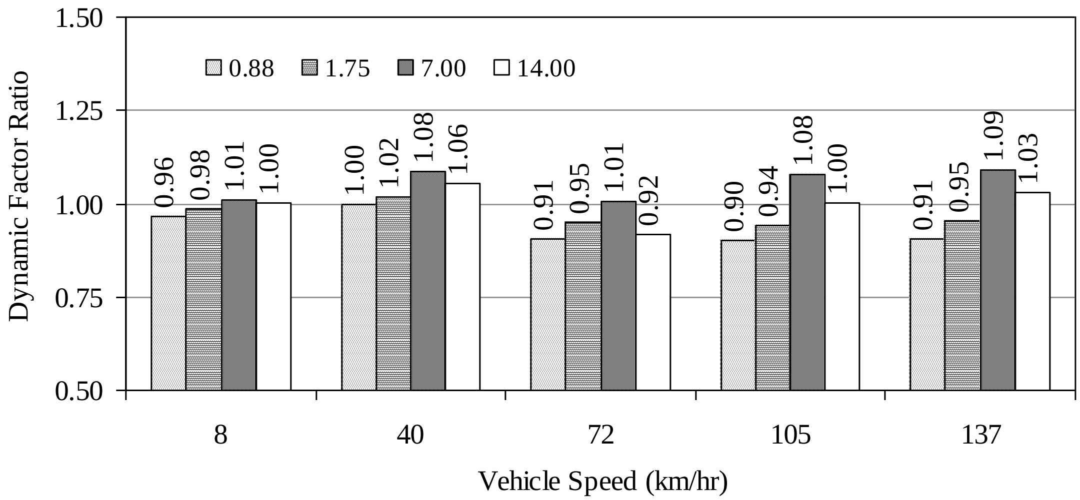

Figure F.14– Comparison of the Impact of Tire Stiffness

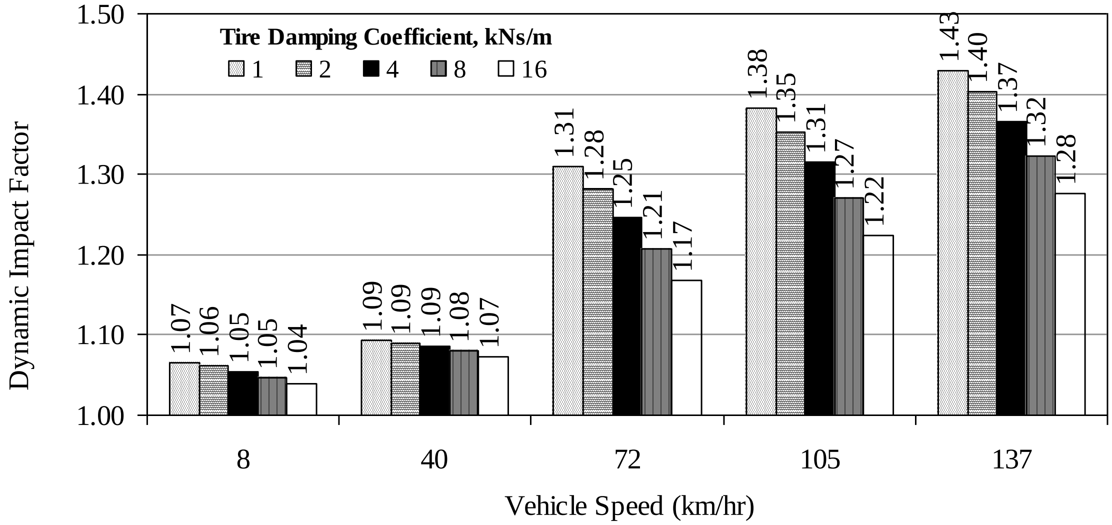

Figure F.15 –Impact of Tire Damping Coefficient on DI

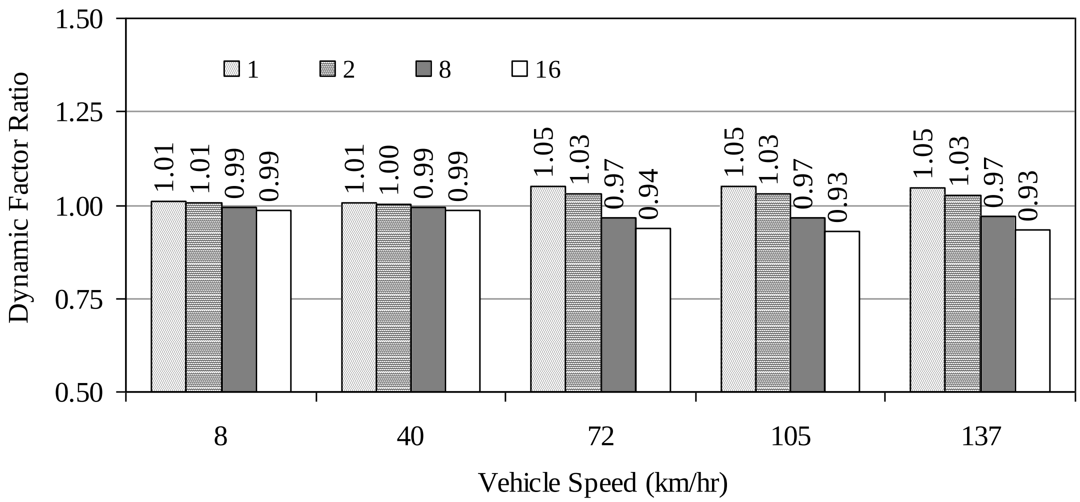

Figure F.16– Comparison of the Impact of Tire Damping Coefficient

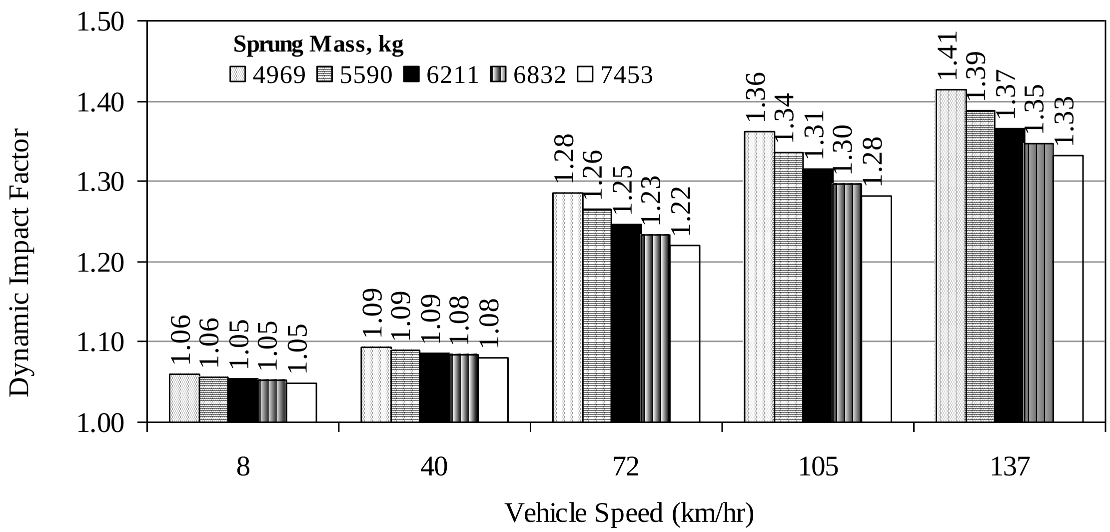

Figure F.17 –Impact of Sprung Mass on DI

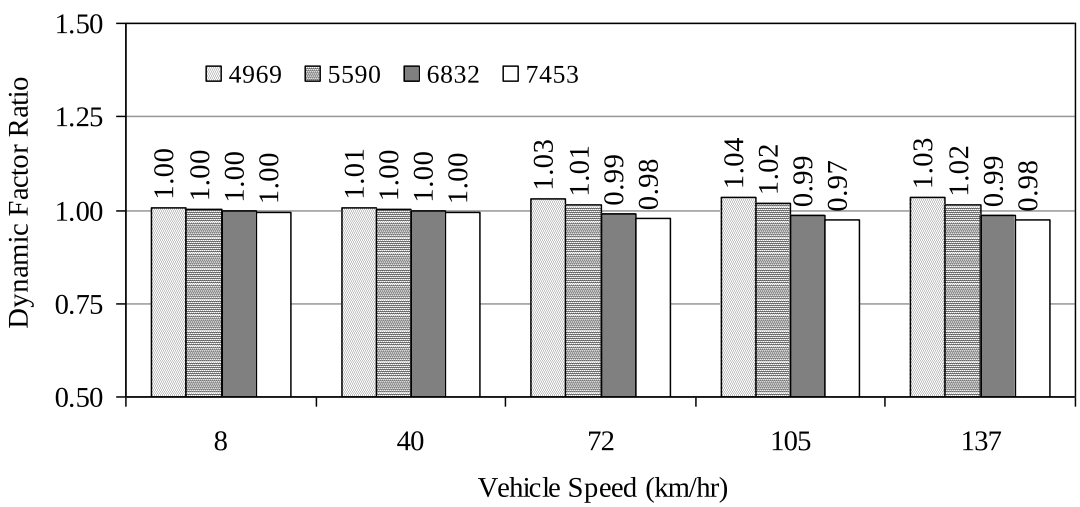

Figure F.18– Comparison of the Impact of Sprung Mass

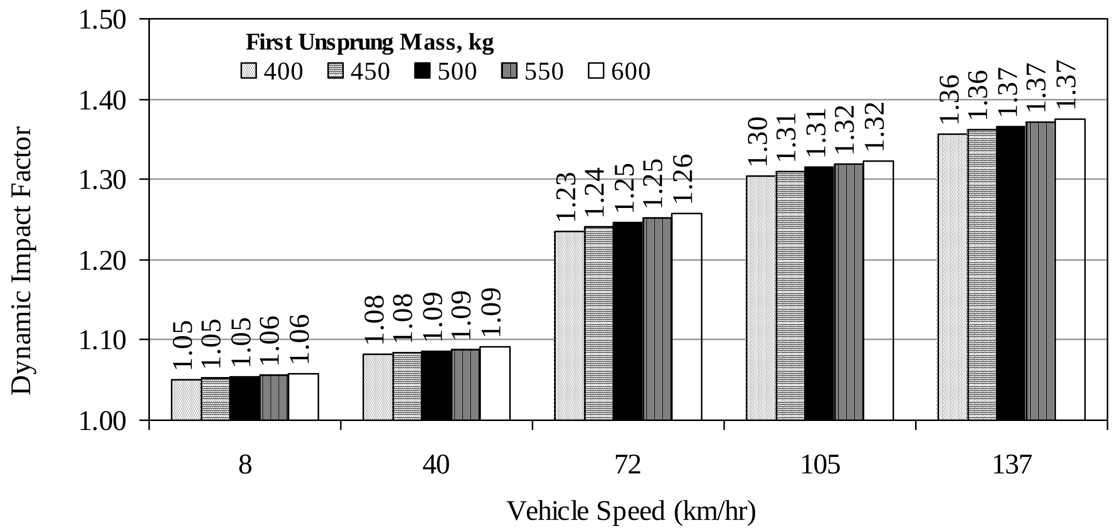

Figure F.19 –Impact of First Unsprung Mass on DI

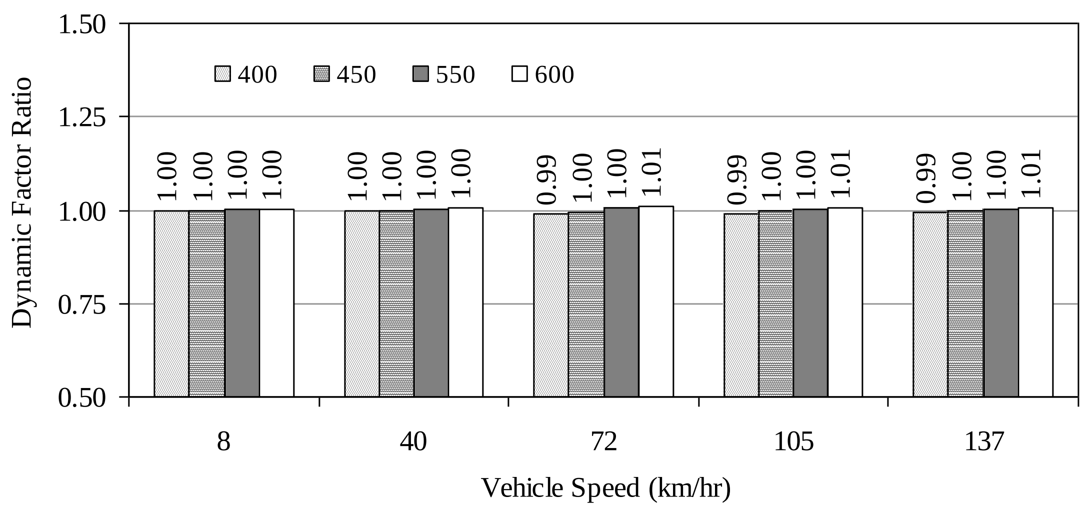

Figure F.20– Comparison of the Impact of First Unsprung Mass

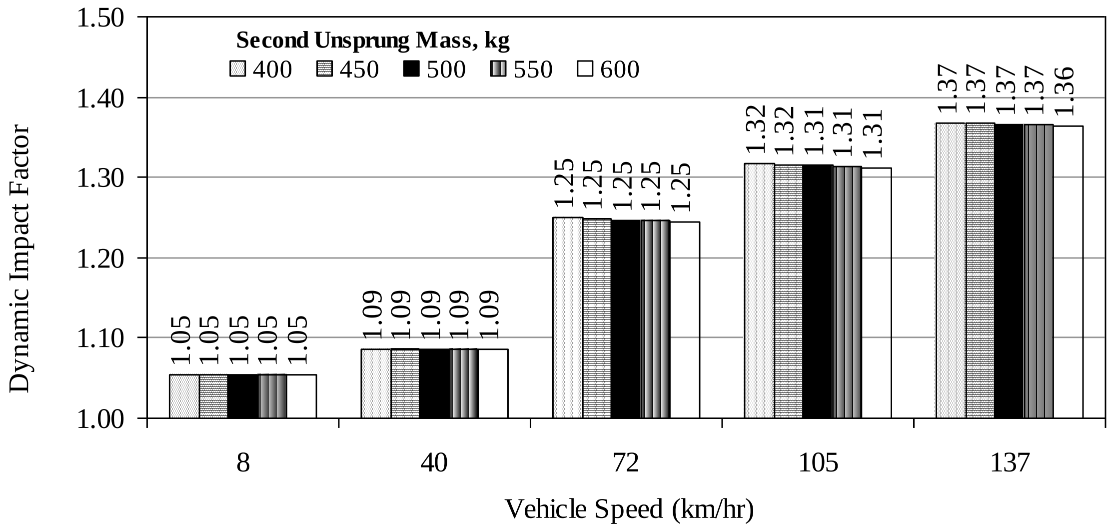

Figure F.21 –Impact of Second Unsprung Mass on DI

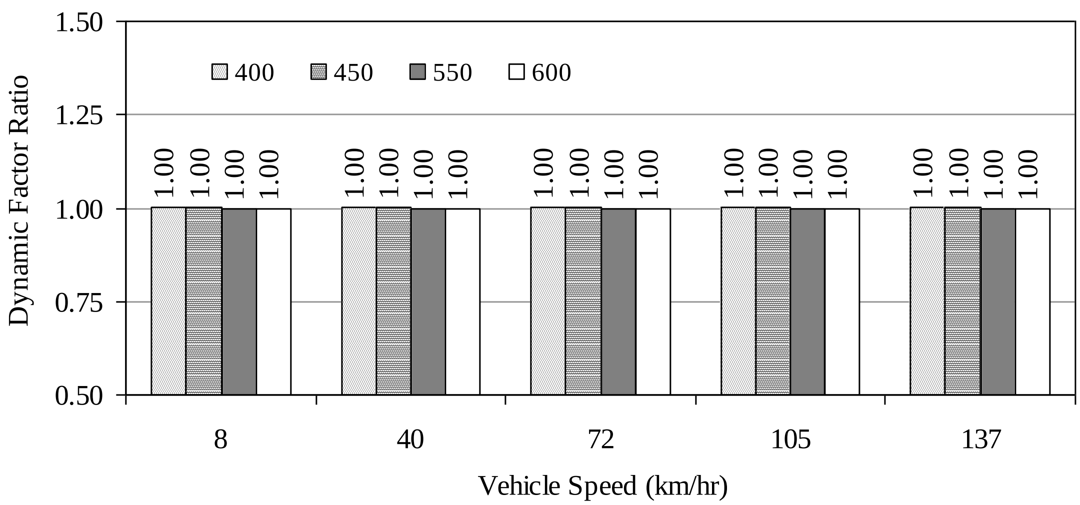

Figure F.22– Comparison of the Impact of Second Unsprung Mass

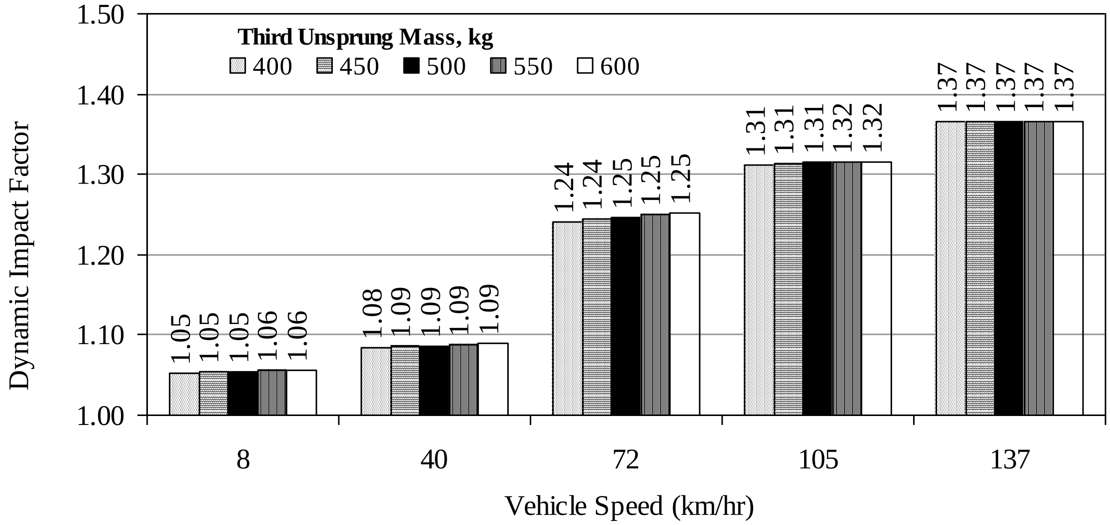

Figure F.23 –Impact of Third Unsprung Mass on DI

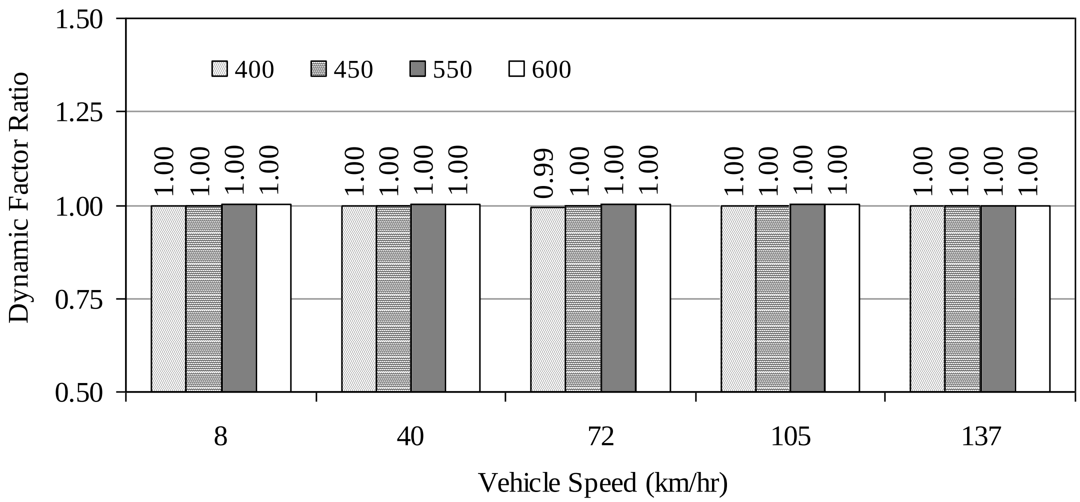

Figure F.24– Comparison of the Impact of Third Unsprung Mass

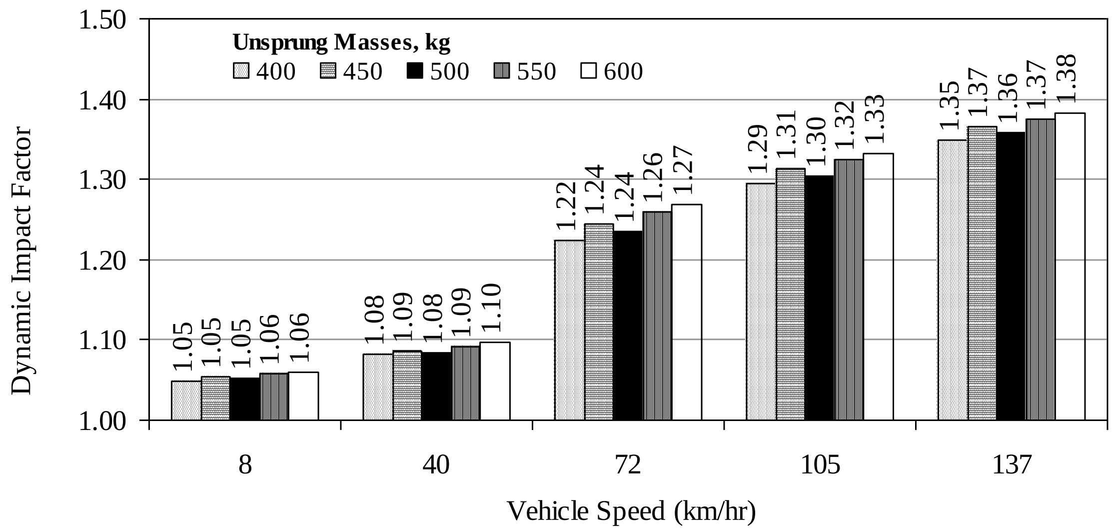

Figure F.25 –Impact of Masses on DI (Standard Truck)

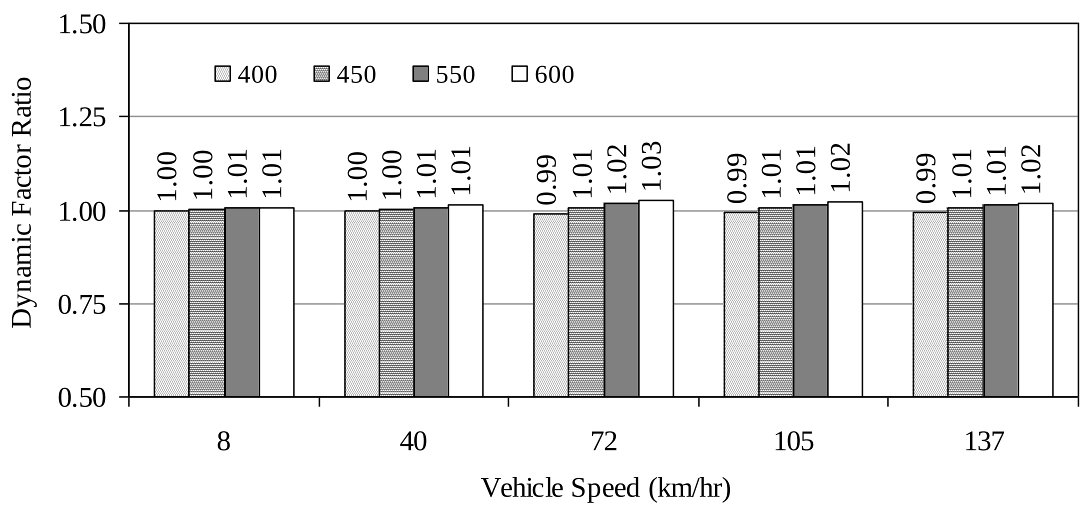

Figure F.26– Comparison of the Impact of Masses

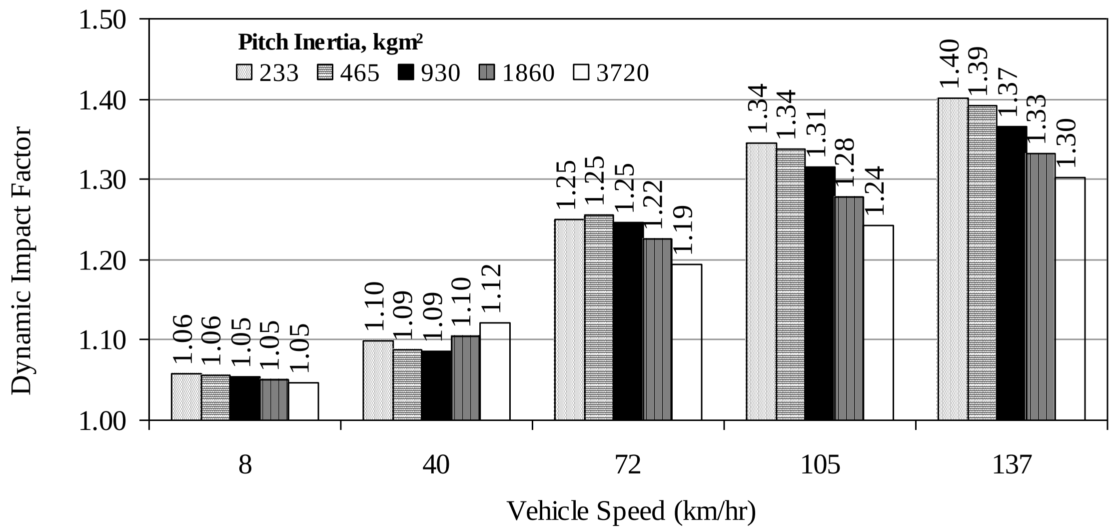

Figure F.27– Impact of Pitch Inertia on DI

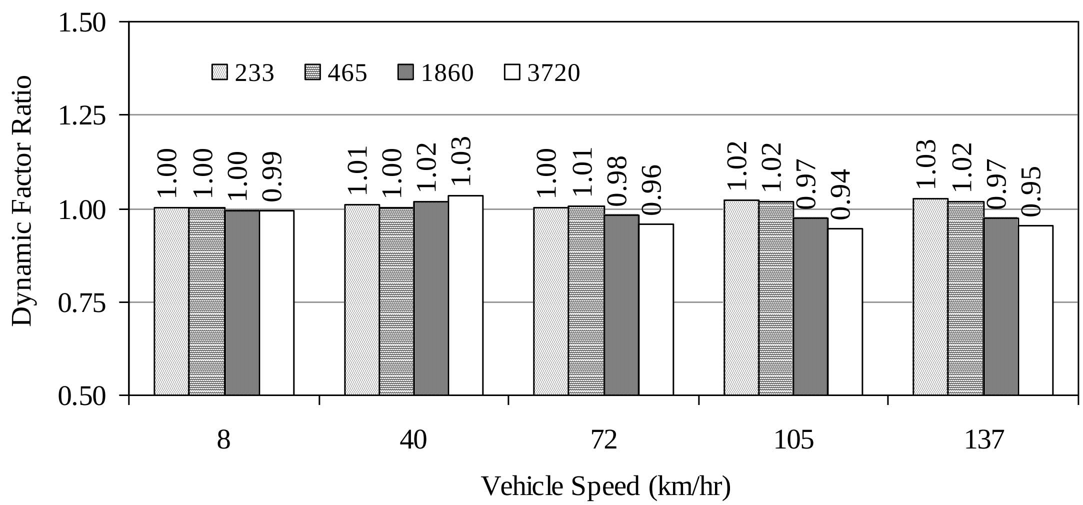

Figure F.28– Comparison of the Impact of Pitch Inertia

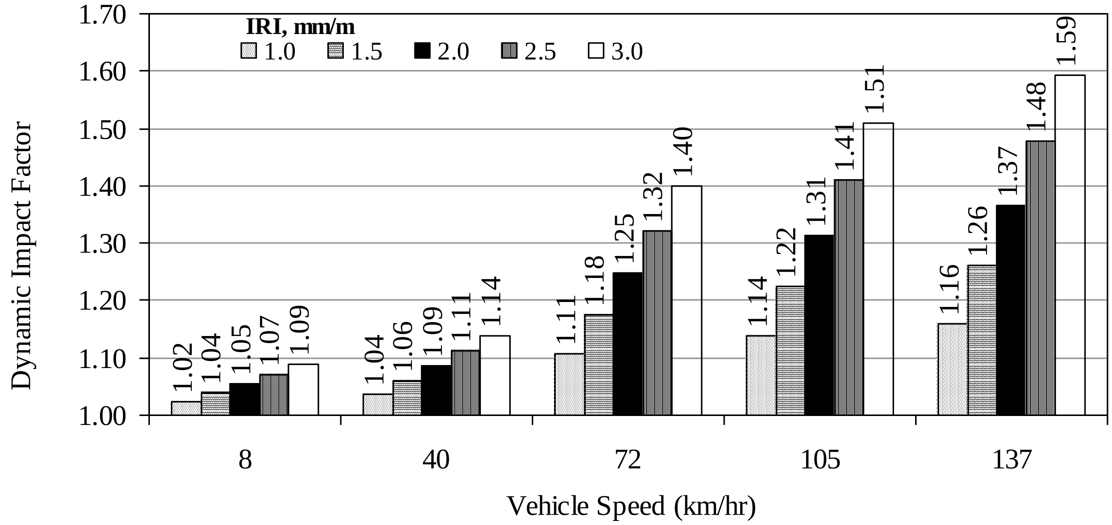

Figure F.29 –Impact of IRI on DI

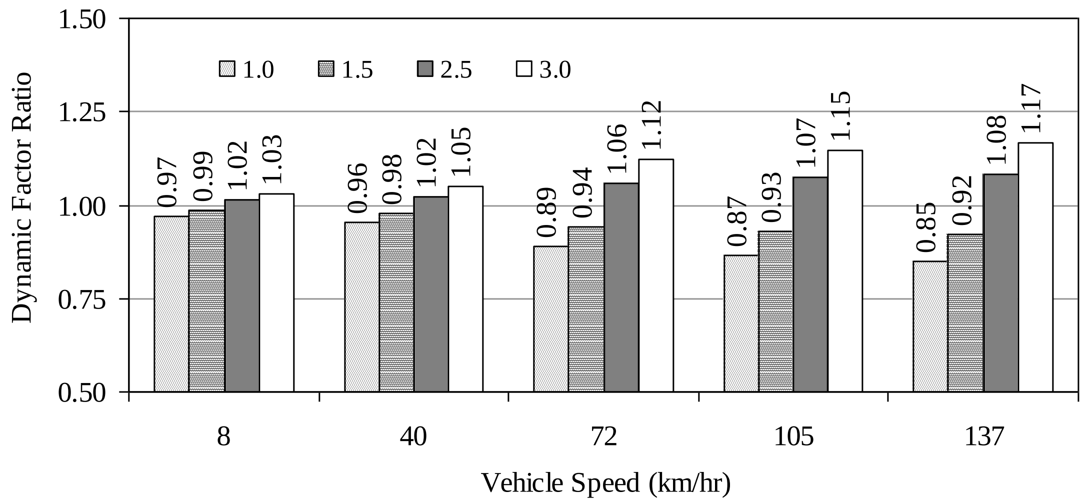

Figure F.30– Comparison of the Impact of IRI

APPENDIX G: WALKING BEAM MODEL PARAMETRIC STUDY

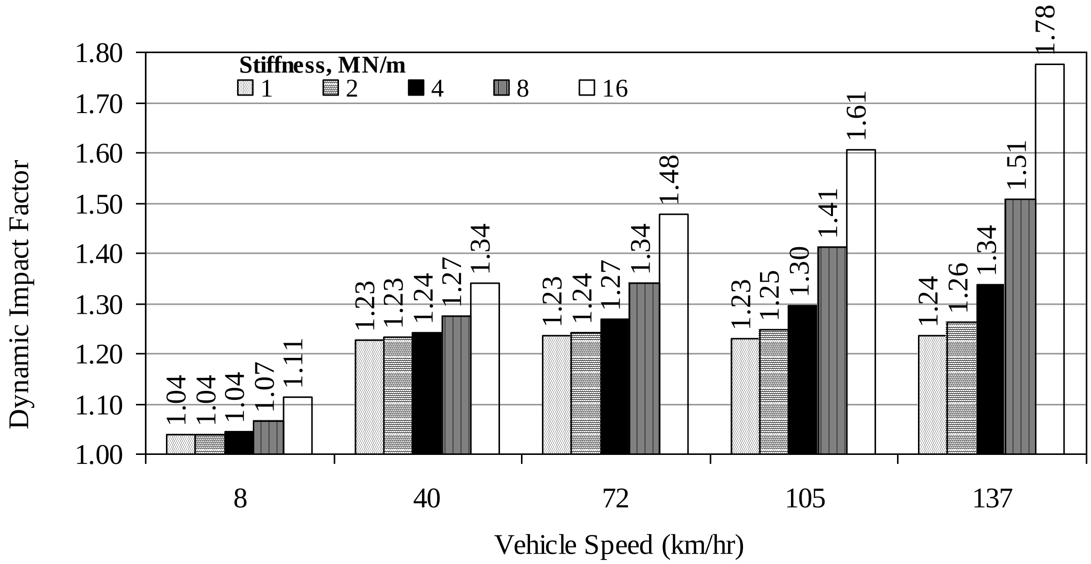

Figure G.1 – Impact of Spring Stiffness on DI

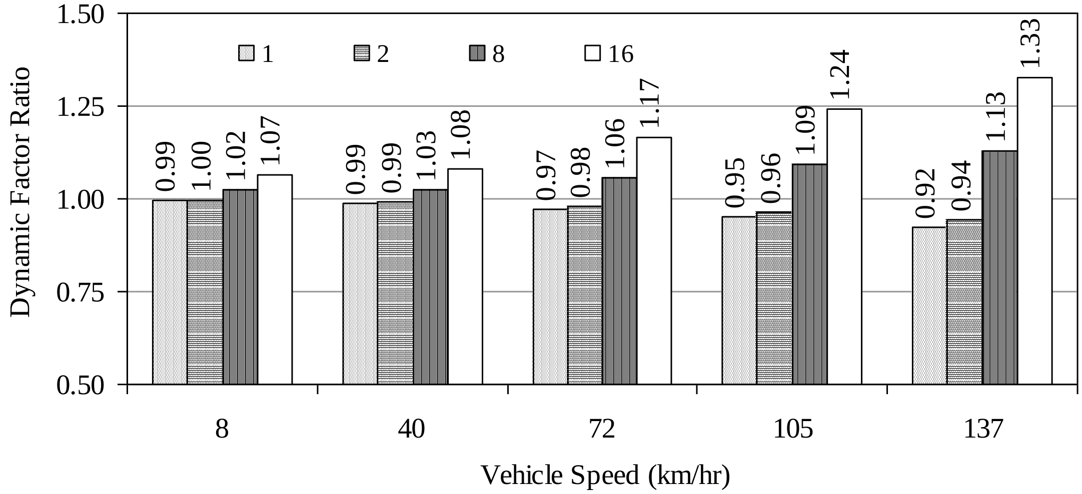

Figure G.2 – Comparison of the Impact of Spring Stiffness

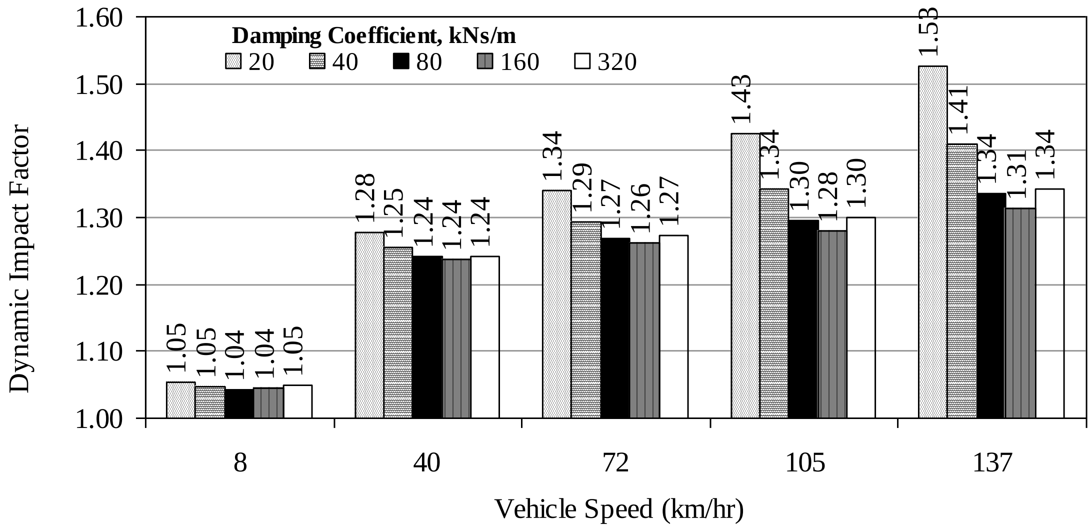

Figure G.3 –Impact of Damping Coefficient on DI

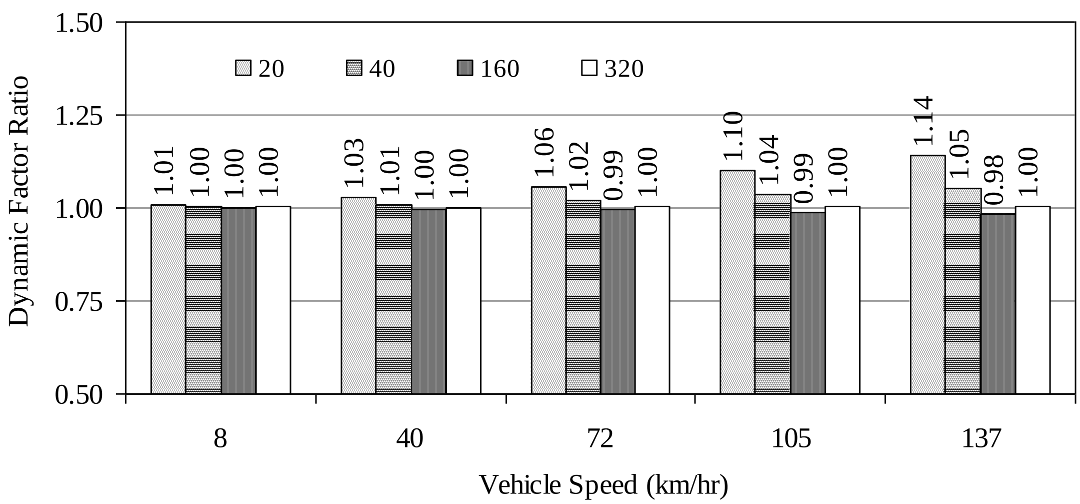

Figure G.4 – Comparison of the Impact of Damping Coefficient

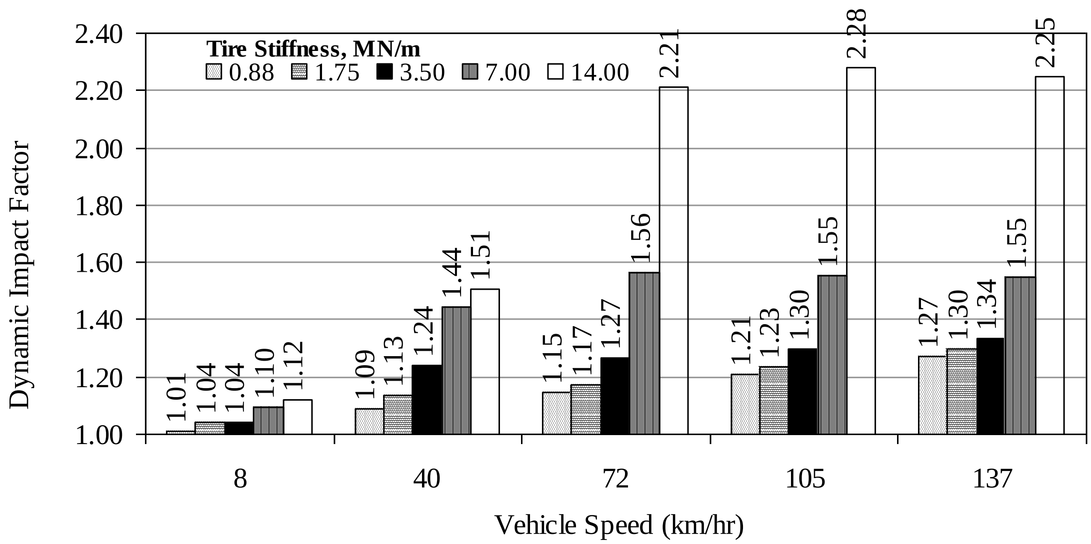

Figure G.5 –Impact of Tire Stiffness on DI

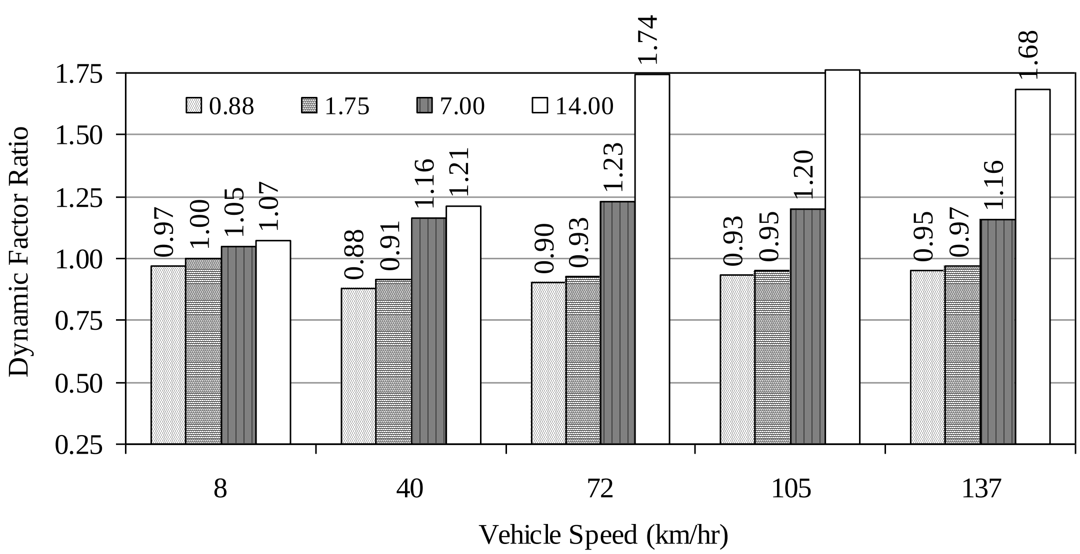

Figure G.6– Comparison of the Impact of Tire Stiffness

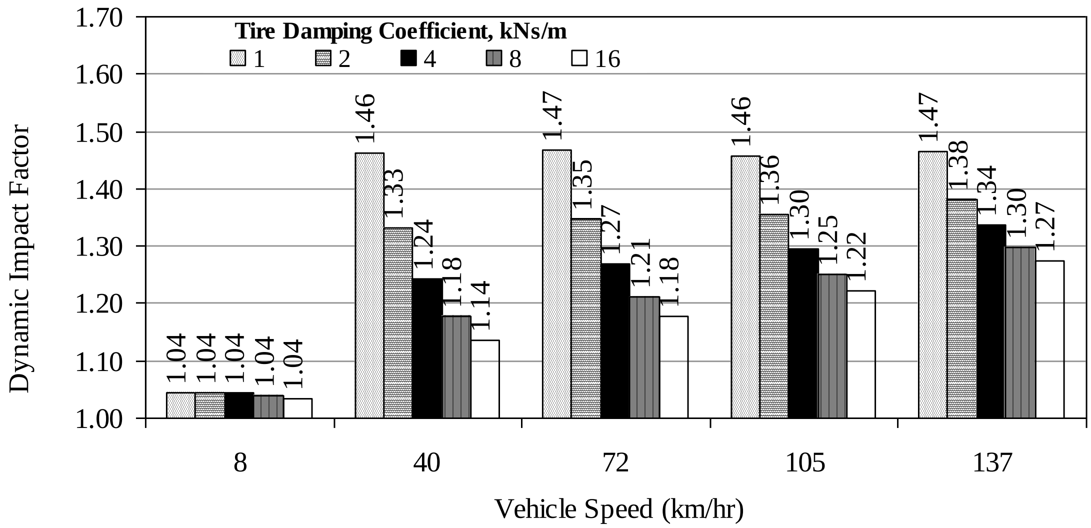

Figure G.7 –Impact of Tire Damping Coefficient on DI

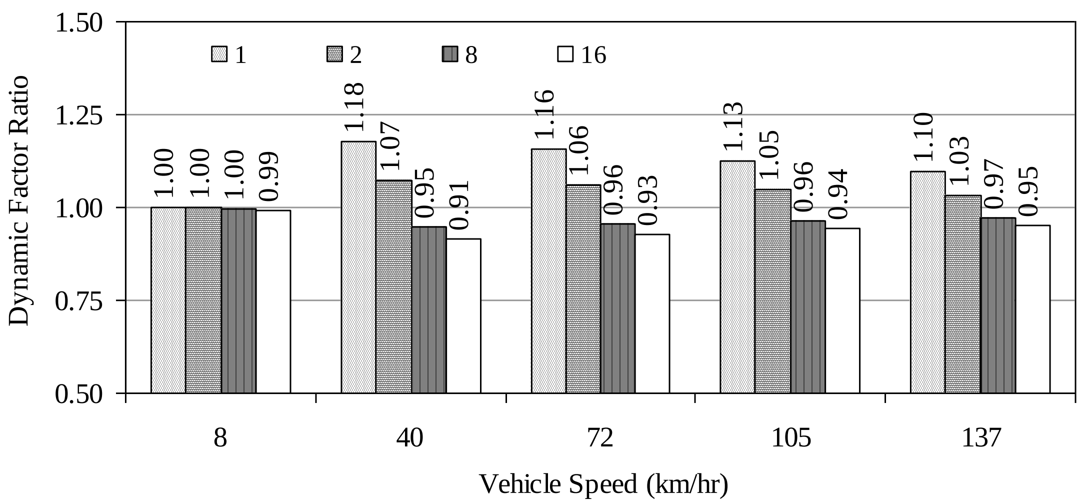

Figure G.8– Comparison of the Impact of Tire Damping Coefficient

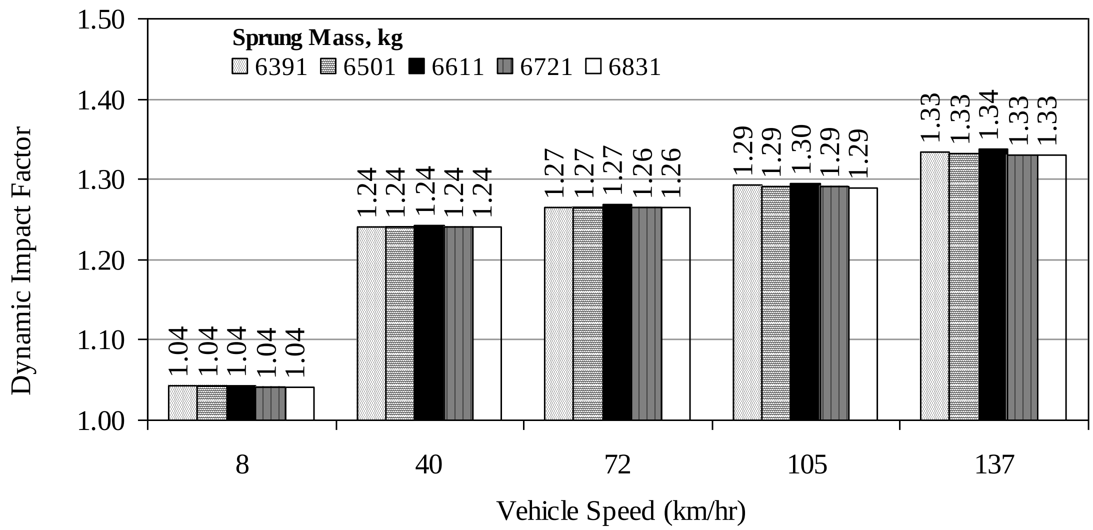

Figure G.9 –Impact of Sprung Mass on DI

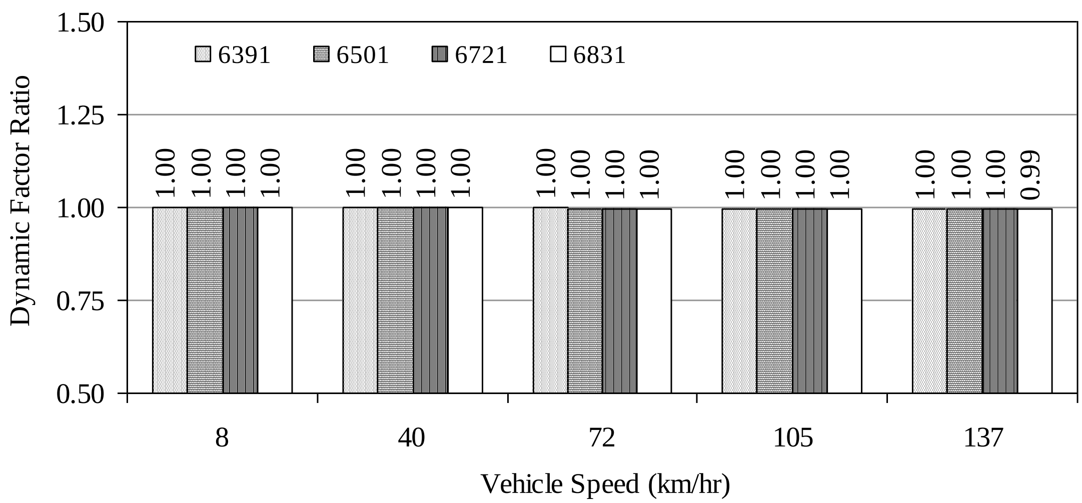

Figure G.10– Comparison of the Impact of Sprung Mass

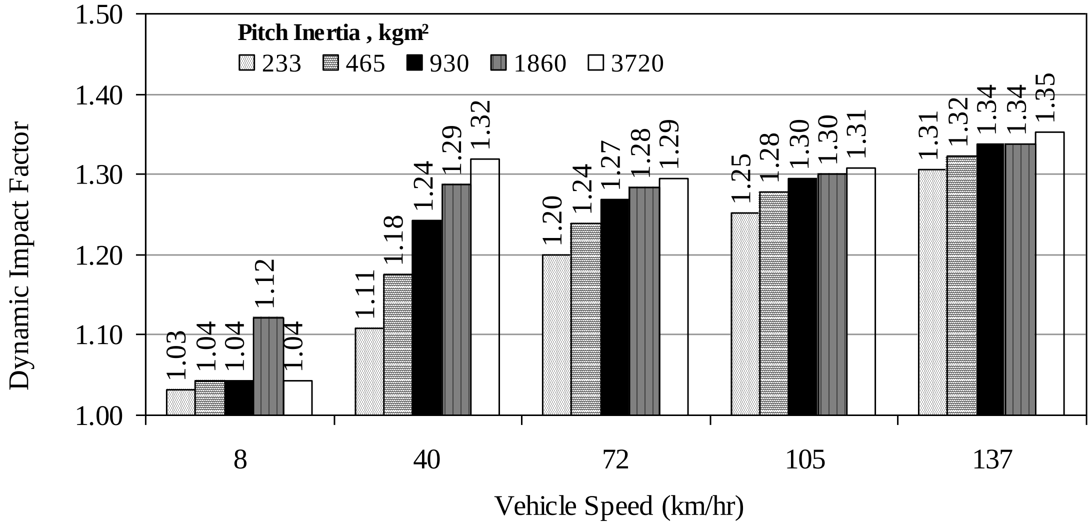

Figure G.11 –Impact of Pitch Inertia on DI

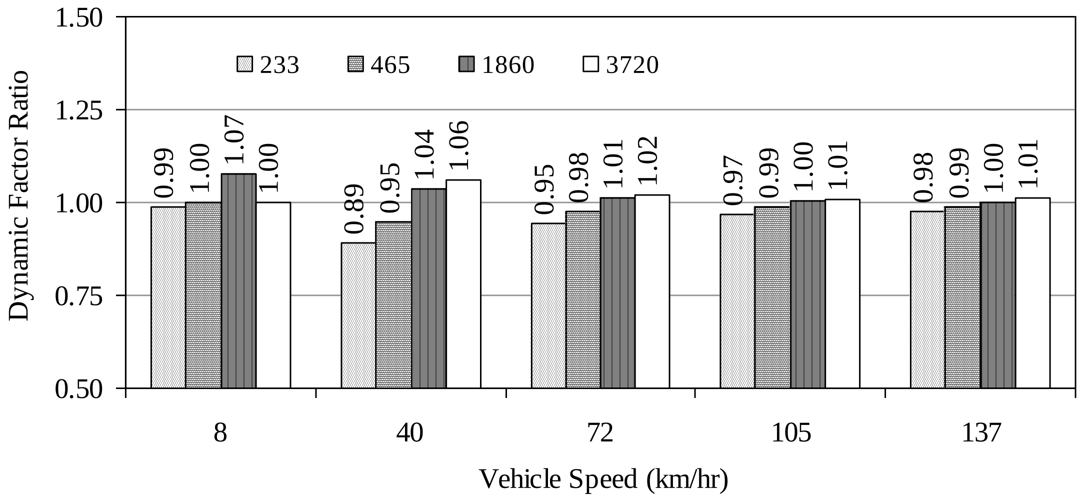

Figure G.12– Comparison of the Impact of Pitch Inertia

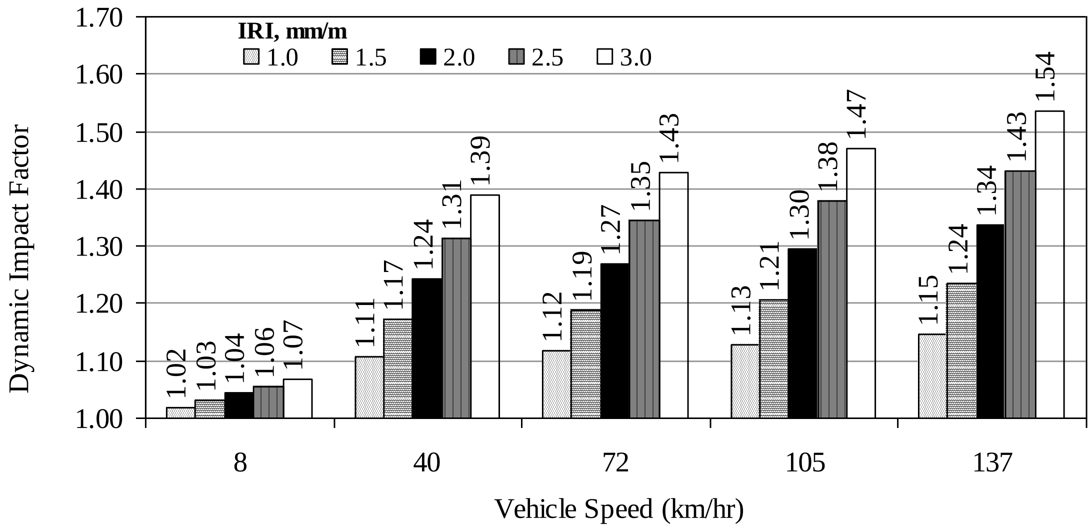

Figure G.13 –Impact of IRI on DI

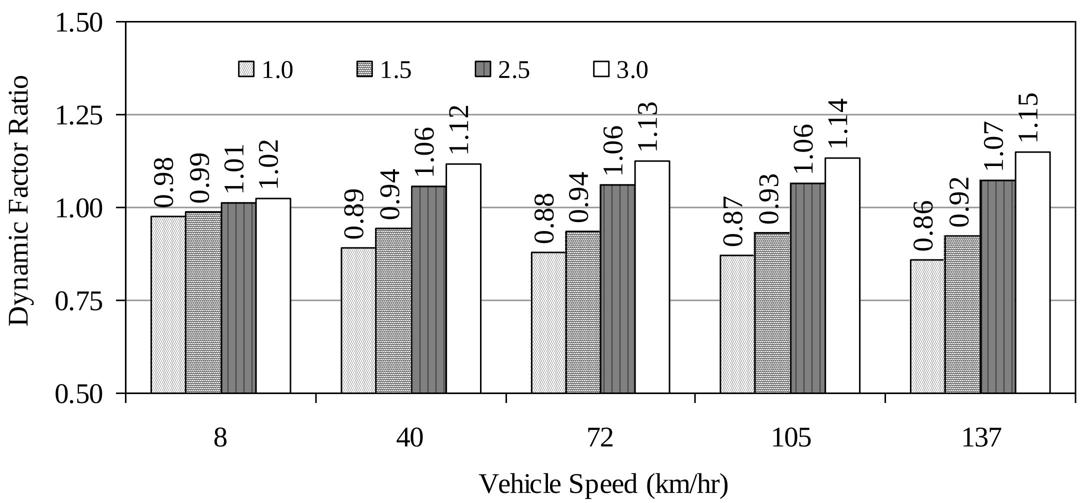

Figure G.14– Comparison of the Impact of IRI